

Voltage-gated sodium channels as non-photonic sensors
for membrane-delimited reactive species

Thesis

in partial fulfillment of the requirements for the degree of
“Doctor rerum naturalium” (Dr. rer. nat.)

submitted to the Council of the Faculty of Medicine
at Friedrich Schiller University of Jena

by M.Sc. Neuroscience Navin Kumar Ojha
born on 07.03.1986 in Katni, Madhya Pradesh, India

Spannungsgesteuerte Natriumkanäle als nicht- photonische Sensoren für membrannahe reaktive Spezies

Dissertation

zur Erlangung des akademischen Grades
„Doctor rerum naturalium“ (Dr. rer. nat.)

vorgelegt dem Rat der Medizinischen Fakultät
der Friedrich-Schiller-Universität Jena

von M.Sc. Neuroscience Navin Kumar Ojha
geboren am 07.03.1986 in Katni, Madhya Pradesh, Indien

Gutachter / Reviewers:

1. Prof. Dr. Stefan H. Heinemann

Institute of Biochemistry and Biophysics, Friedrich Schiller University, Jena

2. apl. Prof. Dr. Thomas Zimmer

Institute of Physiology II, University Hospital, Jena

3. Prof. Dr. Barbara Niemeyer

Department of Molecular Biophysics, University of Saarland, Homburg

Tag der öffentlichen Verteidigung / Date of the public disputation: 06.03.2018

Contents

Table of contents	I – III
List of abbreviations	IV – VI
Summary	VII – X
1. Introduction	1 – 19
1.1. Reactive species.....	1
1.1.1. Sources of cellular reactive species.....	1
1.1.2. Cellular RS are neither hero nor villain.....	2
1.1.3. Biochemistry of cellular reactive species.....	3
1.2. Cell membrane and reactive species.....	3
1.3. Redox modulation of ion channels.....	7
1.4. Voltage-gated Na ⁺ channels.....	9
1.5. Detection of cellular reactive species.....	14
1.5.1. roGFP2.....	15
1.5.2. Grx1 – roGFP2.....	16
1.6. Artifacts of light in cellular reactive species detection.....	17
1.7. Objectives.....	18
2. Materials and methods	20 – 31
2.1. Bacterial strain and cell lines.....	20
2.2. Expression plasmids.....	20
2.3. Other chemicals.....	22
2.4. Buffers and solutions.....	23
2.5. Plasmid amplification, extraction, and purification.....	23
2.6. Cell culture and transfection.....	24
2.7. Patch-clamp electrophysiology.....	25
2.8. Photometry.....	26
2.9. Reactive species generation.....	28
2.10. Data acquisition, analysis, and statistics.....	28
2.10.1. Voltage-dependent channel activation.....	29
2.10.2. Voltage-dependence of channel inactivation.....	29
2.10.3. Steady-state current and the time course of inactivation.....	29
2.10.4. Fractional recovery.....	30
2.10.5. Time course of inactivation removal.....	30
2.10.6. Fluorescence ratios.....	30

3. Results	32 – 81
3.1. Selection of Na ⁺ channel mutants sensitive to reactive species.....	32
3.2. Generation and heterologous expression of seleno-Na ⁺ channel.....	34
3.3. Biophysical properties of roNav1 and roNav2.....	36
3.3.1. Voltage-dependent channel activation.....	37
3.3.2. Voltage-dependent channel inactivation.....	39
3.3.2.1. Residual steady-state current.....	39
3.3.2.2. Inactivation kinetics.....	41
3.3.2.3. The half-maximal inactivation voltage and corresponding slope factor.....	43
3.3.2.4. Time course of fractional recovery from inactivation.....	46
3.4. The response of roNav1 and roNav2 to endogenous redox stimuli.....	49
3.4.1. The response of roNav1 and roNav2 to basal redox status of HEK 293T cells.....	49
3.4.2. Detection of mitochondrial reactive oxygen species.....	51
3.4.2.1. The response of mutant channels to mtROS.....	51
3.4.2.2. The response of fluorescent redox reporters to mtROS.....	52
3.5. The response of roNav1 and roNav2 to exogenous redox stimuli.....	53
3.5.1. The response of roNav1 to chloramine T.....	53
3.5.2. Redox sensitivity comparison of roNav1 with roGFP2.....	55
3.5.3. The response of roNav2 to chloramine T.....	56
3.5.4. A comparison of RS-sensitivity of roNav1, roNav2, and roGFP2.....	57
3.5.5. Detection of hydrogen peroxide-mediated redox changes.....	58
3.5.5.1. Monitoring of H ₂ O ₂ mediated redox changes with roNav1, roNav2, and roGFP2.....	58
3.5.5.2. Reversibility of roNav2 from H ₂ O ₂ mediated redox modifications....	60
3.5.6. The response of roNav1 and fluorescent redox reporters to HDPs.....	60
3.5.6.1. The response of roNav1 and roGFP2 to carbon monoxide.....	61
3.5.6.2. The response of roGFP2 and Grx1-roGFP2 to BOXes.....	63
3.5.7. The response of roNav1 to photo-activated KillerRed-induced ROS.....	65
3.5.8. The response of roNav1 and roNav2 to visible-light induced reactive species.....	67
3.5.8.1. Detection of visible-light induced reactive species with roNav1.....	68
3.5.8.2. Detection of blue-light induced reactive species with roNav2.....	69
3.5.8.3. Reversibility of roNav2 from light-induced chemical modification..	70
3.5.8.4. The response of roGFP2 variants to blue-light irradiation.....	71

3.6. Gated RS sensitivity of roNav1 and roNav2.....	72
3.6.1. Gated RS sensitivity of roNav1.....	73
3.6.2. Gated RS sensitivity of roNav2.....	80
4. Discussion.....	82 – 97
4.1. Challenges in monitoring cellular reactive species.....	82
4.2. Detection of cellular reactive species with fluorescent reporters: advantages and limitations.....	83
4.3. Development of non-photonic alternatives to fluorescent redox reporters.....	84
4.4. Comparison of channel-based RS sensors with fluorescent redox reporters.....	86
4.5. Advantages of channel-based RS sensors.....	88
4.6. Cysteine and selenocysteine as oxidation sensing elements in channel-based sensors	91
4.7. Limitations of channel-based RS sensors.....	95
5. Conclusions.....	97
6. References.....	98 – 109
7. Appendix.....	XI – XVI
A. Declaration.....	XI – XII
B. Acknowledgments.....	XIII
C. CV and publication list.....	XIV – XVI

List of abbreviations

A°	- Angstrom
Ala	- Alanine
Asn	- Asparagine
Asp	- Aspartic acid
BAM15	- N5,N6-bis(2-fluorophenyl)-[1, 2, 5]oxadiazolo[3,4-b]pyrazine-5,6-diamine
BOXes	- Bilirubin oxidation end products
CFC	- Mutant voltage-gated sodium channel with inactivation motif: Cysteine-Phenylalanine-Cysteine
ChT	- Chloramine T
CO	- Carbon monoxide
Cys	- Cysteine
DHE	- Dihydroethidium
DMEM	- Dulbecco's modified eagle's medium
DMSO	- Dimethylsulfoxide
DTT	- 1,4-Dithiothreitol
<i>E. coli</i>	- <i>Escherichia coli</i>
eGFP	- Enhanced green fluorescent protein
EGTA	- Ethylene glycol-bis(2-aminoethylether)-N, N, N', N'-tetraacetic acid
FCS	- Fetal calf serum
GFP	- Green fluorescent protein
Glu	- Glutamic acid
Gly	- Glycine
Grx1-roGFP2	- Glutaredoxin fused with redox-sensitive green fluorescent protein 2
GSH	- Glutathione (reduced)
GSHPX	- Glutathione peroxidase
GSSG	- Glutathione (oxidized)
H ₂ DCF	- Dihydrodichlorofluorescein
HBI	- 4-(p-hydroxybenzylidene) imidazolidin-5-one
HDPs	- Heme degradation products
HEK 293	- Human embryonic kidney cell 293

HEK 293T	- Human embryonic kidney cell 293 expressing SV40 large T antigen
HEPES	- 4-(2-hydroxyethyl)-1-piperazineethanesulfonic acid
HepG2	- Human hepatoma-derived cell lines
His	- Histidine
ICL	- Mutant voltage-gated sodium channel with inactivation motif: Isoleucine-cysteine-Leucine
ICM	- Mutant voltage-gated sodium channel with inactivation motif: Isoleucine-Cysteine-Methionine
IFC	- Mutant voltage-gated sodium channel with inactivation motif: Isoleucine-Phenylalanine-Cysteine
IFL	- Mutant voltage-gated sodium channel with inactivation motif: Isoleucine-Phenylalanine-Leucine
IFM	- Wild-type, voltage-gated sodium channel with inactivation motif: Isoleucine-Phenylalanine-Methionine
IFU	- Mutant voltage-gated sodium channel with inactivation motif: Isoleucine-Phenylalanine-Selenocysteine
kDa	- kilodalton
kHz	- kilohertz
KR	- KillerRed
Leu	- Leucine
LY	- Lucifer Yellow
Lys	- Lysine
Met	- Methionine
MFM	- Mutant voltage-gated sodium channel with inactivation motif: Methionine-Phenylalanine-Methionine
mM	- Millimolar
MMM	- Mutant voltage-gated sodium channel with inactivation motif: Methionine-Methionine-Methionine
μ M	- Micromolar
μ s	- Microsecond
ms	- Millisecond
Msr	- Methionine sulfoxide reductase
mV	- Millivolt
M Ω	- Megaohm

mtROS	- Mitochondrial reactive oxygen species
NA	- Numerical aperture
nm	- Nanometer
PUFA	- Polyunsaturated fatty acid
rFP	- Redox-sensitive fluorescent protein
R _I	- Relative non-inactivating current fraction
rNav	- Rat voltage-gated sodium channel
roGFP2	- Redox-sensitive green fluorescent protein 2
roNav	- Redox-sensitive voltage-gated sodium channel
RS	- Reactive species
Sec	- Selenocysteine
SECIS	- Selenocysteine insertion sequence
Ser	- Serine
SF	- Selectivity filter
TCEP	- Tris(2-carboxyethyl)phosphine
TM	- Transmembrane
Trx	- Thioredoxin reductase
VSD	- Voltage-sensing domain
Z-BOX A	- Z-2-(4-methyl-5-oxo-3-vinyl-1,5-dihydro-2H-pyrrol-2-ylidene)acetamide
Z-BOX B	- Z-2-(3-methyl-5-oxo-4-vinyl-1,5-dihydro-2H-pyrrol-2-ylidene)acetamide

Summary

Reactive species (RS) play important roles in vital physiological processes. However, excessive RS damages cells and may contribute to the onset of several diseases. Therefore, there is a clear demand for sensitive probes that precisely monitor cellular RS with a high spatio-temporal resolution to understand the multifaceted role of RS in redox biology. Genetically encoded redox probes derived from green fluorescent protein (GFP), such as roGFP2 and Grx1-roGFP2, are promising tools for quantitative and dynamic observation of RS with spatio-temporal resolution. However, the excitation light used to read-out the fluorescence of these proteins can lead to irreversible modification of cell constituents, which may result in either immediate or long-lasting alterations of molecular functions.

Herein, we introduce two genetically engineered non-photonic RS sensors: roNav1 and roNav2, both based on the rat skeletal muscle voltage-gated Na⁺ channel (rNav1.4). rNav1.4 was equipped with a cysteine (roNav1; rNav mutant IFM1305C) or a selenocysteine (roNav2; rNav mutant IFM1305U) residue in the inactivation motif to yield membrane-based RS sensors. roNav2 is the first functional selenocysteine-containing ion channel that adequately expresses in the heterologous expression system. By means of the hinged-lid mechanism, roNav1 and roNav2 respond to local changes in redox milieu by their diminished fast inactivation, and hence, yield a ratiometric signal (ratio of non-inactivated current component and peak current) that can be measured with high precision in a non-photonic fashion.

Whereas roNav1 can detect oxidative modification that occurs near the plasma membrane with a sensitivity similar to existing fluorescence-based RS sensors, e.g., roGFP2, roNav2 responds about 100-fold faster to extracellularly applied chloramine T and hydrogen peroxide induced oxidative modifications compared to roNav1. Moreover, roNav2 can sense mitochondrial RS arising due to an elevated glucose metabolism with a comparable sensitivity to the GSH-dependent cytosolic redox sensor Grx1-roGFP2. The usefulness of roNav1 and roGFP2 for detecting such endogenous RS signals is limited by the slow reaction kinetics of cysteine. Nevertheless, roNav1 may suit well to monitor RS that exist for a longer time.

Because the current measured in patch-clamp experiments arises only from ion channels located in the plasma membrane, channel-based RS sensors safely report membrane-delimited processes, whereas the spatial resolution of fluorescent proteins, even when targeted to the cell membrane, is diffraction limited and confounded by background fluorescence arising from proteins close but not inside the plasma membrane.

Advantageously, channel-based RS sensors do not need excitation light for RS sensing, and hence, can be used to detect phototoxic cellular modifications on a real-time scale. Employing roGFP2 and its variants, e.g., Grx1-roGFP2, eGFP:S147C, eGFP:S147U, and eGFP:S147U:Q204C, we showed that excitation light (470 nm) can trigger RS formation and/or chemical modifications in the living cell. roNav1 and roNav2, both sensors indicate such light induced-modification of cells, roNav2 responds about 1,000-fold faster to these changes in comparison to roNav1 under epifluorescence experimental settings. Noticeably, the response of roNav2 to blue light is fully reversed in the dark.

While fluorescent redox sensors are always active, channel-based RS sensors can be turned on or off by means of the endogenous channel inactivation mechanism. This is an important property of the channel-based sensors, which may allow investigation of dynamics of RS distribution and lifetime. Measurements using roNav1 on RS liberated from intracellular Lucifer Yellow and genetically encoded KillerRed have revealed an assessment of RS lifetime in individual mammalian cells. For example, kinetics of roNav1 modification by RS liberated from intracellular Lucifer Yellow showed that Lucifer Yellow-induced RS concentration decayed with two major time constants of about 10 and 1000 ms. These two time constants indicated at least two major species of reactive components with the respective mean lifetimes are released when Lucifer Yellow is excited with blue light. Moreover, channel-based RS sensors indicate dynamic changes in the redox milieu based on the oxidative modification of a single cysteine (roNav1) or a single selenocysteine (roNav2) and they are switchable (gateable) by means of membrane voltage; thus, they are suited for single-molecule measurements and they can easily be employed for complex kinetic analysis.

Complementing other methods of RS detection in living cells, channel-based sensors add non-photonic variants with strict membrane-delimited RS sensors for redox processes. These channel-based sensors allow for the assessment of chemical modification induced in fluorescence microscopy settings with high sensitivity and time resolution.

[German translation]

Zusammenfassung

Reaktive Spezies (RS) sind für lebensnotwendige physiologische Prozessen wichtig. Zuviel RS hingegen führen zu oxidativen Schäden und Zelltod und tragen möglicherweise zur Entstehung verschiedener Krankheiten bei. Hieraus resultiert ein klares Bedürfnis an sensitiven Sonden, mit denen sich RS mit hoher raum-zeitlicher Auflösung detektieren lassen, um die vielseitigen Funktionen von RS in der Redox-Biologie zu verstehen. Genetisch kodierte, vom GFP (grün-fluoreszierendes Protein) abgeleitete Sonden, wie z.B. roGFP2 und Grx-roGFP2, sind hierbei vielversprechende Kandidaten, RS-Konzentrationsänderung mit entsprechender Auflösung verfolgen zu können. Ihr Nachteil liegt darin, dass das für ihre Fluoreszenz notwendige Anregungslicht zu irreversiblen Veränderungen von Zellbestandteilen führen kann, was zu unmittelbaren oder länger-dauernden Veränderungen ihrer molekularen Funktionen führen kann.

In dieser Arbeit werden zwei genetisch-veränderte, nicht-photonische, RS-Sensoren vorgestellt: roNav1 und roNav2, beide basierend auf rNav1.4, dem spannungsabhängigen Natriumkanal aus der Skelettmuskulatur der Ratte. rNav1.4 wurde im Inaktivierungsmotiv mit einem Cystein (roNav1; Mutation IFM1305C) oder einem Selenocystein (roNav2; Mutation IFM1305U) ausgestattet, um membranständige RS-Sensoren zu erhalten. roNav2 ist der erste funktionelle, Selenocystein-enthaltende Ionenkanal, der adäquat in heterologen Systemen exprimiert wird. Bedingt durch den *hinged-lid*-Mechanismus reagieren roNav1 und roNav2 auf lokale Änderungen des Redox-Milieus in Form einer verringerten schnellen Inaktivierung und liefern somit ein ratiometrisches Signal (Verhältnis von nicht-inaktiviertem Strom und Spitzenstrom), das mit hoher Präzision auf nicht-photonischen Weise gemessen werden kann.

Während roNav1 oxidative Modifikationen nahe der Plasmamembran mit etwa der gleichen Sensitivität wie fluoreszenzbasierte RS-Sensoren (z.B. roGFP) detektieren kann, reagiert roNav2 etwa 100-mal schneller auf extrazellulär appliziertes Chloramin-T und Wasserstoffperoxid. Darüberhinaus kann roNav2 einen durch erhöhten Glucose-Metabolismus induzierten Anstieg der mitochondrialen RS detektieren und dies mit einer vergleichbaren Sensitivität wie der GSH-abhängige zytosolische Redox-Sensor Grx1-roGFP2. Die Verwendbarkeit von roNav1 und roGFP2 zur Detektion solcher endogener RS-Signale ist durch die langsame Reaktionskinetik von Cysteinen limitiert. Nichtsdestotrotz sollte roNav1 zur Messung langlebiger RS gut geeignet sein.

Da die in Patch-Clamp-Experimenten gemessenen Ströme ausschließlich auf in der Plasmamembran lokalisierte Ionenkanäle zurückzuführen sind, lassen sich mit diesen Kanälen Prozesse verfolgen, die auf den Membran-Bereich begrenzt sind. Demgegenüber ist die räumliche Auflösung von Fluoreszenzproteinen, selbst wenn sie in der Membran verankert sind, beugungsbegrenzt und wird durch Hintergrundfluoreszenz von Proteinen, die sich nahe bei aber eben nicht innerhalb der Membran befinden, verfälscht.

Zweckmäßigerweise benötigen Kanäle kein Anregungslicht zur RS-Messung und können somit zur Detektion phototoxischer Zellmodifikationen in Echtzeit verwendet werden. Unter Verwendung von roGFP2 und roGFP2-Varianten, wie Grx1-roGFP2, eGFP:S147C, eGFP:S147U, und eGFP:S147U:Q204C, konnten wir zeigen, dass Anregungslicht (470 nm) die Bildung von RS und/oder chemische Modifikationen in lebenden Zellen auslösen kann. Beide kanalbasierte Sensoren deuten auf derartige Licht-induzierte Modifikationen in Zellen hin, wobei roNav2 etwa 1000-fach schneller in derartigen Epifluoreszenz-Bedingungen reagiert als roNav1. Bemerkenswerterweise ist die Antwort von roNav2 auf Blaulicht im Dunkeln vollständig reversibel.

Fluoreszenz-basierte Redoxsensoren sind ständig aktiv. Kanalbasierte Sensoren hingegen lassen sich über den endogenen Inaktivierungsmechanismus an- und ausschalten, was ihren Einsatz zur dynamischen Messung von RS-Verteilung und -Lebensdauer ermöglichen könnte. Messungen mittels roNav1 an von intrazellulärem *Lucifer Yellow* und dem genetisch kodierten *KillerRed* haben erste Abschätzungen von RS-Lebensdauern in einzelnen Säugerzellen ermöglicht. Zum Beispiel wurde beobachtet, dass die Konzentration von durch Lichtblitze erzeugten RS mit zwei Zeitkonstanten von ca. 10 und 1000 ms abnahmen. Dies zeigt an, dass zwei Hauptspezies von RS mit den genannten Lebensdauern durch Blaulicht-Anregung von *Lucifer Yellow* freigesetzt werden. Außerdem zeigen Kanalsensoren dynamische Veränderungen des Redox-Milieus auf Grundlage der oxidativen Modifikation einzelner Cysteine (roNav1) und einzelner Selenocysteine (roNav2) an und sie sind schaltbar (steuerbar) mithilfe der Membranspannung. Somit sind sie für Einzel-Molekül-Messungen geeignet und können leicht für komplizierte kinetische Analysen verwendet werden.

In Ergänzung anderer Methoden zur Detektion von RS in lebenden Zellen, sind kanalbasierte Sensoren nicht-photonische Varianten zur Messung von strikt membranbegrenzten Redox-Prozessen. Diese kanalbasierten Sensoren ermöglichen die Abschätzung von chemischen Modifikationen, wie sie bei der Fluoreszenz-Mikroskopie hervorgerufen werden können, mit hoher Empfindlichkeit und Zeitauflösung.

1. Introduction

1.1. Reactive species

Reactive species (RS) is a collective term for ‘radicals’ and ‘non-radicals’. Radicals are molecules and ions that contain one or more unpaired electron(s) in their atomic or molecular orbital and exist independently, such as hydroxide ($^{\circ}\text{OH}$) and superoxide ($\text{O}_2^{\circ-}$). Non-radicals are typically covalent compounds, such as hydrogen peroxide (H_2O_2) and hypochlorous acid (HOCl). The production of cellular RS in the living cell is triggered by biological signals, enzymatic activities, catalysts, and other RS existing *in vivo*. RS are categorized into different groups based on their active atom, such as reactive oxygen species (ROS, e.g., $^{\circ}\text{OH}$ and H_2O_2), reactive nitrogen species (RNS, e.g., HNO_2 and NO°), and reactive chlorine species (RCS, e.g., Cl° and Cl_2). However, the term ‘ROS’ is more often perceived as ‘RS’ in redox biology due to their greater presence in the living system compared to other groups of reactive species (Halliwell, 2006). The molecular oxygen prefers to accept one electron at a time (Halliwell & Gutteridge, 1984), hence, sequential addition of electrons to oxygen produces varieties of reactive oxygen species in a stepwise fashion (Bayir, 2005; Lambeth, 2004), such as superoxide ($\text{O}_2^{\circ-}$), hydroxyl radical (OH°), hydrogen peroxide (H_2O_2), hypochlorous acid (HOCl), singlet oxygen ($^1\text{O}_2$), and ozone (O_3).

1.1.1. Sources of cellular reactive species

The cell metabolism produces sufficient amount of energy to maintain the structural and functional integrity of the cell. Varieties of cellular RS are continuously produced as by-products of the cellular metabolism. Additionally, RS are also generated either intentionally by the living cell, for example, activated phagocytes generate RS to fight pathogens, or accidentally, for instance, cells exposed to ionizing radiations produce RS (Nathan & Ding, 2010). The nature of RS mainly depends on the source from which they are generated. Typically, sources of cellular RS have been categorized into three major classes:

- (a) *Endogenous sources*: mitochondria, endoplasmic reticulum, lysosomes, and peroxisomes are the major sites of endogenous RS production (Brand, 2010; Dixon & Stockwell, 2014; Lambeth, 2004).
- (b) *Exogenous sources*: exogenous sources of RS include radiation (UV-light, x-rays, and gamma rays), ultrasound, toxins, industrial waste products, cigarette smoking, ozone, and chemicals that produce/promote RS formation like quinones, bipyrimidinium herbicides, and phenols (Leach et al., 2001; Nathan & Ding, 2010; Sharma et al., 2012).

(c) *Pathological sources:* viral, fungal, & bacterial infections, immune cell-activation, and inflammation (Butz et al., 1994; Ghosh et al., 1994; Noori, 2012).

1.1.2. Cellular RS are neither hero nor villain

The paradox of cellular RS is well recognized in the redox research because RS play dual roles, both beneficial and harmful, in cell physiology depending on their concentration and spatio-temporal distribution within the cell. Generation and concentration of RS within the cell are tightly controlled by the redundant protective mechanism of the antioxidant defense system. The antioxidant defense system comprises RS scavenging enzymes, for instance, superoxide dismutase (SOD), catalase, and glutathione peroxidase (GSHPX), and radical scavengers, such as glutathione (GSH), thioredoxin (TXN), α -tocopherol (vitamin-E), and ascorbic acid (vitamin-C) (Halliwell, 2001). These antioxidant enzymes and radical scavengers control the concentration of cellular RS that is essential for healthy cell functions. Controlled oxidative conditions are stimulating factors for several physiological functions, such as signal transduction, activation of nuclear transcription factors, gene expression, cellular defense, cell proliferation, and migration (Ambrozova et al., 2010; Bayir, 2005; Kennett & Kuchel, 2003; Lambeth, 2004; Wu, 2006). Failure of the antioxidant defense system leads to oxidative stress, which is associated with deleterious consequences, such as diabetes, cancer, heart failure, sepsis, frequent aging and neurodegenerative diseases (Dexter et al., 1994; Hensley et al., 1996; Hentze et al., 2010; Matough et al., 2012; Salvemini & Cuzzocrea, 2002) (Fig. 1). Hence, cellular RS are neither good nor bad but they always entertain researchers by their perplexed behavior in the cellular milieu.

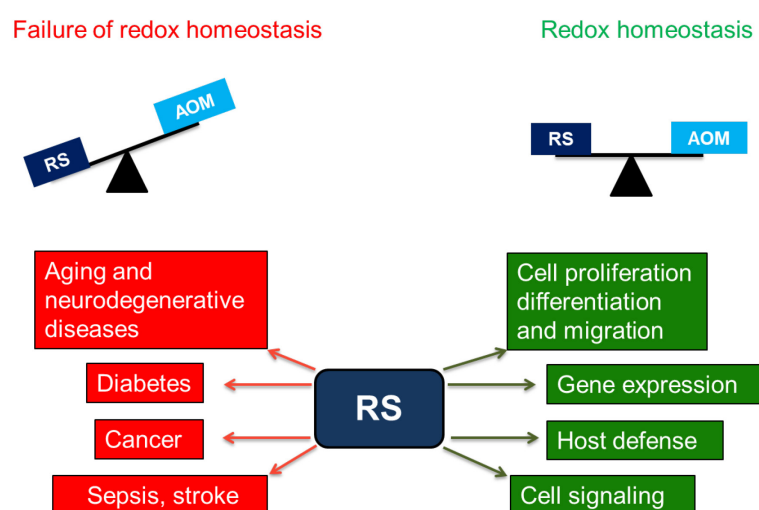


Figure 1: The paradox of reactive species. The antioxidant mechanism (AOM) maintains the cellular RS level; hence, finely adjusted concentrations of cellular RS are crucial for the indicated physiological functions. Failure of the antioxidant defense system may lead to the indicated pathophysiological consequences.

1.1.3. Biochemistry of cellular reactive species

Reactive species (RS) oxidatively modify biomolecule in either reversible or irreversible manner. Oxidative modification of biomolecules leads to downstream multiform biological consequences ranging from signaling functions to detrimental effects. The consequences of oxidative modifications depend on the chemical nature of RS and the nature of microenvironments in which RS are generated. The chemical reactivity of an individual RS is imposed by whether it prefers one or two electron oxidations (Dickinson & Chang, 2011). Additionally, the reactivity of RS depends on the half-life of individual RS in the cellular milieu and molecular targets existing in the vicinity where RS are generated. For example, the half-life of hydroxyl radicals (OH°) in the cellular milieu is only about 10^{-9} s; therefore, OH° can react with biomolecules existing in its vicinity only. However, the half-life of hydrogen peroxide (H_2O_2) is about 1 ms that means it can react with neighboring targets or may diffuse in the cellular milieu to modify distant targets (D'Autréaux & Toledano, 2007; Sharma et al., 2012). Hence, RS specificity to the molecular target depends on the relative reactivity of RS or lifespan of RS in the cell.

Distribution of intracellular RS may not be homogeneous because sources of intracellular cellular RS are localized in specific regions, which means the concentration of RS near a source of production can reach a high local concentration. Under such conditions, the reactivity of elevated RS must be modulated to avoid harmful consequences. For that reason, cells themselves can control the increased local concentration of RS mediated oxidative damage of nearby targets by altering the local redox buffering capacity (Dickinson & Chang, 2011). Besides that, the cell itself can control the localized production of a specific RS as it was previously shown for intracellular local production of H_2O_2 and its adjacent signaling target via a 'floodgate' model (Briehl, 2015; Wood et al., 2003; Woo et al., 2003). However, the physiological importance of the crosstalk between reactive species formed at different subcellular sites, such as cell membrane, mitochondria, and endoplasmic reticulum, is an open field of research.

1.2. Cell membrane and reactive species

The cell membrane is a fundamental structural unit of a cell that separates intracellular structures from the external environment. The structural and functional integrity of the cell membrane is important to maintain the healthy biological system on cellular, tissue, and organismal levels. The cell membrane can be either directly or indirectly affected by cellular RS. In the case of direct effect, RS interact with the membrane constituents and oxidatively modify them whereas in the indirect case, oxidation of membrane constituents is triggered by

oxidative stress (Fig. 2). Controlled oxidative modifications of the cell membrane are important for certain physiological functions, for example cell signaling, immune, and inflammatory processes, while excessive membrane modifications can lead to pathological consequences, for instance, arteriosclerosis, Alzheimer's disease, and Parkinson's disease (Ambrozova et al., 2010; Fisher, 2009; Hensley et al., 1996; Hentze et al., 2010; Volinsky & Kinnunen, 2013). In particular, nerve and muscle cells have an excitable cell membrane that generates and propagates physiological signals by electrical means. Electrical properties of excitable cells arise due to physical constituents of the cell membrane, e.g., lipid bilayer, pumps, transporters, and ion channels (Hille, 2001). Excessive oxidation of membrane lipids and proteins can change the cell excitability (Elliott et al., 1991; Killig & Stark, 2002; Tarr et al., 1995), which may result in several neural and/or neuromuscular disorders.

The cell membrane is one of the favorite subcellular targets of RS due to the abundance of polyunsaturated fatty acids (PUFAs). RS attack double bonds present in PUFAs and produce several fragmented reactive molecules, such as lipid radicals (R°) and lipid peroxide radicals (ROO°). These reactive lipid radicals can oxidatively modify neighboring PUFAs, membrane proteins, cytoplasmic proteins, and enzymes (Kohen & Nyska, 2002; Møller & Wallin, 1998). The lipid oxidation is finally terminated by either the action of antioxidants or by the formation of non-radical end-products (Stark, 2005) (Fig. 2). A single reaction can initiate chain reactions, which may result in the complete oxidation of all PUFAs and/or membrane components if it is not terminated by other means.

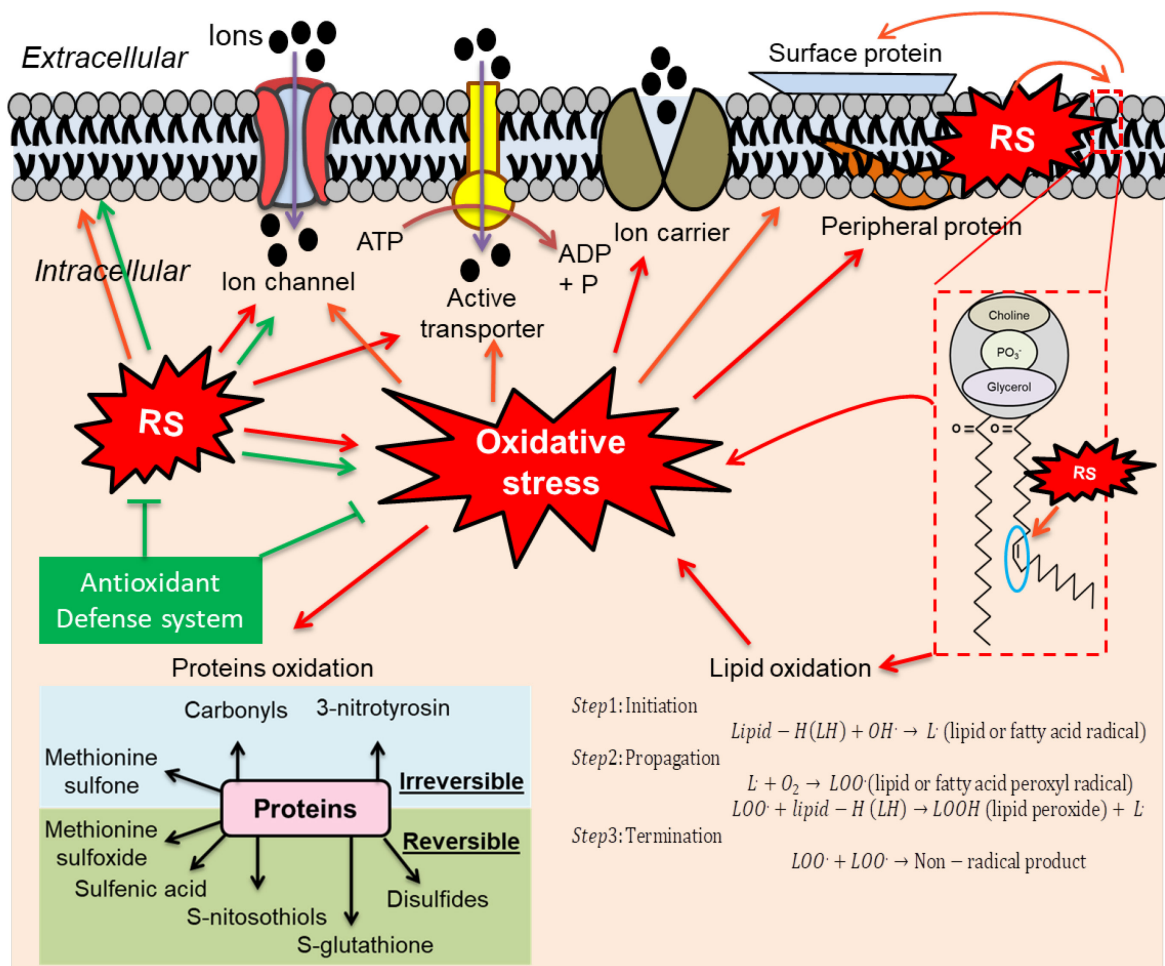


Figure 2: Reactive species attack of the cell membrane. Reactive species can directly interact with membrane proteins and oxidatively modify amino-acid residues, such as cysteine, methionine, and tyrosine present in proteins either in a reversible or irreversible manner. Reversible oxidative modifications of amino-acid residue(s) are important for physiological functions; however, irreversible oxidative modification may have deleterious consequences. Excess accumulation of reactive species within the cell leads to oxidative stress, which may have indirect effects on the membrane constituents, such as ion channels, active ion transporters, ion carriers, peripheral, and surface proteins. The antioxidant defense system counterbalances the cellular RS level to maintain redox homeostasis in the cell. RS can also directly interact with membrane lipids and oxidatively modify them. Polyunsaturated fatty acid (PUFA) chains of membrane lipids are susceptible to RS attack due to the presence of double bonds. Oxidation of membrane lipids produces a variety of radicals and non-radicals that may affect functional properties of membrane proteins and/or contribute to oxidative stress. Red arrows indicate deleterious consequences, while green arrows indicate the physiological relevance.

Further, RS may directly interact with membrane proteins and disturb either the tertiary structure of proteins and/or chemically modify building blocks of proteins, i.e. amino-acid residues, as a direct effect. Accumulating evidence suggests that reversible and irreversible oxidative modifications of cellular proteins are indispensable for cell survival and regeneration (Fedorova et al., 2009; Groeger et al., 2009; Love et al., 2013; Stadtman &

Levine, 2003). Although positive stress conditions are important for cell survival, excessive modification of membrane proteins can contribute to clinical conditions, such as neurodegenerative diseases, atherosclerosis, and heart failure (Hajieva et al., 2015; Pacher et al., 2007; Stark, 2005). Identification of protein nitrotyrosine modification in atherosclerosis and brain ischemia gained the attention of researchers and encouraged them to investigate further and unravel the protein oxidation at the amino acid level (Beckmann et al., 1994). It has now been firmly recognized that oxidation end-products of amino-acid residues are potential markers for oxidative stress.

Oxidative modification of amino-acid residues

Amino-acid residues in proteins are the major targets of RS. Cellular RS can covalently adduct to specific amino acids and alter the overall properties of the amino acids, thus modify protein functions. The oxidative modification of methionine, cysteine, lysine, arginine, proline, and histidine in presence of certain metal ions, for instance, Fe^{2+} and Cu^{2+} , have been frequently shown in relevance to physiology or pathology (Cai & Yan, 2013; Stadtman, 2006; Wall et al., 2012). Different amino acids differ markedly in how easily their side chains are oxidatively modified. The role of oxidative modification of methionine, cysteine, lysine, arginine, proline, and histidine in presence of certain metal ions, for instance Fe^{2+} and Cu^{2+} , have been frequently shown in the modulation and/or alteration of protein functions (Cai & Yan, 2013; Stadtman, 2006; Wall et al., 2012). Among the mentioned amino acids, methionine and cysteine are well characterized in redox signaling. Cysteine has been described for its ease of oxidation in the cellular milieu compared to the methionine.

The thiol group (-SH) of cysteine in proteins serves as redox switch. Upon oxidative modification, thiol switches determine different conformational and functional states of a protein. Therefore, spatio-temporal operation and specificity of thiol switches in signal transduction may be of great interest for further research. The thiol group of cysteine is readily oxidized to different degrees due to multiple oxidation states of the sulfur. For instance, a cysteine is oxidized in the presence of an oxidative stressor and produces sulfenic acid (R-SOH), hyper peroxidized sulfenic acid (R-SO₂H), and sulfonic acid (R-SO₃H) (Cai & Yan, 2013; Poole et al., 2004). Cysteine modification to sulfenic acid can be reversed by the actions of glutathione and thioredoxin enzyme system, and thus, it may function in signaling. However, cysteine modification to the sulfonic acid is irreversible, which may lead to the oxidative damage of proteins.

Cysteines present in a protein vary in terms of their redox reactivity because the reactivity of a thiol group in cysteine depends on diverse contributing factors, such as its

accessibility for oxidation, substrate binding, microenvironment, and the dissociation constant (pKa) (Lim et al., 2012; Rhee et al., 2000; Roos et al., 2013). Under physiological conditions at neutral pH, the oxidative modification of cysteine residues is impossible because of the high pKa value (about 8.5) of cysteines (Roos et al., 2013). The thiol group of cysteine is modified to form thiolate (thiolate anion) when the pKa value of cysteine becomes lower than that of the physiological value. Thiolated cysteine residues are redox active. The chemical conversion of thiol to thiolate may be achieved via different contributing factors as mentioned above.

Identification of catalytically active sites in glutathione peroxidases (GPX) and thioredoxin reductases (Trx) revealed the importance of selenocysteine over cysteines in redox regulation. The selenocysteine (Sec/U/Se-Cys) is 21st, naturally occurring, selenium-containing, proteinogenic amino-acid residue and is encoded by TGA in DNA. It differs from its structural analogue cysteine as selenocysteine contains selenium instead of sulfur in cysteine. At physiological pH, selenol group (-SeH) possess relatively low pKa value (about 5.2) compared to thiol (-SH) of cysteine (about 8.3), which makes selenocysteine a better nucleophile (Huber & Criddle, 1967). Thus, selenocysteine exhibits high redox reactivity with an increased reaction rate compared with cysteine (Arnér, 2010). Moreover, the selenocysteine exhibits greater tendency to be reversed from oxidative modification compared with cysteine due to the relative greater electrophilicity of selenium in selenocysteine compared with sulfur in cysteine (Ruggles et al., 2011). These properties of selenocysteine make it an important redox-sensing element in redox regulating enzymes, e.g., thioredoxin reductases.

1.3. Redox modulation of ion channels

Ion channels are multimeric membrane proteins, which form an ion-selective pore that opens and closes in response to voltage change, ligand binding, mechanical or cellular stimuli. They produce electrical signals that are crucial for diverse physiological functions, for example, generation of electrical activity in nerves and muscles, cardiac excitability, hormone secretion, intracellular signaling, cell growth, cell proliferation, and cell volume regulation (Alberts et al., 2002; Lang et al., 2005; Nadal et al., 2004). Accumulating evidence suggests that the mild or reversible oxidation of ion channels is an important regulatory mechanism for regulating membrane potential, vasomotor functions, gene expression, and protective mechanism against hypoxia (Bogeski & Barbara, 2014; Bogeski et al., 2011; Kozai et al., 2014; Olschewski & Weir, 2015; Sahoo et al., 2014). However, excessive or irreversible oxidative modification of ion channels can produce pathological conditions, e.g., seizure

susceptibility, altered cardiac excitability, disorders of muscle cells, and neurodegenerative diseases (Ertel et al., 1997; Hool & Corry, 2007; Huguenard, 1996; Kolbe et al., 2010).

Cellular RS can modulate ion channel activities either indirectly, for example, oxidized glutathione (GSSG) reduces BK channel activity in neonatal rat hippocampus (Soh et al., 2001) or directly, such as RS can directly modify a single methionine located in the P-segment of the shaker potassium channel, which leads to accelerated P/C-type inactivation of the channel (Chen et al., 2000). Several mutagenesis studies helped to spot the molecular targets of RS in ion channels. Such studies not only revealed the oxidation targets but also provided information on insensitive targets and the importance of specific amino-acid residues that are important for the functional expression of channels. Ion channel proteins contain a number of potentially RS-sensitive amino-acid residues, e.g., methionine, cysteine, tyrosine, histidine, and tryptophan; however, methionine and/or cysteine have always been reported as the prime targets of cellular RS because of their relatively higher oxidation sensitivity compared to other amino acids (Stadtman 1993; Stadtman & Levine, 2003). Ciorba et al. (1997) showed that the oxidation of a single methionine located at the position 3 in the N-terminal ball region of a splice variant of shaker K⁺ channel, Sh C/B, drastically slowed the N-type inactivation of the channel, an effect that can be reversed when channels are co-expressed with MsrA (methionine sulfoxide reductase A). Hence, such reversible oxidative modification of the channel may have a role in physiological functions, such as controlling membrane excitability during the oxidative stress or aging. Like methionine oxidation, oxidation of certain cysteine residues present in various channels may also affect the functional properties of ion channels, such as oxidation of a cysteine residue in the N-terminus of the Kv1.4 channel protein modulates N-type inactivation of the channel (Ruppersberg et al., 1991).

Further, more than one type of amino-acid residues can be oxidatively modified depending on the accessibility of amino-acid residues for RS attack and the vigorousness of oxidative stress. For example, Su et al. (2007) and Kolbe et al. (2010) showed that the oxidation of a cysteine residue (C723), located in a linker between pore domain and the cytoplasmic cyclic nucleotide-binding domain of hERG1 channel results to accelerated deactivation kinetics. Additionally, three methionine residues (M554, M651, and M713) in the C-terminus of hERG1 channel are also likely to contribute in accelerated deactivation kinetics of the channel when RS stimuli exist for a longer duration. Whereas cysteine most likely forms disulfides, methionine forms methionine sulfoxide by the addition of oxygen during oxidation under physiological condition (Creighton, 1993; Hoshi & Heinemann, 2001). Mild oxidation of methionine and cysteine can be reversed by the action of methionine

sulfoxide reductase (Msrs) and cellular glutathione (GSH), respectively; in such a way the reversible oxidation of amino-acid residues may have a role in physiological functions (Drazic & Winter, 2014; García-Santamarina et al., 2014). Excessive or irreversible oxidation of either cysteine or methionine may cause the functional loss of channels. A comprehensive list of specific methionine and/or cysteine that are susceptible to RS attack in several ion channels, e.g., voltage-gated potassium channels (K_v), voltage-gated calcium channels (Cav), transient receptor potential (TRP) channels, and store-operated Ca^{2+} entry (SOCE)/Orai channels, is found elsewhere (Bogeski et al., 2011; Bogeski & Niemeyer, 2014; Sahoo et al., 2013). Identification of the RS targets in ion channel proteins may allow developing therapeutic strategies for several human diseases that are associated with altered ion channel functions that arise due to oxidative stress, for example, cardiac arrhythmia.

1.4. Voltage-gated Na^+ channels

Voltage-gated Na^+ channels are members of the ion channel superfamily that includes voltage-gated K^+ channels, voltage-gated Ca^{2+} , TRP related channels and cyclic-nucleotide-gated channels (Hille, 2001). A variety of different Na^+ channel isoforms have been identified by means of molecular cloning, biochemical purification, and electrophysiological recording (Goldin, 1999). The eukaryotic Na^+ channels comprise of two subunits: α and β . Whereas the α subunit is a large protein (about 260 kDa) that forms channel pore and allows voltage-dependent Na^+ conductance, the auxiliary β subunit (about 33-39 kDa) facilitates membrane localization of channel protein and functions in modulating channel properties (Catterall, 1984; Catterall, 2000; O'Malley & Isom, 2015).

There are nine genes that encode the α subunit of voltage-gated Na^+ channels in mammals (Goldin et al., 2000; Goldin, 2002). Additionally, a tenth poorly homologous gene to voltage-gated Na^+ channels is also included in the Na^+ channel family; however, it has not been shown to encode a functional channel (Goldin et al., 2000; Goldin, 2002; Noda & Hiyama, 2015). The nomenclature of voltage-gated Na^+ channels is based on the commonly used nomenclature of voltage-gated K^+ channels. The name consists of the chemical symbol of principal permeating ion (Na), a principal physiological regulator (V, voltage) as a subscript (Nav), a number that indicates the gene subfamily (e.g., $Nav1$), and a number following the decimal point that indicates the channel isoform (e.g., $Nav1.1$) (Chandy, 1991; Goldin et al., 2000). The transmembrane and extracellular domains of various isoforms of the voltage-gated Na^+ channel (Nav channel) exhibit greater than 50% identical amino acid sequences (Frank & Catterall, 2003). A phylogenetic tree for nine Nav isoforms ($Nav1.1$ - $Nav1.9$) together with a tenth sodium channel-like protein (Nax) and the primary expression area of each channel are shown in Fig.3.

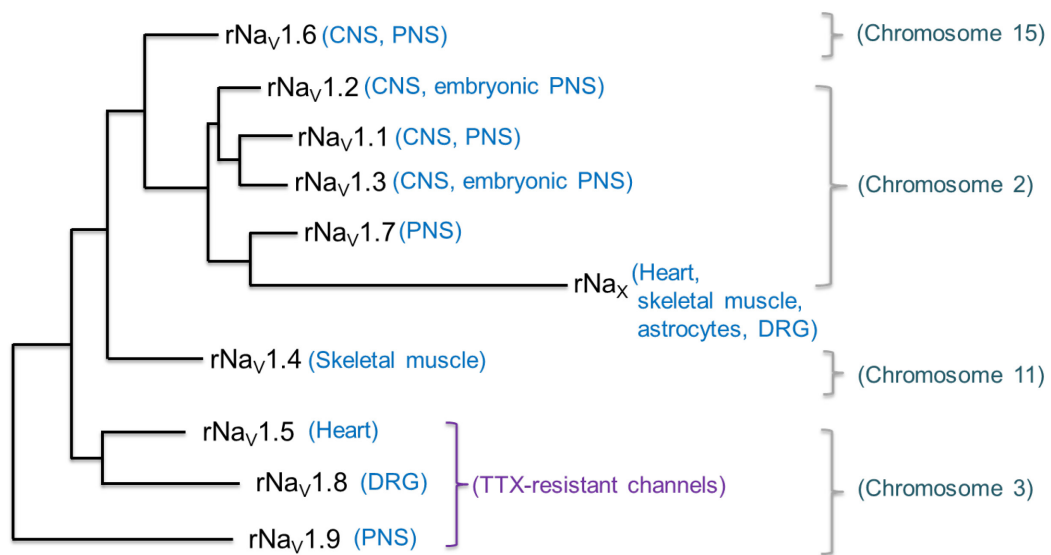


Figure 3: A phylogenetic tree for Nav channels. Phylogenetic relationships of rat sodium channel sequences Nav_V1.1–Nav_V1.9 and Nav_X obtained by maximum parsimony analysis. Nav_X is evolutionarily more distant. The human chromosomes on which the human ortholog of corresponding rat gene is found are shown on the right. The primary expression of each channel isoform in specific cell/tissue system is indicated (blue letters). The tetrodotoxin (TTX) is a neurotoxin that can block all channels except Nav_V1.5, Nav_V1.8, and Nav_V1.9. CNS: Central nervous system; PNS: Peripheral nervous system; DRG: Dorsal root ganglia. (Adapted and modified from Goldin et al., 2000).

As shown in Fig. 4, the α subunit of Nav channels consists of four homologous domains/repeats (I–IV). Each homologous domain has six transmembrane α -helical segments (S1–S6) (Catterall, 2000; Noda et al., 1983; Trimmer et al., 1989). Four sets of S5–S6 segments and intervening sequences (P-loop) form a selectivity filter (SF) that make channel pore selective for Na⁺. Four amino-acid residues, Asp/Glu/Lys/Ala (DEKA), in the SF are critical for ion selectivity in Nav channels (Favre et al., 1996; Heinemann et al., 1992; Sun et al., 1997). Above DEKA, there is a negative ring comprises of Glu378/Glu704/Asp1065/Asp1356 that guards the entrance to the SF vestibule in human Nav channels. Extracellular loop L5 in repeats I–II and L6 in repeat IV form a negative ring, which attracts cations and excludes anions (Shen et al., 2017). Extracellular loops that guard the SF vestibule are heavily glycosylated and stabilized by disulfide bonds (Catterall, 2014; Shen et al., 2017). S5 and S6 segments of each repeat enclose the ion-conducting pore. S6 segments line the wall of the central cavity and contain a number of polar and charged amino-acid residues including highly conserved Asn residue (Asn409/Asn729/Lys1105/Asn1404) (Shen et al., 2017). S1–S4 segments of each homologous domain together form voltage-sensing domain (VSD). The S4 segment is crucial for channel gating and it contains positively charged Arg or Lys residues at every third position (Catterall, 2010; Noda et al., 1984). Upon membrane depolarization, the central pore of the channel opens due to the outward transfer of basic

residues, also called gating charges (Aggarwal & MacKinnon, 1996; Yang & Horn, 1995). The cytosolic linker between domains III and IV mediates rapid channel inactivation where the conserved inactivation motif IFM (isoleucine–phenylalanine–methionine) is of prime importance (West et al., 1992).

There are four Nav β subunits (β 1- β 4) have been identified, which express in heart and central nervous system of vertebrates. The Nav β 1 expresses in adult skeletal muscles only. Whereas β 1 and β 3 interact with the α subunit non-covalently, β 2 and β 4 are each disulfide-bonded to the Nav α (Brackenbury & Isom, 2011; Catterall, 2000; Isom et al., 1992, 1995; Morgan et al., 2000; Yan et al., 2017; Yu et al., 2003). Typically, a β subunit consists of an amino-terminal immunoglobulin (Ig) and a single transmembrane segment (Kazen-Gillespie et al., 2000; Yan et al., 2017) (Fig. 4). Extracellular large P-loops, particularly in repeats I and III of the Nav α subunit provide a scaffold for binding auxiliary β subunit (O'Malley & Isom, 2015; Yan et al., 2017). Although it is known that Nav β subunit functions in modulating kinetics of Nav channels and toxin binding to the channel, a detailed mechanism by which Nav β subunit modulate the functions of Nav channels (α subunit) is still not very clear.

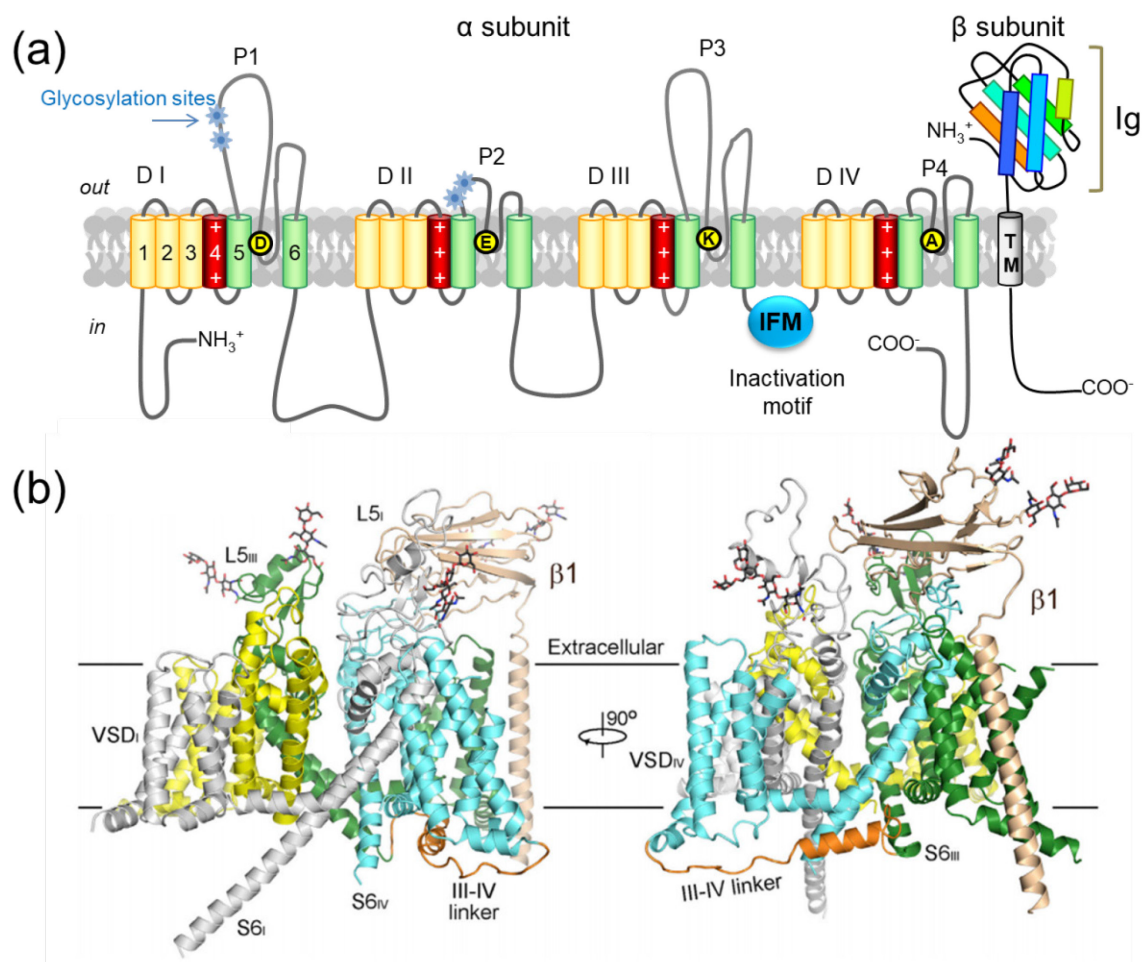


Figure 4: Transmembrane topology of a voltage-gated Na^+ channel α and β subunit and the cryo-EM Structure of $\text{Na}_v1.4$ homolog from electric eel EeNav1.4 in complex with the $\beta1$ subunit. (a) The α subunit of a Na_v channel consists of four homologous domains (DI-DIV). Each domain comprises of six transmembrane alpha-helical segments (S1–S6). S1 to S4 segments in each repeat form voltage-sensing domain. Segment S4 is crucial for channel gating. The four sets of segment S5-S6 and their intermediate sequences form the ion-selective channel pore. Indicated four conserved amino-acid residues, Asp/Glu/Lys/Ala (DEKA), play important role in Na^+ selectivity. Pore-forming loops (1-4) and glycosylation sites are indicated. The intracellular linker between DIII and DIV consist of conserved IFM motif that is essential for channel inactivation. An amino-terminal immunoglobulin (Ig) domain and a single transmembrane (TM) segment of the Na_v β subunit are shown. (b) The cryo-EM structure of the Na_v channel (EeNav1.4) from an electric eel, in complex with the $\beta1$ subunit at 4.0 Å resolution. The $\beta1$ subunit is shown in wheat color along with four homologous colored domains of EeNav1.4 channels. Black sticks represent the glycosyl moieties. (Panel b is adapted from Yan et al., 2017)

The α subunit of voltage-gated Na^+ channels (Nav) opens, i.e. activates in about 100 μs upon membrane depolarization, activation is followed by spontaneous inactivation, i.e. closing of channels, in about 1 ms. Voltage-dependent conformational changes in DIII and DIV mediates occlusion of channel pore with the IFM (Isoleucine-Phenylalanine-

Methionine) motif (inactivation motif), and hence, the flow of Na^+ is terminated, the process is so-called inactivation (Eaholtz et al., 1999; McPhee et al., 1998; Ulbricht et al., 2005; West et al., 1992) (Fig. 5). The inactivation of Nav channels is essential for timely elicitation of action potentials and propagation of signals in excitable cells. Abnormal inactivation of Nav channels may contribute to several human diseases of skeletal muscle, cardiac muscle and the CNS, such as periodic paralysis, paramyotonia congenital, long QT syndrome, Brugada syndrome, and epilepsy (Balsler, 2002; Cannon, 2000; Escayg et al., 2000; Goldin, 2003; Wallace et al., 1998).

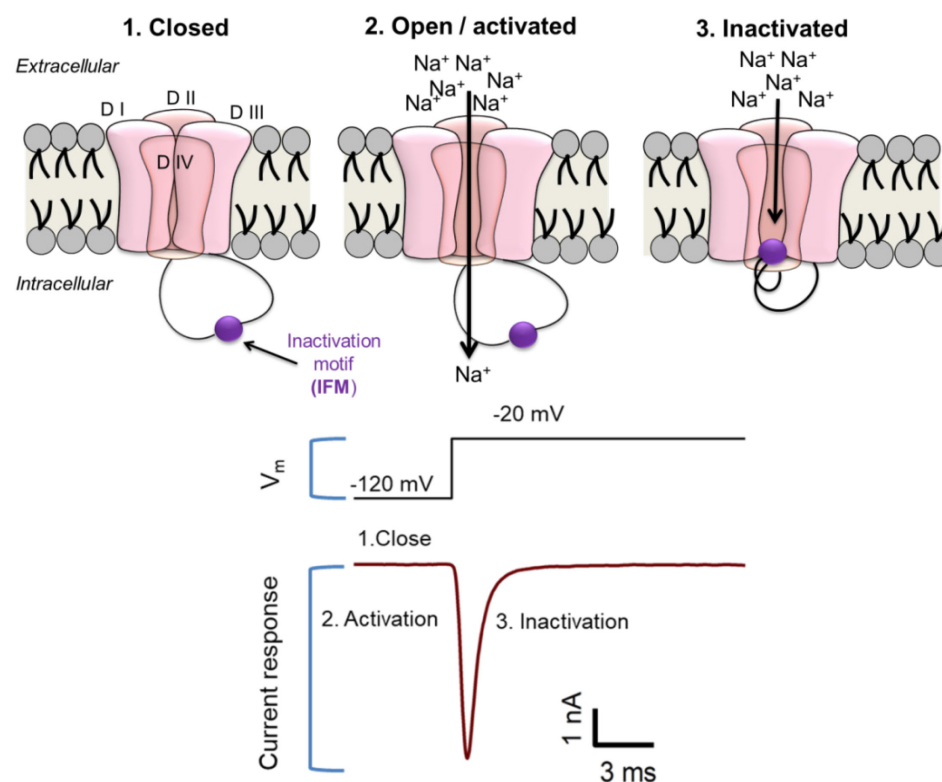


Figure 5: Three states of a voltage-gated Na^+ channel. Three simplified states, closed, opened (activated), and inactivated (closed), of a voltage-gated Na^+ channel (top) and the current response (bottom) of the channel in corresponding states are shown. At resting or very negative (e.g., -120 mV) membrane potential, the gate of the channel remains closed; hence, permeation of Na^+ ions into the cell is not possible. The conformation change upon membrane depolarization (e.g., -20 mV) leads to the opening of channel gate, which allows permeation of Na^+ ions into the cell. During sustained depolarization, the inactivation motif (IFM) of the channel occludes the channel pore and terminates ionic flow; the state is so-called ‘inactivation’. A representative current response of the channel in closed, activated, and inactivated states is shown at the bottom.

Oxidative modification of voltage-gated Na^+ channels

It is evident that excessive oxidative modifications of voltage-gated sodium channels may contribute to pathophysiology (Desaphy et al., 1998; Mao et al., 2012; Wang & Wang, 2002;

Zhang, 2005), the underlying mechanism, however, remains to be elucidated. Since the majority of redox-related functional changes in proteins arise due to the indirect effect of RS, it is more likely that indirect effects of cellular RS may have an impact on the functional properties of voltage-gated sodium channels. Previously, it has been shown that excess oxidation of polyunsaturated fatty acids affects inactivation of Nav channels (Rack et al., 1986; Wang, 1984). Additionally, oxidation of histidine residues of Nav channels substantially affects the steady-state inactivation (Rack et al., 1986). Further, Kassmann et al. (2008) showed that the methionine located in the inactivation motif of the rat Nav1.4 channel is a potential target of RS, however, oxidation of methionine at position 1469 and 1470 in the S4-S5 linker of domain IV may also have an important role in modulating functional properties of sodium channels. Like methionine oxidation, cysteines present in Nav channels may also be oxidatively modified under mild and/or vigorous oxidative condition. Since the Nav channel is rich in cysteine residues, it can be expected that these cysteines may play important role in redox modulation of the channel. About 33-40 cysteines are present in various isoforms of Nav channels, oxidation of these cysteines may affect the kinetics of the channel in a complex manner (Li et al., 1998; Evans & Bielefeldt, 2000; Gonzalez et al., 2009; Kurata et al., 1998).

1.5. Detection of cellular reactive species

In order to understand the precise role of reactive species in physiological and pathophysiological processes, it is essential to understand the molecular mechanism of RS generation, distribution, and related signals. However, living cells exhibit complex redox systems with distinct and independent regulatory systems. Besides that, high reactivity and relative instability of cellular RS make their detection extremely challenging. In order to understand the explicit descriptive role of RS in health and diseases, there is a deliberate demand of a rapid and sensitive redox-sensing tool that can capture cellular RS with high precision.

In conventional approaches of RS detection, the detection of RS mainly relies on the detection of oxidation end-products of oxidatively modified cellular lipids, proteins, and nucleic acids (Pryor & Godber, 1991; Owusu-Ansah et al., 2008). Additionally, several synthetic redox-sensitive fluorescent dyes, such as H₂DCF (dihydrodichlorofluorescein) and DHE (dihydroethidium), have been developed for the real-time assessment of RS concentrations and/or activities (Gomes et al., 2005; Wardman, 2007). Such dyes report intracellular oxidation by changing their fluorescent properties. However, redox-sensitive fluorescent dyes are mostly irreversible and cannot be targeted to subcellular sites. Moreover, these dyes chemically interfere with the intracellular milieu thereby perturb natural cell

environment (Karlsson et al., 2010). Therefore, genetically encoded redox-sensitive reporters, such as redox-sensitive green fluorescent proteins (roGFPs) and their variants, have received much attention for monitoring real-time dynamic changes in the cellular redox milieu.

Reduction-oxidation sensitive green fluorescent proteins (roGFPs) are genetic variants of wild-type GFP. The wild-type GFP is a soluble protein, which is composed of 238 amino-acid residues (27 kDa). It has a β -can or β -barrel structure that consists of 11 β -strands, each strand assembled to form nearly a perfect cylindrical structure. Both ends of the β -barrel are capped with a short segment of α -helices. The chromophore 4-(p-hydroxybenzylidene) imidazolidin-5-one (HBI) is located coaxially in the center of the helix (Meyer & Dick, 2010; Tsien, 1998; Yang, 1997; Yang et al., 1996). roGFPs possess two cysteines at position 147 and 204 into the barrel structure of either wild-type GFP or eGFP (Dooley et al., 2004, 2006; Meyer & Dick, 2010). The redox state of cysteines that are genetically introduced in the roGFPs affect their spectral properties.

1.5.1. roGFP2

The reduction and oxidation-sensitive green fluorescent protein of second generation, i.e. roGFP2, is a genetically engineered fluorescent redox reporter, which was developed by inserting two cysteines at position 147 (on β strand 7) and 204 (on β strand 10) into the barrel structure of eGFP (wild-type GFP with mutation S65T and C48S) (Fig. 6a). Oxidation promotes the formation of a disulfide-bridge between 147C and 204C (Fig. 6b). Due to the formation of a disulfide-bridge, one β strand of roGFP2 shifts relative to the other that produces several structural rearrangements. These structural changes result in the shift of excitation spectra of roGFP2 where spectral peak near 400 nm increases at the expense of spectral peak near 470 nm (Dooley et al., 2004; Meyer & Dick, 2010) (Fig. 6d). Ratiometric changes in these two excitation peak of roGFP2 indicate real-time dynamic changes in cellular redox state. Ratiometric observation overcomes artifacts arise due to photo-bleaching and inhomogeneous distribution of the sensors. Since roGFP2 is genetically encoded, it can be targeted to specific subcellular sites where redox processes have to be assayed.

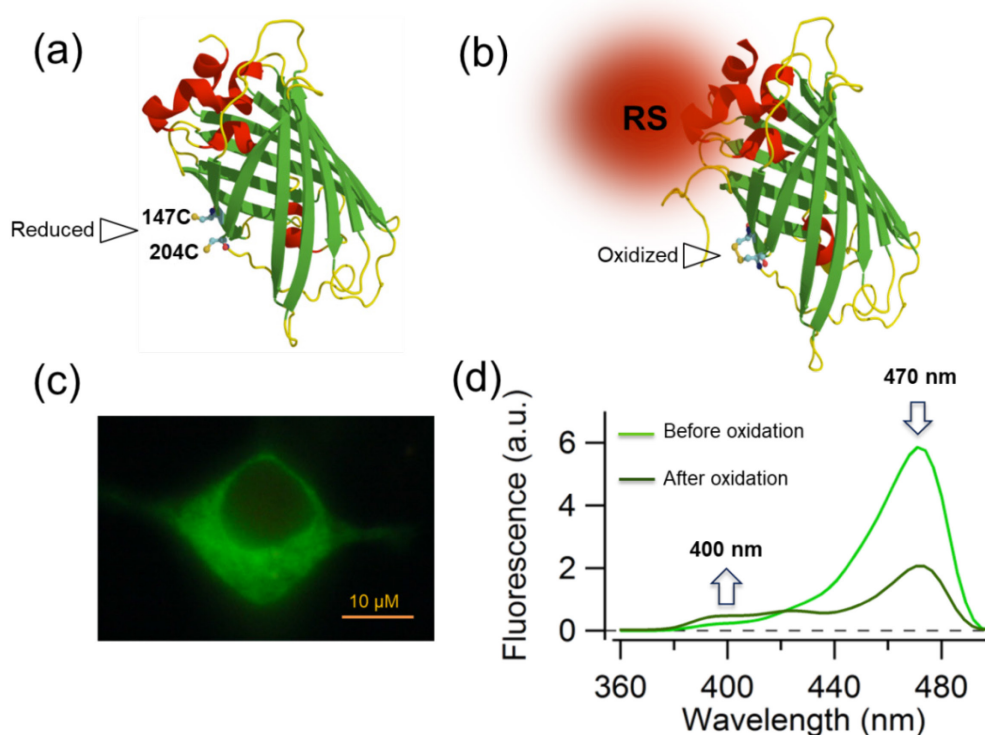


Figure 6: roGFP2. (a) Reduced roGFP2. Under reduced condition, cysteines at positions 147 and 204 remain apart. (b) Oxidized roGFP2. Two cysteines located at position 147 and 204 form a disulfide-bridge in response to oxidation. (c) A green fluorescent HEK 293T cell. Upon blue-light excitation, transiently expressed roGFP2 emits green fluorescence. (d) Excitation spectra of roGFP2 before and after oxidation. The formation of disulfide-bridge in roGFP2 leads to increase in the spectral peak near 400 nm at the expense of spectral peak near 470 nm.

1.5.2. Grx1-roGFP2

Although the sensitivity of roGFP2 to oxidation is limited by the slow reaction kinetic of cysteine oxidation, the sensitivity and dynamics of roGFP2 can be increased by fusing appropriate enzymes/regulatory proteins that can catalyze and accelerate the disulfide bond formation in roGFP2. Fusion of a particular enzyme/regulatory protein to the roGFP2 can yield a fusion product sensitive to specific redox couple, while roGFP2 alone is not specific for any redox pair. The fusion of human glutaredoxin-1 to roGFP2 by means of a flexible spacer of 30 amino-acid residues (Gly-Gly-Ser-Gly-Gly)₆ provides strongly accelerated formation of a disulfide bridge, and hence, increases the sensitivity of Grx1-roGFP2 in the physiologically relevant range for glutathione-mediated RS modification (Gutscher et al., 2008) (Fig. 7). The nucleophilic cysteine C23 of Grx1 reacts specifically with GSSG (oxidized glutathione) to form a mixed Grx1-glutathione disulfide intermediate in response to oxidative stress. Hence, Grx1-roGFP2 allows live imaging of both short- and long-lived dynamic change in cellular glutathione homeostasis with high sensitivity and spatio-temporal

resolution (Gutscher et al., 2008; Meyer & Dick, 2010). Grx1-roGFP2 exhibits the spectral properties similar to roGFP2.

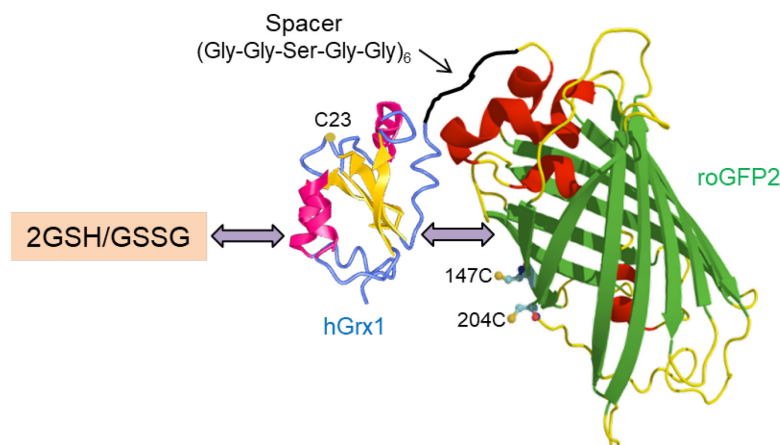


Figure 7: Grx1-roGFP2. Grx1-roGFP2 was developed by fusing roGFP2 to the human Grx1 by means of an indicated spacer. It catalyzes equilibration between glutathione and roGFP2.

1.6. Artifacts of light in cellular reactive species detection

Fluorescent techniques have become indispensable in life science research. Developments of numerous synthetic optical probes allow to study and visualize complex structures, functions, and organization of biomolecules with high spatio-temporal resolution on a real-time scale. Despite several advantages of fluorescent techniques in life science research, phototoxicity has long been recognized as an unavoidable problem and is often associated with dysregulation in cell physiology.

In context to redox research, fluorescent redox reporters, such as roGFP2 and its variants, offer several useful features, such as the choice of localized sub-cellular targeting, real-time RS detection, and ratiometric observation. However, excitation light that is required to readout the state of reporters can lead to lasting irreversible destruction of cellular structures and may even result in immediate alteration of molecular function. Despite the obvious detrimental consequences of visible light in cell physiological studies, the issue of phototoxicity has been only infrequently considered in life science research (Editorial, *Nat. Meth.*, 2013). It was reported that mammalian cells exposed to visible light for minutes to hours may suffer to damage mainly due to excess RS production (Hockberger et al., 1999). Endogenous photosensitizers, such as riboflavin and flavin adenine dinucleotide (FAD), can absorb excited visible light and produce RS, e.g. hydroxyl radical, superoxide anion, and singlet oxygen (Cunningham et al., 1985; Edwards & Silva, 2001; Eichler et al., 2005; Godley et al., 2005). Thus, these endogenous photosensitizers upon visible-light exposure may oxidatively modify the cell environment. Moreover, it has also been reported that

monochromatic visible light (450 nm) can degrade aromatic amino-acid residues, for instance, tryptophan and tyrosine, in the presence of riboflavin, thereby altering structure and function of cellular proteins (Edwards & Silva, 2001). Additionally, photo-activated GFP disturbs cellular redox homeostasis by either producing endogenous superoxide or altering the glutathione homeostasis (Goto et al., 2003; Greenbaum et al., 2000; Niwa et al., 1996). All these evidence clearly indicate that fluorescence techniques are inherently prone to excitation-light-induced artifacts.

1.7. Objectives

Approaches involving the employment of genetically encoded redox-sensitive fluorescent proteins for cellular RS detection have several advantages over traditional methods of RS detection. However, excited fluorescent proteins and excitation light itself may perturb the native intracellular environment. Although genetically encoded fluorescent reporters can be targeted to subcellular sites, signals of targeted fluorescent proteins may be contaminated with signals that arise from somewhere else in the cytoplasm. To avoid life artifacts in RS detection, the present study is designed to answer the following three questions:

- 1) Is it possible to develop non-photonic redox sensors that can capture real-time dynamic changes in cellular RS with high precision?
- 2) Can it be possible to monitor photo-damage induced by excitation light?
- 3) Is it possible to target a non-photonic RS sensor to the cell membrane in order to monitor report redox process and/or photo-damage that occur exactly at the cell membrane?

A previous study from our laboratory demonstrated that the inactivation of Nav channels is susceptible to oxidative modification mainly due to the presence of methionine in the inactivation motif (IFM) (Kassmann et al., 2008). Kassmann et al. (2008) showed that Nav channels progressively lose their rapid inactivation because of the oxidative modification of methionine located in the inactivation motif. The removal of inactivation can be monitored in real-time and with high precision by repeatedly recording current mediated by Nav channels using the whole-cell patch-clamp technique. Therefore, we hypothesized that the introduction of either additional methionine or cysteine residues in the inactivation motif of the Nav channel might enhance the inactivation susceptibility to oxidation. In the present study, we genetically engineered several mutants based on rat skeletal Nav1.4 with additional methionine and cysteine residues in the inactivation motif. We examined functional properties of channel mutants. Subsequently, we selected a channel mutant that exhibits

functional properties close to the wild-type channel to further investigate its response to various RS stimuli in order to employ the variant as a membrane-delimited RS sensor.

Increasing evidence showed that the selenocysteine is a more redox-sensitive element in redox enzymes compared with cysteine (Arnér, 2010; Gonzalez-Flores et al., 2013; Johansson et al., 2015). Thus, we hypothesized that by introducing a selenocysteine in the inactivation motif of the voltage-gated sodium channel, the oxidation sensitivity of the channel may be even greatly enhanced. Therefore, we genetically engineered a Nav1.4 mutant with a single selenocysteine in its inactivation motif and investigated its functional properties and response to RS stressors.

We further examined the response of selected Nav1.4 channel variants amongst several channel mutants with additional methionine and cysteine residues and a Nav1.4 channel variant containing selenocysteine in its inactivation motif to various stressors and compared their sensitivity with genetically encoded fluorescent redox reporters. Moreover, the effect of excitation light that is used to read the state of redox sensitive fluorescent proteins on cellular redox milieu and/or fluorescent proteins was monitored using roGFP2, Grx1-roGFP2, eGFP variants with a cysteine (147C) and a selenocysteine (147U), and channel variants with a cysteine (IFC) and a selenocysteine (IFU). Since voltage-gated Na⁺ channels are operated by means of the electrical membrane potential and they do not require light, the applicability of selected channel mutants was investigated for monitoring photo-damage/chemical modification induced by excited light under epifluorescence settings.

2. Materials and methods

2.1. Bacterial strain and cell lines

E. coli strain

XL1-Blue competent cells (Stratagene, Darmstadt, Germany)

Cell lines

- HEK 293 cells (CAMR, PortonDown, Salisbury, UK)
- HEK 293T cells (Leibniz Institute DSMZ-German Collection of Microorganisms and Cell Cultures, Braunschweig, Germany)
- HepG2 cells (Leibniz Institute DSMZ-German Collection of Microorganisms and Cell Cultures, Braunschweig, Germany)

2.2. Expression plasmids

The α -subunit-encoding rat skeletal muscle Nav1.4 (SCN4A; P15390; Trimmer et al., 1989) in the plasmid vector pcDNA3 (wild-type rNav1.4) was used. All Nav channel mutants containing mutations in their inactivation motif 1303I:1304F:1305M (IFM) were based on rNav1.4 (Fig. 8). Additionally, all Nav constructs carried mutation M1316L; the purpose of this mutation was to remove the potentially oxidation sensitive methionine of the inactivation linker. All the mutants were generated by site-directed mutagenesis and later verified by DNA sequencing (Kassmann et al., 2008; Ojha et al., 2014; Ojha et al., 2017). Mutants are termed by their inactivation motif, which are as follows:

1. rNav1.4_1303I:F1304C:1305M (ICM)
2. rNav1.4_1303I:F1304C:M1305L (ICL)
3. rNav1.4_1303I:1304F:M1305C (IFC)
4. rNav1.4_I1303C:1304F:M1305L (CFL)
5. rNav1.4_I1303C:1304F:M1305C (CFC)
6. rNav1.4_I1303M:1304F:1305M (MFM)
7. rNav1.4_I1303M:F1304M:1305M (MMM)
8. rNav1.4_1303I:1304F:M1305U_selN (IFU)
9. rNav1.4_1303I:1304F:M1305L (IFL)

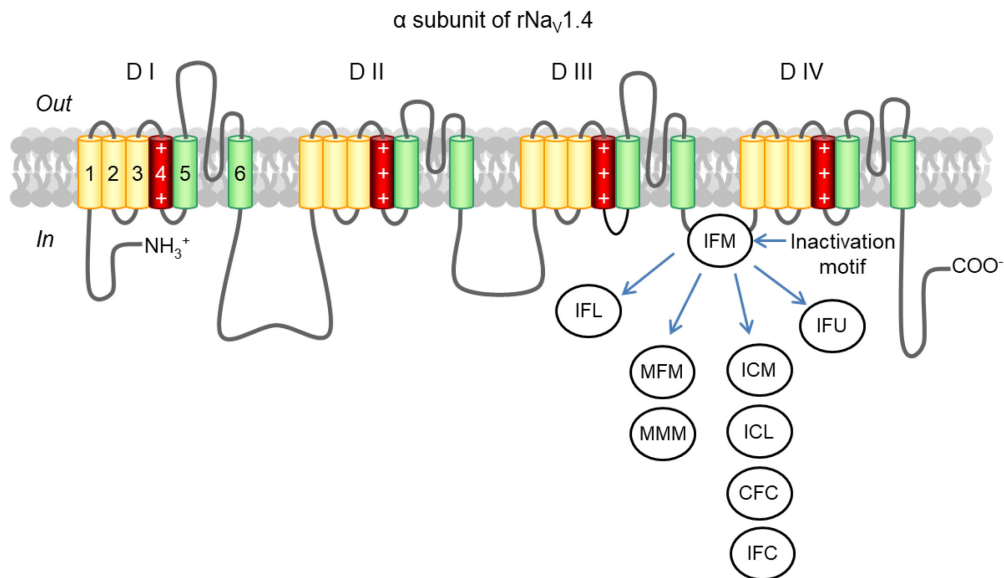


Figure 8: Transmembrane topology of the α subunit of rat Nav1.4. Wild-type channel and mutations in the inactivation motif (IFM) are illustrated. (Modified from Ojha et al., 2014)

Other plasmids that were used: roGFP2 (eGFP_S147C:Q204C; (Dooley et al., 2004)), Grx1-roGFP2 (Gutscher et al., 2008), eGFP_S147U:Q204C (Dooley, 2006) eGFP_S147C:204Q, eGFP_S147U:204Q (Ojha et al., 2017), and humanCD8. All constructs were in pcDNA3 expression vectors.

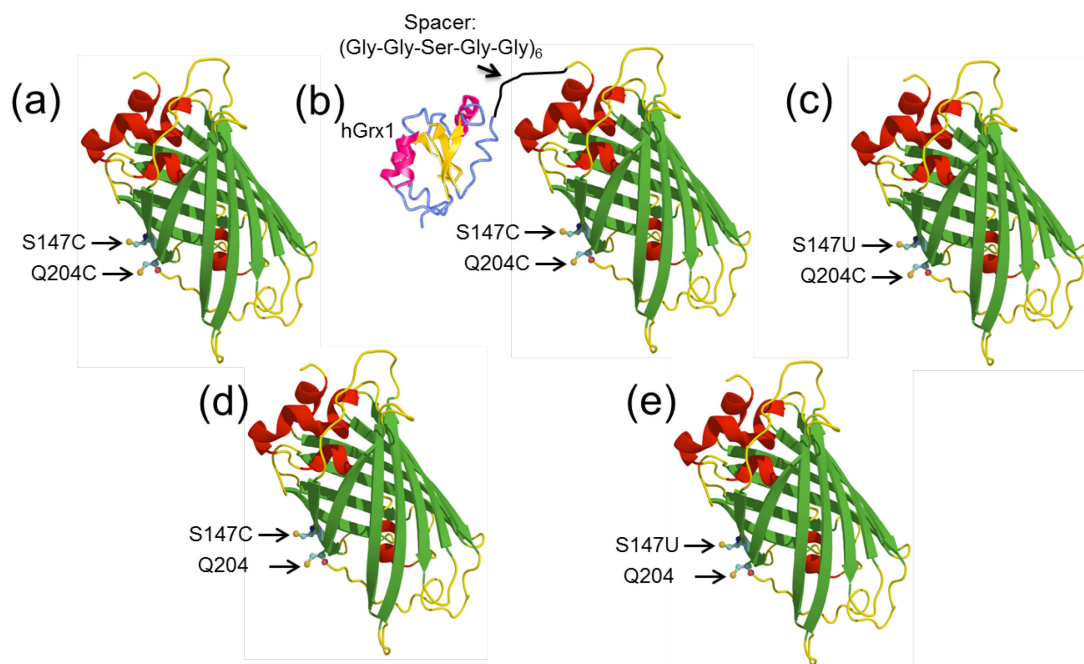


Figure 9: Illustration of roGFP2 and its variants. (a) roGFP2 (eGFP_S147C:Q204C): two surface-exposed cysteines at position 147 and 204 respond to oxidative modification. (b) Grx1-roGFP2: human glutaredoxin-1 fused to roGFP2 with an indicated spacer. (c) eGFP with a selenocysteine and a cysteine at position 147 and 204, respectively. (d) eGFP with a single cysteine at position 147. (e) eGFP with a single selenocysteine at position 147.

A cytoplasmic pKillerRed (Evrogen, Moscow, Russia) was used as a genetically encoded photosensitizer. KillerRed expressed in HEK cells generates reactive species upon light-irradiation. In some experiments, pNav β 1-KillerRed was used to generate light-induced reactive species delimited to the cell membrane (Fig. 10). This construct was generated by fusing C-terminus of the Nav β 1 subunit to the N-terminus of KillerRed (the work was done by Dr. Enrico Leipold, Center for Molecular Biomedicine, Department of Biophysics, Friedrich Schiller University of Jena, Germany).

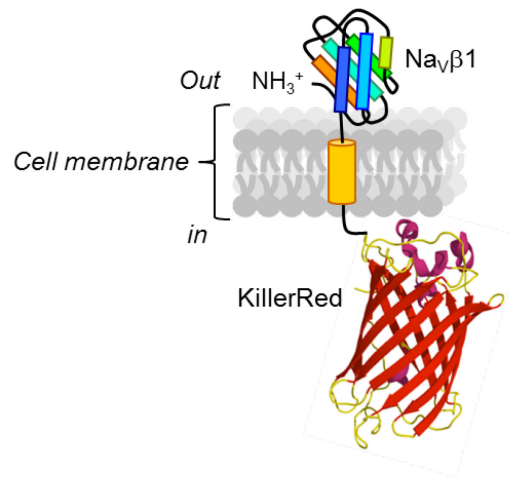


Figure 10: Cartoon illustrating the fusion product of KillerRed and Nav β 1 localized in the cell membrane.

2.3. Other chemicals

Hydrogen peroxide (FLUKA, St. Gallen, Switzerland) and chloramine T (Sigma-Aldrich, Taufkirchen, Germany) were used as the oxidant. Redox properties of CORM-2 (Sigma-Aldrich) and bilirubin oxidation end products (BOXes: Z-BOX A and Z-BOX B; obtained from Prof. Dr. Georg Pohnert, Friedrich Schiller University, Jena, Germany) were investigated using oxidation-sensitive fluorescent proteins. These chemicals were diluted in the respective bath solution immediately before extracellular application.

In some experiments either the reducing agent DTT (1,4-Dithiothreitol) at 1 mM concentration or a general RS scavenger ascorbic acid at 2 mM concentration (both from Sigma-Aldrich) in bath saline was used for the extracellular application. Some whole-cell measurements were performed with the reducing agent TCEP (tris(2-carboxyethyl) phosphine hydrochloride) (Sigma-Aldrich) added in the internal patch pipette solution at 1 mM concentration with readjustment of the pH. BAM15 (TimTec Inc, Newark, DE, USA) was used as a mitochondrial uncoupler.

2.4. Buffers and solutions

Medium for *E.coli* growth

E. coli plating medium: 15 g agar in 1 liter of LB (Luria Broth) medium (constituents in g: 10 Tryptone/peptone, 5 yeast-extracts, 5 NaCl added in 1 liter of H₂O and autoclaved; pH 7.0 adjusted with NaOH) with antibiotic (either ampicillin or kanamycin with a final concentration of 100 µg/ml).

TY media for E.coli mass culture (in g): 10 Tryptone/peptone, 5 yeast-extracts, 5 NaCl added in 1 liter of H₂O and autoclaved; pH 7.0 adjusted with NaOH. During the mass culture of *E. coli* strain, an antibiotic (ampicillin or kanamycin) with a final concentration of 100 µg/ml in the media was used to allow the growth of successfully transformed cells only.

Buffer for cell washing

Phosphate buffered saline (PBS) (in mM): 4.3 Na₂HPO₄·7H₂O, 1.4 NH₂PO₄, 137 NaCl, and 2.7 KCl; pH 7.4

Solutions for whole-cell voltage-clamp measurements

Internal (patch pipette) solution (in mM): 35 NaCl, 105 CsF, 10 EGTA, and 10 HEPES;
pH: 7.4 (CsOH)

External (bath) solution (in mM): 150 NaCl, 2 KCl, 1.5 CaCl₂, 1 MgCl₂, and
10 HEPES; pH: 7.4 (NaOH)

2.5. Plasmid amplification, extraction, and purification

The desired plasmid (1 µg) and *E. coli* strain XL1-blue (100 µl) mix were kept on ice for 1 hour. Subsequently, cells were seeded on TY 1.5% agar plate containing antibiotic (ampicillin or kanamycin) and grown for overnight at 37 °C. Next day, a single bacterial colony was selected, which further amplified in TY medium containing antibiotic for overnight in a shaker at 37 °C. After adequate growth of transformed *E. coli* cells, the plasmid was extracted and purified using Promega PureYield™ Plasmid Midiprep kit (Promega GmbH, Mannheim, Germany) following the instructions of the supplier. The concentration of purified plasmid was determined by GeneQuant™ 1300 spectrophotometer (GE Healthcare, Munich, Germany).

2.6. Cell culture and transfection

Cell lines (HEK 293, HEK 293T, HepG2) were maintained in T75 flasks containing DMEM (Dulbecco's Modified Eagle's Medium)/Ham's F12 nutrient mix with L-glutamine and supplemented with 10% fetal calf serum (Gibco[®] by Fisher Scientific GmbH) in a humidified 5% CO₂ incubator (Thermo Electron LED GmbH, Langenselbold, Germany) at 37 °C. About 90% confluent cells were trypsinized (0.05% trypsin-EDTA; Gibco[®] by Fisher Scientific GmbH), diluted with culture medium, and grown in either 35-mm dishes or 24 well cell-culture plates. The cells were plated in 35-mm dishes explicitly for photonic experiments. These 35-mm dishes were made by sticking the glass coverslip of thickness 170 μm and diameter 25 mm (Gerhard Menzel GmbH, Braunschweig, Germany) using silicone elastomer (RTV615, KVD, Bad Wimpfen, Germany) to the bottom of hollow 35-mm dishes (Fig. 11). The cells grown on the glass surface (diameter=25 mm) only were used in experiments. About 70% confluent cells were transfected with the desired plasmid using Roti[®]-fect (Roth, Karlsruhe, Germany) transfection reagent following the instructions of the supplier.

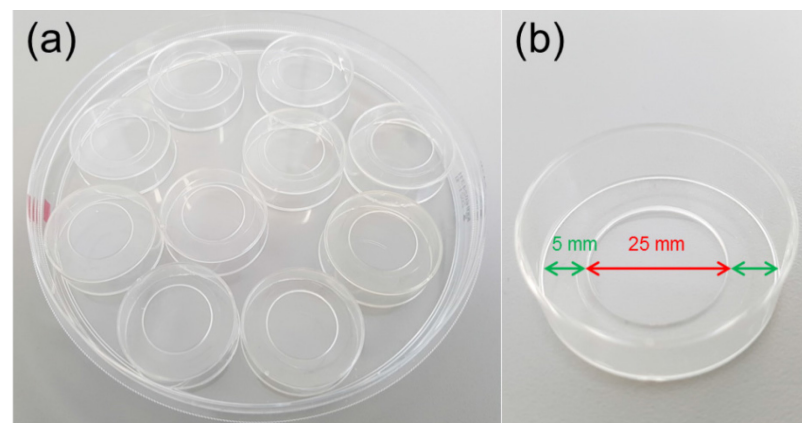


Figure 11: Glass bottom dishes for photonic experiments. (a) 35-mm cell culture dishes stored in a petri plate. (b) A single 35-mm cell culture dish with a glass coverslip (diameter of 25 mm) (red) and plastic space (5 mm) around the glass coverslip (green) is shown.

The culture of rNav1.4 mutant IFU (roNav2) expressing cells was supplemented with sodium selenate (Na₂SeO₄; 300 nM) for 12 hours from the day of transfection. After 12 hours, transfected cells were maintained in fresh cell culture media without sodium selenate. Unless otherwise stated, cells expressing ion channels other than mutant IFU were grown in absence of sodium selenate.

Electrophysiological and/or photometrical experiments were performed 1-3 days after the cell transfection. Cells not transfected with fluorescent proteins were co-transfected with human-CD8 plasmid and transfected cells were identified by the binding of anti-CD8-coated beads (Invitrogen by Life Technologies GmbH). These anti-CD8 beads (diameter 4.5 μm)

contain a coating of a mAb (ITI-5C2) specific for the CD8 antigen; therefore, beads allow identification of positively transfected cells.

2.7. Patch-clamp electrophysiology

Patch-pipettes were fabricated from filament glass capillaries (Inner/outer \varnothing : 0.86/1.50 and length: 80-mm) using pipette puller (Sutter Instruments, Novato, USA). Fabricated pipettes were coated with either silicone elastomer (RTV615) or white wax (Modern Materials[®], Saint Paul, USA) and fire-polished to yield resistances of 0.7-1.5 M Ω .

Voltage-clamp experiments in the whole-cell configuration were performed with the patch-clamp setup that consisted of Zeiss inverted microscope (Axio Observer.D1), micromanipulator (Sutter Instruments), and an EPC 10 USB double patch-clamp amplifier operated by PatchMaster software (both from HEKA Elektronik, Lambrecht, Germany). In some experiments, an EPC 9 patch-clamp amplifier (HEKA Elektronik) was used.

The series resistance was corrected electronically by more than 70% to minimize voltage errors. Unless otherwise stated, holding voltage in all experiments was set to -120 mV. Leak and capacitive currents were corrected with a p/6 method with a leak holding voltage of -120 mV. A p/4 method was used during the assessment of voltage-dependent channel activation and the fractional recovery of channels from inactivation. Currents were low-pass filtered at 5 kHz and data were sampled at 50 kHz. Currents were sampled at 25 kHz during the assessment of voltage-dependent channel inactivation.

Perforated-patch clamp recordings were performed by supplementing escin (Sigma-Aldrich) as a perforating reagent at 1-10 μ M to the patch pipette solution in the on-cell configuration. Escin formed pores in the membrane within 10-15 minutes thereby a series resistance was achieved between 3 and 20 M Ω .

Most of the electrophysiological experiments were performed at room temperature (19-24 $^{\circ}$ C). Some experiments were performed at a constant temperature of either 32 $^{\circ}$ C or 30 $^{\circ}$ C as stated in results. The temperature was controlled by an electronic peltier temperature control system (PTC-10) (NPI Electronic GmbH, Tamm, Germany).

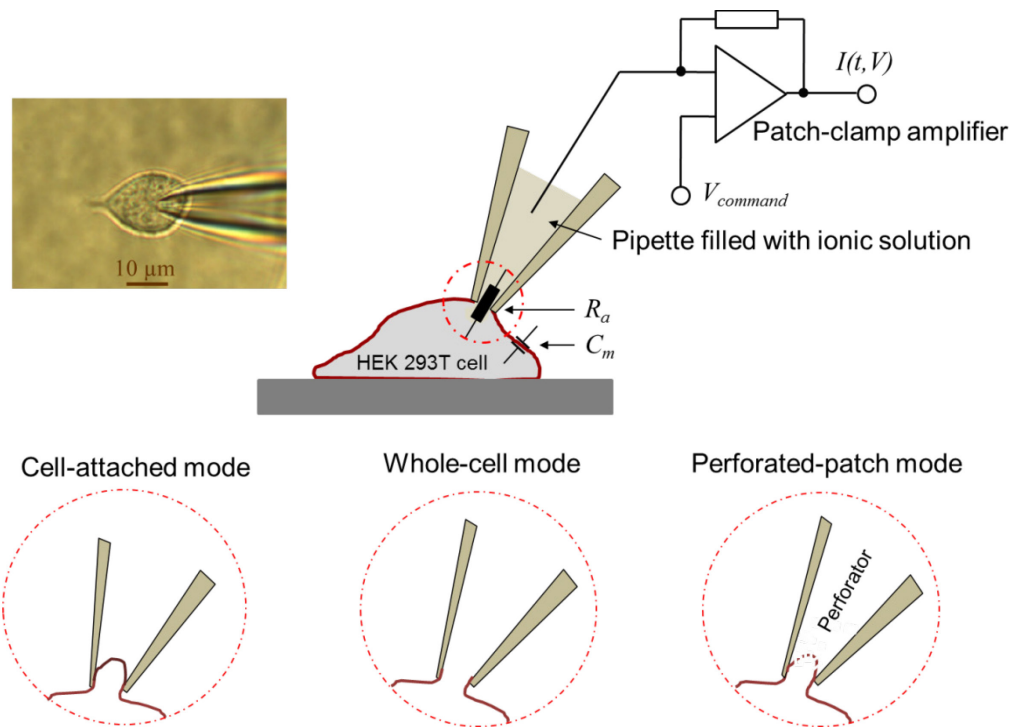


Figure 12: Illustration of patch-clamp measurements (not drawn to scale). Patch pipette with recording electrode in contact with cytosol of a HEK 293T cell. Three patch-clamp recording configurations: on-cell (cell-attached), whole-cell, and perforated-patch are shown.

2.8. Photometry

A Zeiss inverted microscope (Axio Observer.D1) with epifluorescence filter set: GFP, 492/SP, FT 495, HC 520/35 and objectives: 40x (NA=1.3; fluar) and 63x (NA=1.4; Plan-Apochromat) coupled to a uEye camera (IDS Imaging Development Systems GmbH, Obersulm, Germany), a viewfinder, and an FDU-photodiode (both from TILL Photonics, Gräfelfing, Germany) was used for fluorescence measurements. A polychrome-V monochromator (150-W Xenon high stability lamp; TILL Photonics) controlled with PatchMaster software (HEKA Elektronik) was used as a light source to excite the transiently expressed fluorescent proteins (Fig. 13). In some photometrical measurements, a polychrome-1 monochromator (TILL Photonics) was used as the light source.

The light was irradiated on cells expressing roGFP2 or its variants via 40x (NA=1.3) fluar oil objective and the fluorescence was measured from a single cell at two excitation maxima near 400 nm and 470 nm (each for either 10 ms or 20 ms). A 63x (NA=1.4) Plan-Apochromat objective was chosen when the oxidative response of fluorescent protein was intended to compare with the mutant IFU channel. A 20x (NA=0.3) Ph1 dry LD A-Plan objective was used to compare the sensitivity to oxidation of roGFP2 and mutant IFC channel co-expressed in a single HEK cell. A single fluorescent cell was selected for the ratiometric fluorescent measurement using a viewfinder coupled with the camera (Fig. 14). The step

interval of ratiometric fluorescence measurements in most of the experiments was either 5 s or 10 s. Unless otherwise stated, all photometrical experiments were performed at room temperature (19-24 °C).



Figure 13: Setup for patch-clamp electrophysiology and photometry: 1-inverted microscope, 2-viewfinder, photo-diode, and camera, 3-patch-clamp amplifier, 4-computer monitor, 5-polychrome-V monochromator, 6-Fluorescence detection unit for single emission (FDU-SE), 7-temperature control device, 8-patch pipette holder, 9-micromanipulator, 10-microscope stage controller, and 11-Faraday cage.

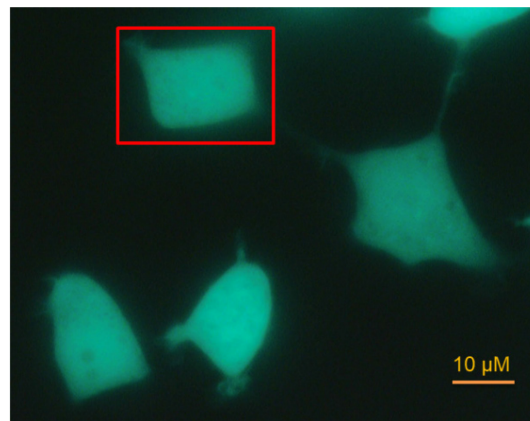


Figure 14: Schematic representation of the viewfinder area (red rectangle) selected for fluorescence measurements. roGFP2 expressing fluorescent HEK 293T cells are shown.

2.9. Reactive species generation

The cell culture was supplemented with high glucose (25 mM) to affect the endogenous RS milieu. Extracellular oxidants, such as chloramine T and H₂O₂, diluted in the bath solution immediately before application, were applied by either changing the entire bath volume or by glass application pipette in the local vicinity of a transfected single cell.

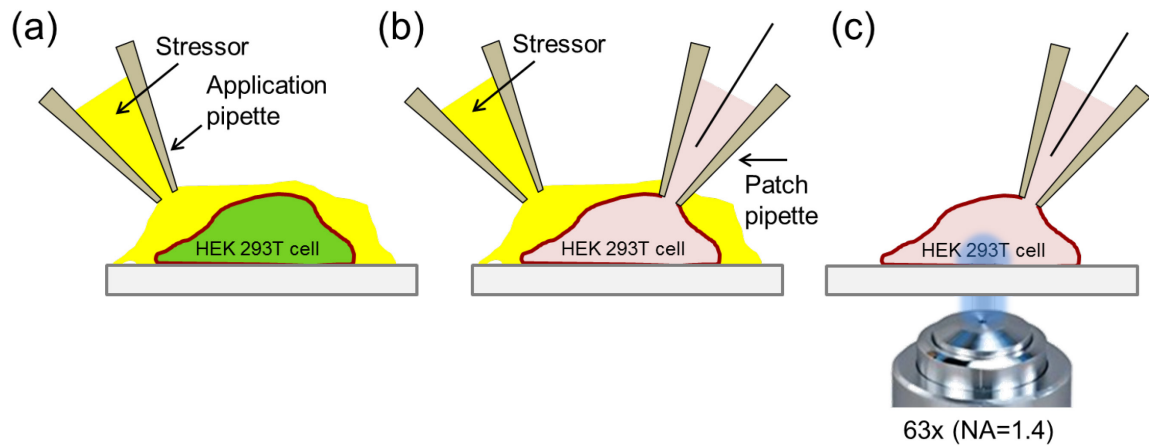


Figure 15: Mode of RS generation. A schematic representation of the local application of stressor (oxidant) on green fluorescent protein (a) and channel expressing cells (b). Blue-light was directed to the cells via the microscope objective to induce reactive species formation (c). (Figures are not drawn to scale).

In some experiments, RS were generated solely by epifluorescence excitation light (blue and green) passed through an epifluorescence filter set and the microscope objective (20x Ph1 dry LD A-Plan (NA=0.30) and 63x oil Plan-Apochromat (NA=1.4)). A genetically-encoded photosensitizer KillerRed was used to generate light-induced RS in some experiments. Epifluorescence filter set for KillerRed: BP 510-560, FT 580 (LP 590).

2.10. Data acquisition, analysis, and statistics

Patch-clamp electrophysiological and fluorescence data were acquired with PatchMaster software and analyzed with FitMaster (HEKA Elektronik), IgorPro (WaveMetrics, Lake Oswego, OR, USA), and MS-Excel (Microsoft Corporation, Redmond, USA). Data were presented as mean \pm s.e.m. for independent measurements (n). Groups of data were compared with a two-sided student's t-test followed by a post hoc Bonferroni correction when appropriate. Differences in the mean data were considered significant: *, $P \leq 0.05$; **, $P \leq 0.01$; ***, $P \leq 0.001$.

2.10.1. Voltage-dependent channel activation

Voltage-dependent channel activation was assayed by depolarizing pulses from -60 mV to 60 mV in steps of 10 mV, every 2 s from a holding membrane voltage of -120 mV. Peak currents as the function of depolarizing voltages were fit according to a Hodgkin-Huxley formalism with three activation gates ($m = 3$) and a single-channel conductance following the Goldman-Hodgkin-Katz equation:

$$I(V) = \Gamma V \frac{1 - e^{-(V - E_{rev})/25mV}}{1 - e^{-V/25mV}} \times \frac{1}{(1 + e^{-(V - V_m)/k_m})^3} \quad (\text{eq. 1})$$

V_m = voltage of half-maximal gate activation, k_m = the corresponding slope factor, Γ = the maximal conductance of all channels, and E_{rev} = the reversal potential.

2.10.2. Voltage-dependence of channel inactivation

Channel inactivation was measured from a holding membrane voltage of -120 mV with conditioning pulses of 500 ms at voltages ranging from -120 mV to -45 mV in steps of 5 mV, every 10 s. Subsequently, the peak current was determined at -20 mV, later normalized to a control peak current measured before conditioning voltages (reference peak current). The normalized peak currents were plotted as a function of conditioning voltage and were fit according to either a single-component Boltzmann function (eq. 2) or two-component Boltzmann function (eq. 3):

$$\frac{I(V)}{I_{control}} = \frac{1}{1 + e^{-(V - V_h)/k_h}} \quad (\text{eq. 2})$$

$$\frac{I(V)}{I_{control}} = \frac{(1 - r_2)}{1 + e^{-(V - V_{h1})/k_h}} + \frac{r_2}{1 + e^{-(V - V_{h2})/k_h}} \quad (\text{eq. 3})$$

V_h = the half-maximal inactivation voltages (V_{h1} and V_{h2} for two-component), k_h = the corresponding slope factor, r_2 = proportionality constant that represents the fraction of channels that inactivate in a secondary inactivation phase, and $(1 - r_2)$ = the fraction of channels that inactivate in the primary inactivation phase.

2.10.3. Steady-state current and the time course of inactivation

Channels were depolarized to -20 mV from a holding membrane potential of -120 mV and currents were fit according to a Hodgkin-Huxley formalism with three activation gates ($m=3$) and a single-channel conductance to estimate the steady-state current and the time course of inactivation.

$$I(t) = I_0 m^3(t) h(t)$$

$$m(t) = 1 - e^{-(t/\tau_m)}$$

$$h(t) = h_\infty + (1 - h_\infty) e^{-(t/\tau_h)} \quad (\text{eq. 4})$$

I_0 = current amplitude, t = time, τ_m = time constant of activation, τ_h = time constants of inactivation, and h_∞ = the fraction of non-inactivating current after infinite time.

2.10.4. Fractional recovery

A control peak current was measured in response to depolarizing pulses of -20 mV for 10 ms from a holding membrane potential of -100 mV afterward channels were conditioned for 0.2 ms and conditioning time was increased by a factor of 2. The step was repeated every 5 s until channels recovered completely from inactivation. The peak current was determined at -20 mV after conditioning, normalized to a control peak current measured before conditioning time. Normalized peak current was plotted as a function of conditioning time and was fit with either a single-exponential (eq. 5) or a double-exponential function (eq. 6):

$$I(t) = A e^{-(t/\tau_1)} \quad (\text{eq. 5})$$

$$I(t) = A e^{-(t/\tau_1)} + (1 - A) e^{-(t/\tau_2)} \quad (\text{eq. 6})$$

A = normalized current amplitude, $(I-A)$ = second component of normalized current amplitude, t = time, τ_1 = first time constant, and τ_2 = second time constant.

2.10.5. Time course of inactivation removal

The time course of oxidation-induced inactivation removal was monitored by measuring the ratio (R_I) of current at 5 ms (I_5) or 10 ms (I_{10}) after the depolarization onset and the peak current (I_p) elicited by pulses to -20 mV. 5 ms was chosen for cases where a direct comparison with wild-type channels was intended because the inactivation of wild type is faster than that of mutant IFC (roNav1) and mutant IFU (roNav2). The remaining non-inactivating current fraction, $R_I(t)$, was plotted as a function of time (t) and was fit with the following function:

$$R_I(t) = R_0 - (R_\infty - R_0) \left(1 - e^{-\left(\frac{t-t_0}{\tau}\right)} \right) \quad (\text{eq. 7})$$

R_0 = ratio before oxidation, R_∞ = the ratio after infinite exposure to oxidant, t_0 = the time of oxidation start, and τ = the time constant.

2.10.6. Fluorescence ratios

Fluorescence of individual cells expressing roGFP2 and its variants was measured at 400 nm and 470 or 475 nm. Due to operational delay (about 5 ms) of the scanner, the second half

episodes of the fluorescence at 400 nm and 470 or 475 nm were chosen for the analysis (Fig. 16). Background fluorescence (F_0) at 250 nm or in absence of excitation light was subtracted from the fluorescence measured at 400 nm (F_1) and 470 or 475 nm (F_2) that yielded absolute fluorescence at 400 nm (dF_1) and 470 or 475 nm (dF_2). The ratio of absolute fluorescence ($dF_1/dF_2 = F_{400} / F_{470}$) was plotted as a function of time and fitted according to equation 7 for the fluorescence ratio instead of inactivation removal.

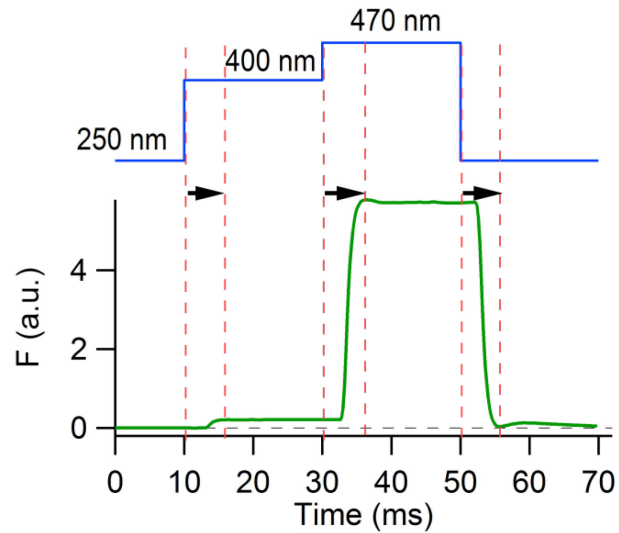


Figure 16: A representative fluorescence trace measured from a HEK 293T cell expressing roGFP2 (lower) in response to indicated pulse protocol (upper). Black arrow shows an operational delay of the scanner (~5 ms).

3. Results

The rapid inactivation of Nav channels is mainly mediated by the inactivation motif “IFM” (Ile-Phe-Met), located in the intracellular linker between domains III and IV (West et al., 1992). The presence of methionine (Met) in the inactivation motif makes the channel inactivation susceptible to oxidative modification. Exposure of rat skeletal muscle Nav1.4 (rNav1.4) to the oxidant chloramine T (ChT) efficiently removes its rapid inactivation; this is mainly due to chemical modification of the Met residue (Met1305 for rat Nav1.4) present in the inactivation motif (Kassmann et al., 2008). The study of Kassmann et al. (2008) clearly indicated that oxidation-mediated removal of channel inactivation depends on the oxidation sensitivity of amino-acid residues located in the inactivation motif. Therefore, it was hypothesized that introduction of either additional Met residues or cysteine residues (Cys) in the inactivation motif might make the inactivation even more susceptible to oxidative modification. Hence, several single- or double-site mutants with either additional Met or Cys were generated and they were termed by their inactivation motif, such as MFM for rNav1.4_I1303M:F1304:M1305. Such mutants were expressed in HEK 293 or 293T cells and their function was evaluated by means of the whole-cell patch-clamp method.

3.1. Selection of Na⁺ channel mutants sensitive to reactive species

For an application of one of the channel mutants containing either additional Met or Cys residues in the inactivation motif as an RS sensor, the rapid inactivation should be nearly complete as to avoid Na⁺ influx into cells under sustained depolarization. Thus, the time course of inactivation and the fraction of steady-state current at a depolarizing voltage of -20 mV were measured for each mutant. All mutants produced current and exhibited rapid inactivation. The steady-state current at the end of the 20-ms depolarizing pulse relative to the peak current was analyzed for wild-type rNav1.4 (in percentage): 1.5 ± 0.2 (n=8), MFM: 2.1 ± 0.3 (n=5), MMM: 6.2 ± 1.6 (n=12), ICM: 11.7 ± 0.4 (n=55), ICL: 9.6 ± 0.6 (n=18), IFC: 2.8 ± 0.3 (n=16), CFL: 6 ± 0.5 (n=18), and for CFC: 18.7 ± 1.3 (n=16). Mutant IFL exhibited the least steady-state current (1.19 ± 0.2 , n=9) among all channels (Fig.17b). Hence, all mutants with either additional Met residues or Cys residues exhibited a greater steady-state current than the wild type (IFM). Mutant MFM and IFC displayed a steady-state current and an inactivation time courses most similar to that of the wild type (Fig. 17).

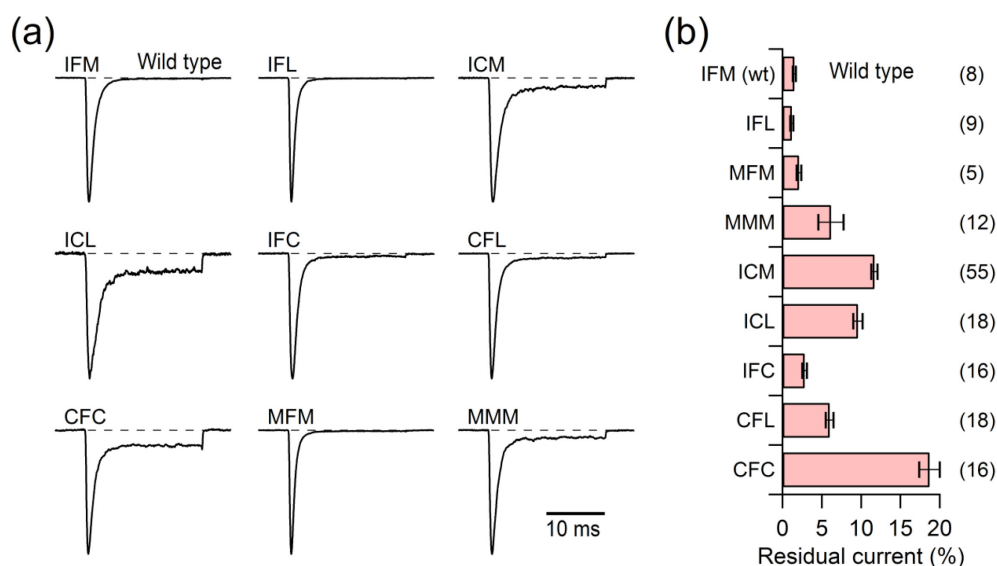


Figure 17: Steady-state inactivation of rNav1.4 mutants. (a) Normalized current responses of rat skeletal muscle Nav1.4 wild-type (IFM) and the indicated mutants expressed in HEK 293 cells in response to depolarization to -20 mV from a holding voltage of -120 mV. (b) The residual current at the end of the 20-ms depolarizing pulse relative to the peak current for the indicated mutants. Data are mean \pm s.e.m. (n). (Ojha et al., 2014)

The mutants with either one or additional Cys residues were subjected to 50 μ M ChT, and those with an altered number of Met residues were exposed to 500 μ M ChT. All mutants carrying either one or additional Cys residues lost inactivation on ChT (50 μ M) exposure with a single-exponential time course characterized by time constants of 50-70 s, while wild-type rNav1.4 showed a very small response only (about 2000 s) (Fig. 18a,b,d). ChT at 10-times higher concentration removed inactivation of wild-type rNav1.4 with a time constant of about 300 s, while an increasing number of Met residues accelerated that process (MFM, about 60 s; MMM, about 30 s). Mutant IFL, i.e. a channel mutant lacking Met residue in its inactivation motif, served as a negative control with a very slow response to 500 μ M ChT (about 700 s) (Fig. 18c,e).

These results indicated that a Cys residue at any position within the IFM motif results in channels with strongly RS-sensitive inactivation; a second Cys in the inactivation motif does not increase the sensitivity. Mutants with two or three Met residues exhibited about 10-times less sensitivity than the mutant with a Cys (Fig. 18d-blue,e-gey). Mutants MFM and MMM are well suited for the study of Met-directed modifications. Since a mutant with the least steady-state current under control conditions was most desirable for the employment of mutant as RS sensor, mutant IFC was selected for further analysis and it was termed by its inactivation motif, IFC, also referred to as ‘roNav’ or ‘roNav1 (reduction-oxidation sensitive Nav channel of generation 1)’.

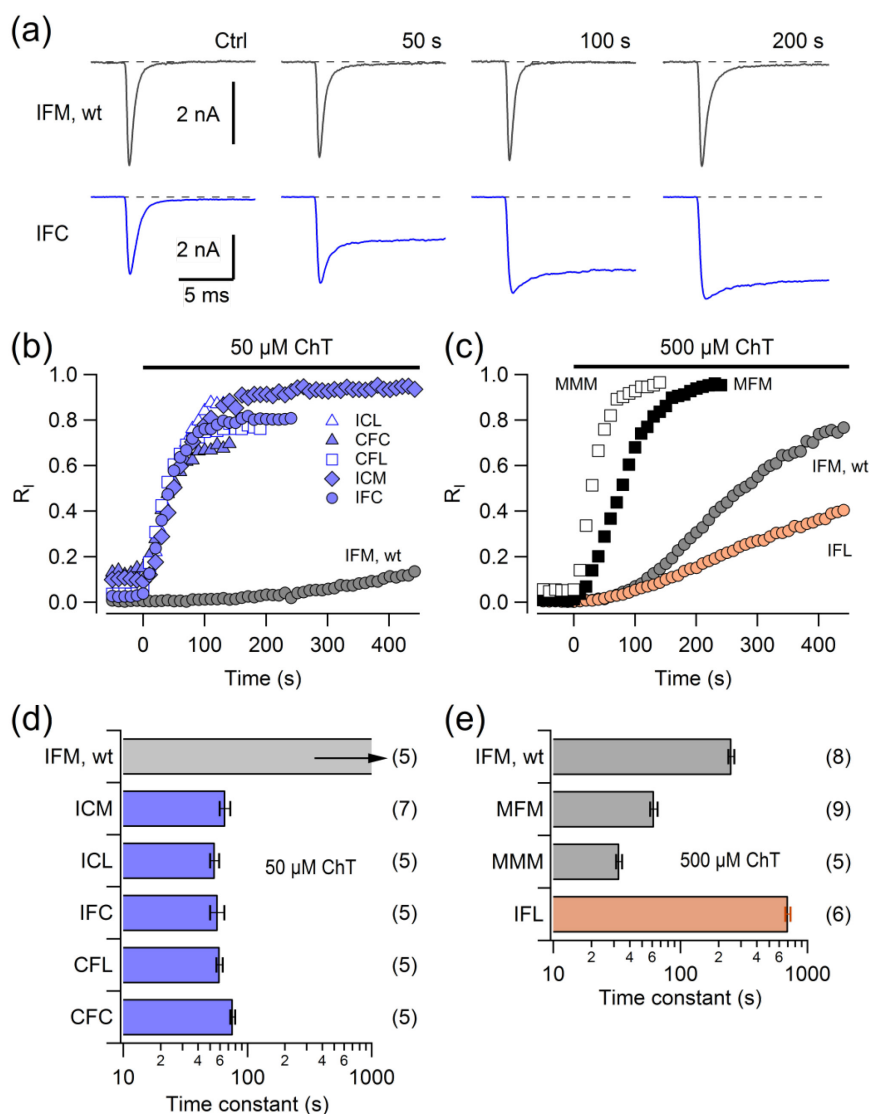


Figure 18: Removal of rapid inactivation by chloramine T. (a) Current traces at -20 mV for wild-type rNav1.4 (IFM, top) and mutant IFC (bottom) in HEK 293 cells before (Ctrl) and after (time indicated) application of 50 μ M ChT. (b) Time course of inactivation removal in response to application of 50 μ M ChT for the wild type and the indicated mutants. (c) Time course of inactivation removal in response to the application of 500 μ M ChT for the wild type and the indicated mutants. Mutant IFL served as a negative control. (d, e) Time constants for inactivation removal for the indicated channels in response to 50 μ M ChT (d) and 500 μ M ChT (e). Data are mean \pm s.e.m. with n shown in parentheses. (Ojha et al., 2014)

3.2. Generation and heterologous expression of seleno-Na⁺ channel

The results shown thus far have demonstrated that RS-sensitivity of channel inactivation can be increased by introducing an oxidation-sensitive amino-acid residue in the inactivation motif. Therefore, it was further hypothesized that the RS-sensitive inactivation of roNav1 might be increased with a more reactive selenocysteine (Sec, U) at the position 1305 instead of Cys. Aiming for even improving the RS-sensitive inactivation of roNav1, a Sec residue was introduced in the inactivation motif (M1305U) of the wild-type rNav1.4 thereby a

seleno- Na^+ channel (rNav1.4_IFU) was genetically engineered. An expression vector was constructed based on wild-type rNav1.4 channels with a TGA stop codon (in DNA) at the position equivalent to M1305, and followed by a Sec insertion sequence element (SECIS; 225-bp fragment containing nucleotides 2811-3065 from human SELENON mRNA, SEP1) downstream of the channel gene (Fig. 19). The seleno- Na^+ channel was termed by its inactivation motif, IFU, also referred to as ‘roNav2’ (reduction-oxidation sensitive Nav channel of generation 2).

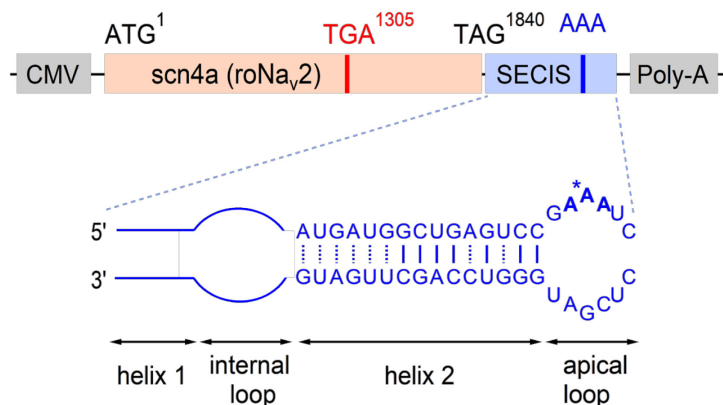


Figure 19: Vector construction for selenocysteine incorporation into Nav1.4. A 225-bp fragment containing nucleotides 2811-3065 from human SELENON mRNA (NM_020451.2, SEP1) was placed directly after the endogenous scn4a stop codon TAG, thereby placing the AAA consensus sequence of the SECIS element. The SECIS element is at 140 nt downstream of the scn4a stop codon. (Ojha et al., 2017)

After constructing an expression vector of roNav2, its production yield in HEK 293T was examined and compared with the yield of roNav1 and wild-type rNav1.4. Transfected cells were depolarized to -20 mV for 20 ms from a holding potential of -120 mV and the peak current amplitude was determined for each channel construct (Fig. 20a-c). Wild-type rNav1.4 and roNav1 were adequately expressed in HEK 293T cells and produced mean peak current amplitudes of -4.5 ± 0.5 nA ($n=20$) and -4.0 ± 0.5 nA ($n=20$), respectively (Fig. 20d, white bars). roNav2 yielded a much smaller current signal (Fig. 20c, black trace) of -0.20 ± 0.02 nA ($n=20$) (Fig. 20d, white bar). Supplementation of the cell culture with sodium selenate (Na_2SeO_4 ; 300 nM) increased the current amplitude of roNav2 by about 8-fold (-1.4 ± 0.1 nA, $n=29$; $P<0.001$) (Fig. 20c,d-red); the current amplitude of rNav1.4 (-3.6 ± 0.6 nA, $n=20$; $P=0.28$) and roNav1 (-4.3 ± 0.5 nA, $n=20$; $P=0.69$) were unaffected by sodium selenate (Fig. 20d). Hence, sodium selenate (300 nM) is essential for the reasonable expression yield of roNav2 in HEK 293T cells; supplementation does not influence the expression of roNav1 and wild-type rNav1.4.

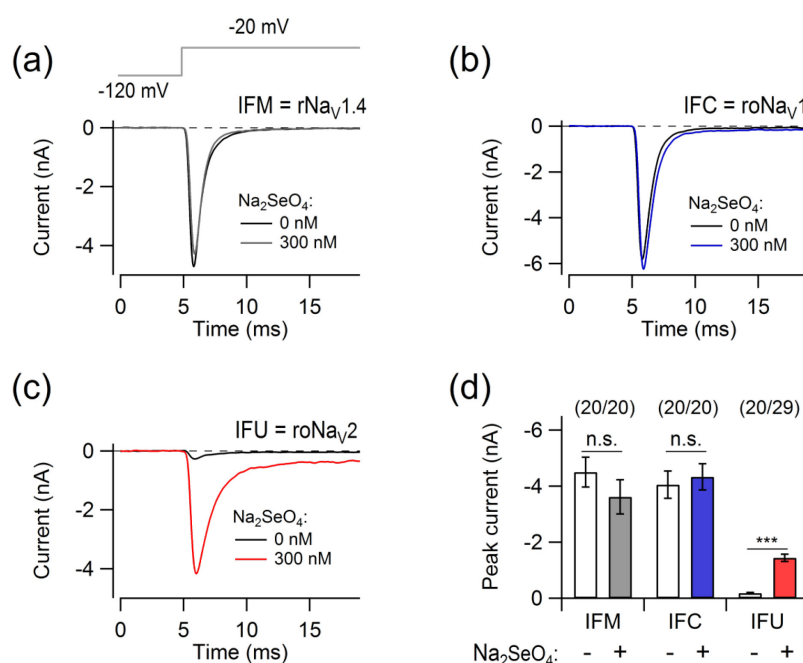


Figure 20: Influence of sodium selenate on the functional expression level. (a-c) Representative current traces at a depolarizing pulse -20 mV from holding voltage of -120 mV of the indicated channel constructs, expressed in HEK 293T cells, either in normal cell culture medium (0 nM) or in culture medium supplemented with 300 nM sodium selenate (Na₂SeO₄). (d) Mean current amplitude of the indicated channel constructs, cultured in medium without (white bars) or with 300 nM Na₂SeO₄ (colored bars). Data in d are mean ± s.e.m (n). Statistical t-test: ***, P<0.001; n.s. (not significant), P>0.05. (Ojha et al., 2017)

roNav1 and roNav2 were selected for further analysis. Biophysical properties of these channels were analyzed and compared with wild-type rNav1.4. Further, the response of mutant channels (roNav1 and roNav2) to RS stimuli was assayed.

3.3. Biophysical properties of roNav1 and roNav2

Introduction of either a Cys (roNav1) or a Sec (roNav2) in the inactivation motif of wild-type rNav1.4 might affect biophysical properties of the channel. Therefore, patch-clamp electrophysiological measurements were performed to investigate the influence of either Cys or Sec in the inactivation motif on the channel properties. Since supplementation of sodium selenate (300 nM) in the cell culture is required for a considerable expression yield of roNav2 in HEK 293T cells, all channels were expressed in presence of sodium selenate to compare channel properties. Because sodium selenate (300 nM) may affect the channel properties, the influence of sodium selenate on the functional properties of wild-type rNav1.4 and roNav1 was examined.

3.3.1. Voltage-dependent channel activation

Channel-expressing cells were depolarized from -60 mV to 60 mV in steps of 10 mV, every 2 s, from a holding voltage -120 mV and currents were measured in response to depolarizing voltages (Fig. 21a, 21b-e, top). Subsequently, current amplitudes were plotted as the function of depolarizing voltages and were fit according to a Hodgkin-Huxley formalism with 3 activation gates and a single-channel conductance according to the Goldman-Hodgkin-Katz (GHK) equation (eq. 1) (Fig. 21b-e, lower).

GHK fit yielded half-maximal activation voltage (V_m) and the corresponding slope factor (k_m) for each channel construct. The half-maximal activation voltage (V_m) of roNav1 (-40.4 ± 1.9 mV, $n=11$; $P=2.0$) and roNav2 (-46.6 ± 1.2 mV, $n=22$; $P=0.1$) were similar to that of wild type (-41.4 ± 1.7 mV, $n=6$). The reducing agent TCEP (1 mM) supplemented to the patch pipette solution did not affect the half-maximal activation voltage of roNav2 (-46.5 ± 0.23 mV, $n=30$; $P=0.09$) (Fig. 21f, left). The corresponding slope factor (k_m) of roNav2 (11.5 ± 0.40 mV, $n=22$; $P<0.001$) significantly varied from the wild-type channel, while roNav1 (8.0 ± 0.41 mV, $n=11$; $P=1.2$) and wild-type rNav1.4 (7.5 ± 0.48 mV, $n=6$) exhibited a similar k_m (Fig. 21f, right). The apparent voltage dependence of roNav2 was less steep compared to wild-type rNav1.4 and roNav1. Even the steepness of voltage dependency of roNav2 (13.8 ± 0.50 mV, $n=30$; $P<0.001$) did not come close to the wild-type channel when the reducing agent TCEP at a concentration of 1 mM was supplemented in the patch pipette solution (Fig. 21f, right).

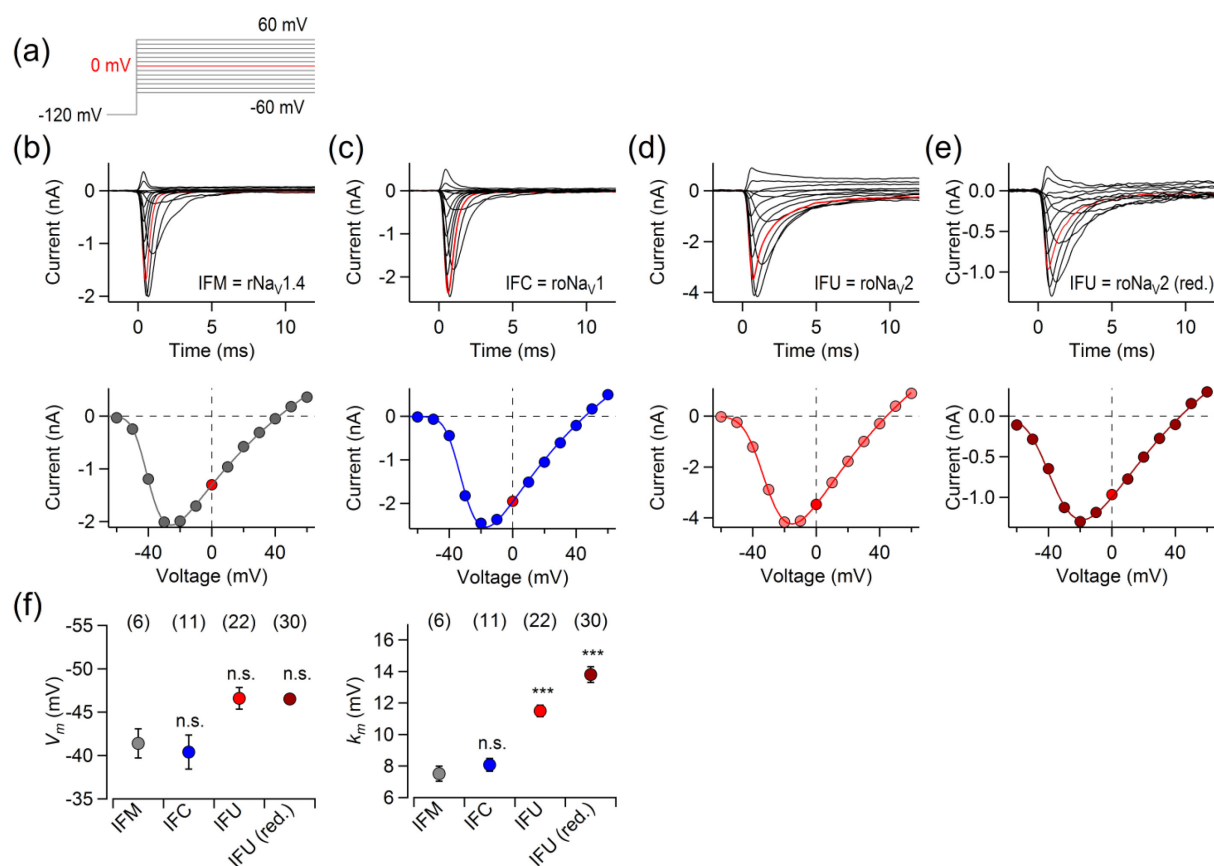


Figure 21: Voltage-dependent activation of wild-type Nav1.4 and mutant channels. (a) Pulse paradigm, red trace indicates 0 mV. (b-d) Representative current traces of indicated channels (upper) obtained in response to pulse paradigm. The current trace at 0 mV is shown in red. Current-voltage relationships with a superimposed GHK fit are shown in lower panel. (e) As in b-d, but for roNav₂ using a pipette solution supplemented with 1 mM TCEP. (f) Half-maximal activation voltage, V_m (left) and the corresponding voltage dependency, k_m (right) of indicated channels. Data in f are mean ± s.e.m. (n). A t-test for mutants (IFC and IFU) versus wild type (IFM) after the Bonferroni correction for multiple comparisons: ***, $P < 0.001$ and n.s., $P > 0.05$. (Ojha et al., 2017).

As illustrated in Fig. 22, wild type and roNav1 expressed in the absence of sodium selenate exhibited a V_m (rNav1.4: -40.5 ± 3.2 mV, $n=8$; $P=0.82$ and roNav1: -41.2 ± 2.6 mV, $n=11$; $P=0.79$) and the k_m (rNav1.4: 7.4 ± 0.9 mV, $n=8$; $P=0.38$ and roNav1: 7.8 ± 0.8 mV, $n=11$; $P=0.77$) similar to as it was for the respective channel when expressed in presence of sodium selenate. Thus, the presence of sodium selenate (300 nM) in the cell culture has no effect on the voltage-dependent channel activation of either wild-type rNav1.4 or roNav1.

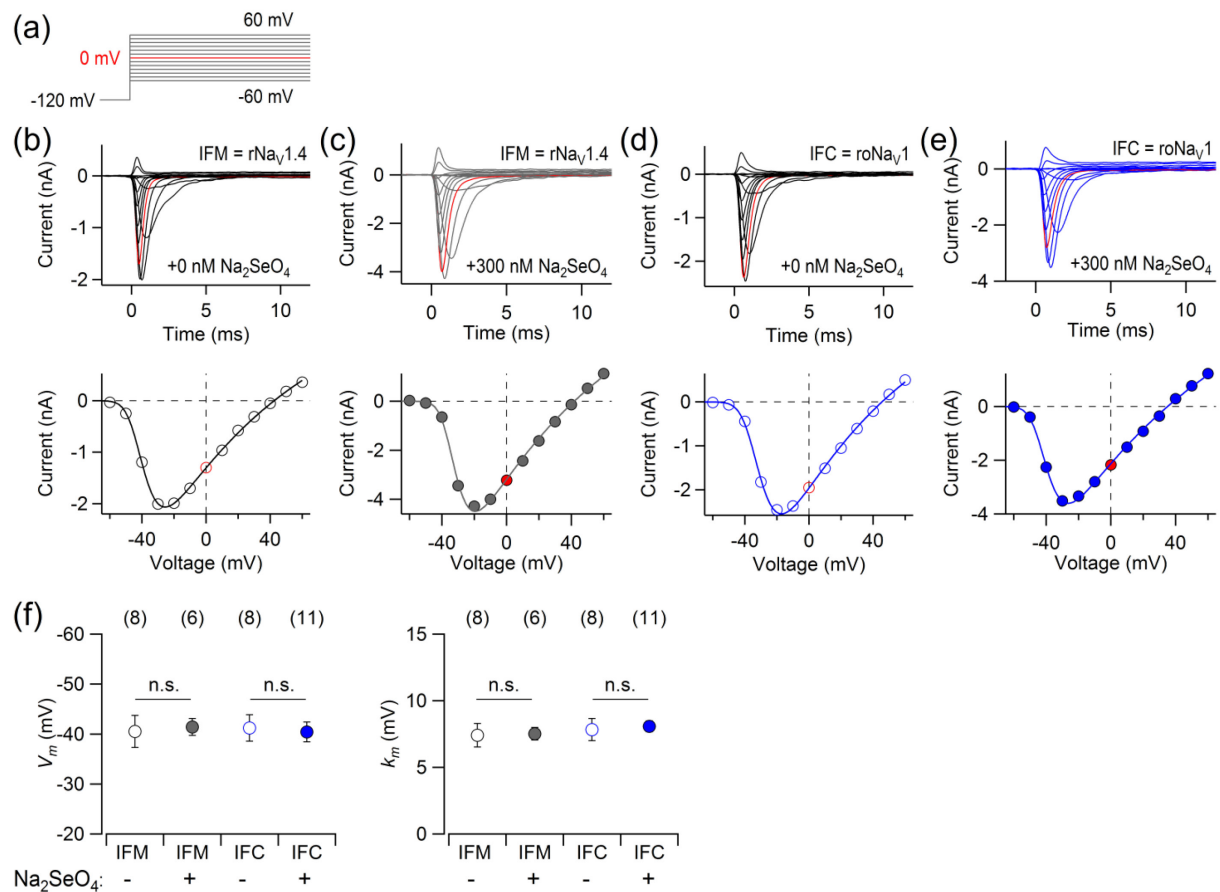


Figure 22: Influence of sodium selenate on voltage-dependent channel activation. (a) Pulse protocol. Red trace indicates 0 mV. (b-e) Current traces (upper) obtained from indicated channels, expressed either in the absence (0 nM) or presence (300 nM) of sodium selenate (Na_2SeO_4), in response to pulse paradigm as indicated in panel a. The current trace at 0 mV is shown in red. Peak currents as the function of voltage with a superimposed GHK fit (lower). (f) The half-maximal activation voltage, V_m (left) and the corresponding slope factor, k_m (right) of indicated channels in indicated cell culture condition. Data in f are mean \pm s.e.m. (n). Statistical t-test: n.s., $P > 0.05$.

3.3.2. Voltage-dependent channel inactivation

Na^+ channels inactivate during sustained membrane depolarization; this process involves occlusion of the channel pore by the inactivation motif. A Cys (roNav1) or a Sec (roNav2) in the inactivation motif may disturb this process. Therefore, inactivation parameters, such as the time constant (τ_h) of inactivation, steady-state inactivation, fractional recovery, half-maximal inactivation voltage (V_h), and the corresponding slope factor (k_h) of roNav1 and roNav2 were analyzed and compared with wild-type rNav1.4.

3.3.2.1. Residual steady-state current

Na^+ current was measured at a depolarizing pulse of -20 mV for 20 ms from a holding membrane potential of -120 mV and the residual steady-state current was analyzed at the end of the 20-ms depolarizing pulse relative to the peak current (Fig. 23a-c). A residual steady-

state current of roNav1 (2.6 ± 0.18 %, $n=24$; $P<0.001$) and roNav2 (12.6 ± 0.57 %, $n=37$; $P<0.001$) was significantly greater than that of wild type (1.7 ± 0.16 %, $n=12$). roNav1 (M→C) and roNav2 (M→U) exhibited about 1.5-fold and 7-fold, respectively, greater residual steady-state current than the wild type (IFM) (Fig. 23f).

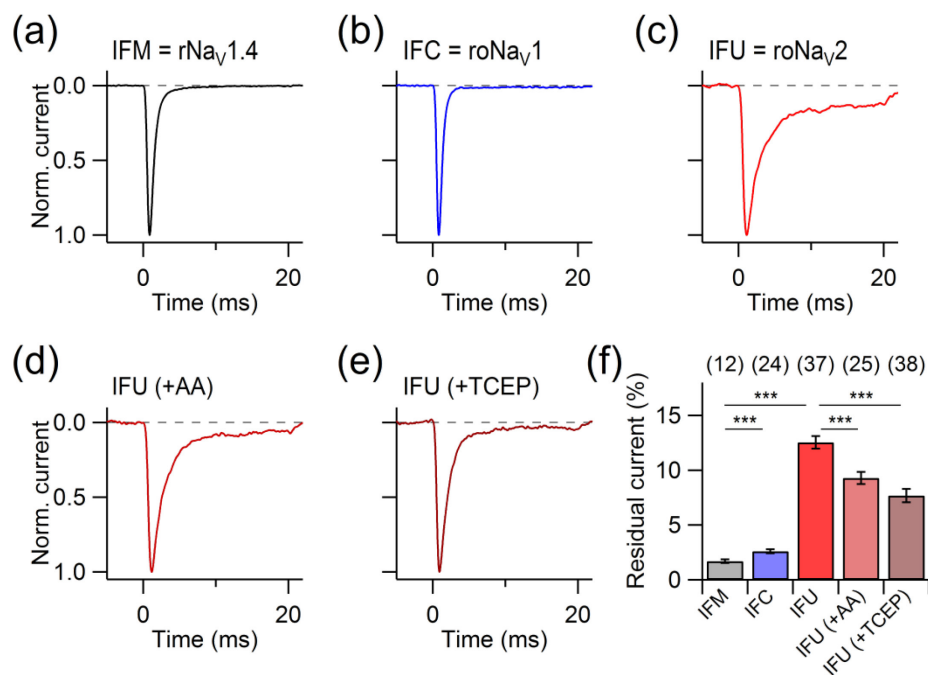


Figure 23: Residual steady-state current of rNav_v1.4, roNav_v1, and roNav_v2. (a-c) Normalized current responses of the indicated channels in response to a depolarization voltage -20 mV for 20 ms from a holding voltage of -120 mV. (d-e) The normalized current response of roNav_v2 in a reducing environment. Reducing conditions were accomplished by supplementing either ascorbic acid (AA; 2 mM) or TCEP (1 mM) to the patch pipette solution during whole-cell current measurement. (f) Percentage residual current at the end of the 20-ms depolarizing pulse relative to the peak current for the indicated constructs. Mean \pm s.e.m. (n in parentheses). t-test with post hoc Bonferroni correction for multiple comparisons: ***, $P\leq 0.001$.

Since the greater steady-state current of roNav1 in compared to wild type is an intrinsic property of roNav1 and it is not caused by the oxidative modification of the Cys residue in the inactivation motif (Ojha et al., 2014), inactivation of roNav2 was also measured in a reducing environment by either supplementing the pipette solution with TCEP (1 mM) or the general RS scavenger ascorbic acid (2 mM). While supplementation of ascorbic acid decreased the residual steady-state current of roNav2 by about 26% (9.3 ± 0.55 %, $n=25$; $P<0.001$), TCEP reduced the residual steady-state current of roNav2 by about 60% (7.7 ± 0.60 %, $n=38$; $P<0.001$) (Fig 23d-f). A partial decrease in the residual steady-state current of roNav2 in presence of either the reducing agent or the RS scavenger might indicate that the greater residual steady-state current of roNav2 has emerged because of the M→U mutation

as well as due to the oxidative modification of its inactivation motif. Noticeably, TCEP (1 mM) provided a stronger reducing environment for roNav2 than ascorbic acid (2 mM).

3.3.2.2. Inactivation kinetics

As shown in Fig. 24, the current was fit according to a Hodgkin-Huxley formalism for $m=3$ activation and $h=1$ inactivation gates to analyze time constant of channel inactivation (τ_h) and steady-state inactivation (h_{inf} or h_∞) of wild-type rNav1.4, roNav1, and roNav2 (Fig. 24a-d; black trace: current, red trace: fit). The mean time constants of inactivation (τ_h) were: rNav1.4, 0.29 ± 0.026 ms ($n=8$); roNav1, 0.51 ± 0.032 ms ($n=20$; $P<0.001$); roNav2, 1.2 ± 0.07 ms ($n=27$; $P<0.001$). Hence, inactivation kinetics of roNav1 was about 2.4-fold faster than the roNav2 and about 1.7-fold slower than the wild-type rNav1.4 at -20 mV. roNav2 exhibited about 4.2-fold slower inactivation kinetics than the wild type. Under reduced conditions (1 mM TCEP in the patch pipette) the inactivation time constant of roNav2 remained unchanged (1.2 ± 0.08 ms, $n=35$; $P=0.95$ with respect to “normal” conditions) (Fig. 24e, left). This might suggest that the slower inactivation kinetics of roNav2 is caused by the intrinsic property of Sec in the inactivation motif and not by its oxidative modification.

Steady-state inactivation (h_∞) of roNav1 (0.0048 ± 0.0007 , $n=20$; $P<0.01$) and roNav2 (0.056 ± 0.007 , $n=27$; $P<0.001$) were significantly differed from the wild-type rNav1.4 (0.0011 ± 0.00023 , $n=8$). Reduced condition (1mM TCEP) lowered h_∞ of roNav2 (0.03 ± 0.0034 , $n=35$; $P<0.001$), but it remained larger than for the wild type (Fig. 24e, right).

The time constant of inactivation and the steady-state inactivation of wild-type rNav1.4 (0.4 ± 0.06 ms and 0.0032 ± 0.0025 , $n=5$; $P=0.07$, 0.3) and roNav1 (0.45 ± 0.074 ms and 0.0036 ± 0.0006 , $n=6$; $P=0.22$, 0.18) were similar when channels were expressed in the absence of sodium selenate (Fig. 25).

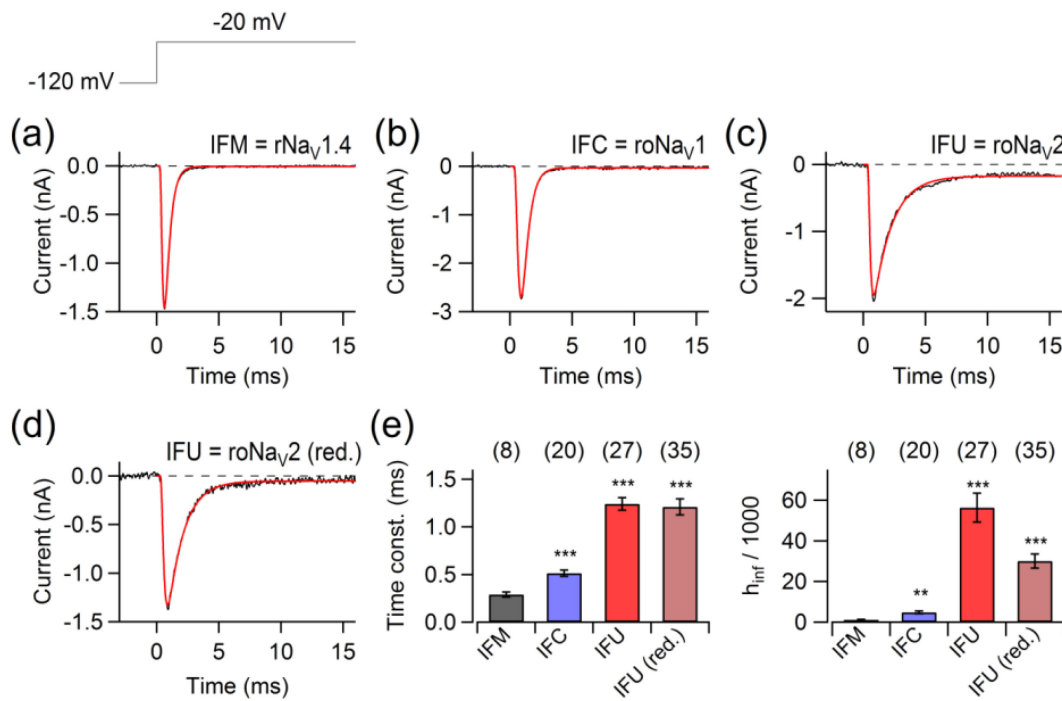


Figure 24: Inactivation kinetics and steady-state inactivation of Nav channels. (a-c) Representative current traces of the indicated channels in response to -20 mV (black) and superimposed fits according to a Hodgkin-Huxley formalism (red). (d) As in a-c, but for roNav_v2 using a pipette solution supplemented with 1 mM TCEP (e) Fit results: mean time constant of inactivation (τ_h) (left) and steady-state inactivation (h_{inf}) (right). Data are mean \pm s.e.m (n in parentheses). Statistical t-test for IFM (rNav_v1.4) vs. IFC (roNav_v1) and IFU (roNav_v2) after a post hoc Bonferroni correction: **, $P \leq 0.01$; ***, $P \leq 0.001$.

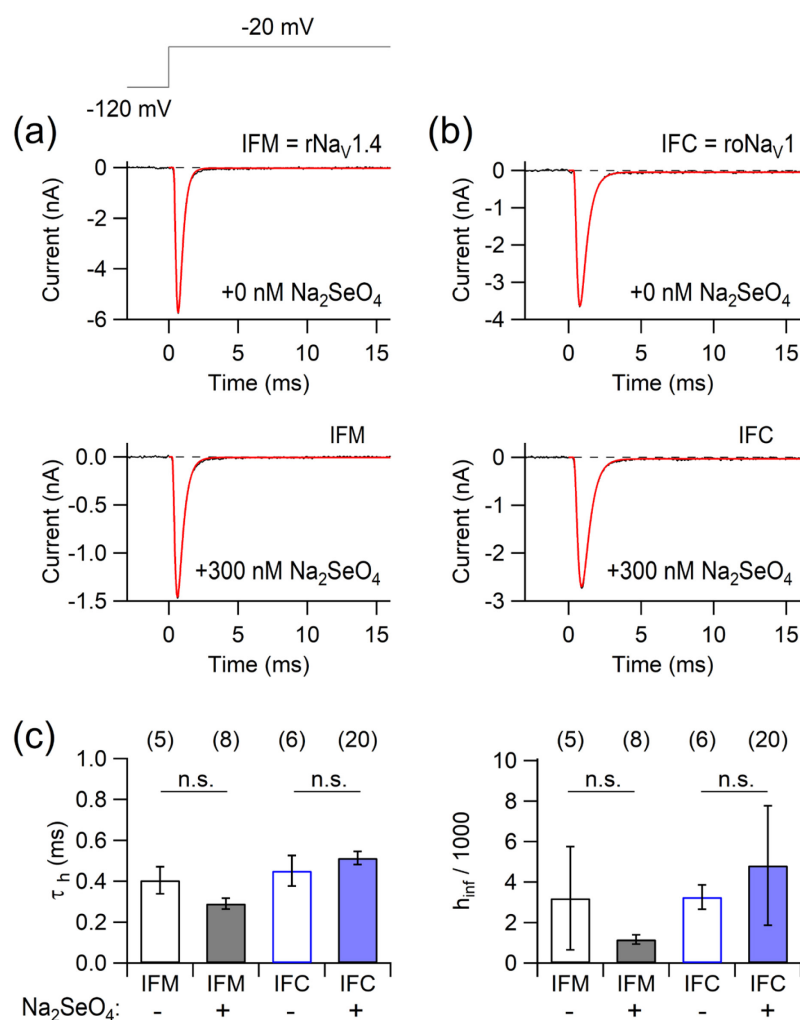


Figure 25: Influence of sodium selenate on inactivation kinetics and steady-state inactivation.

(a) Pulse protocol (top). Representative current traces of rNav1.4 expressed in the absence (middle) and presence (bottom) of 300 nM sodium selenate (Na₂SeO₄) (black) and superimposed fits according to a Hodgkin-Huxley formalism (red). (b) Current traces and fits as in a, but for mutant IFC (roNav1). (c) Fit results: time constant of inactivation (left) and steady-state inactivation (right) of the indicated constructs. Data are mean \pm s.e.m. (n in parentheses). Statistical t-test: n.s., $P > 0.05$.

3.3.2.3. The half-maximal inactivation voltage and the corresponding slope factor

To determine the half-maximal inactivation voltage (V_h) and the corresponding slope factor (k_h), channel-expressing cells were conditioned for 500 ms at voltages ranging from -120 mV to 45 mV in steps of 5 mV, every 10 s from a holding membrane voltage of -120 mV (Fig. 26a-d). Subsequently, the peak current monitored at -20 mV after conditioning was normalized to the peak current obtained at -20 mV before conditioning. Normalized peak current was plotted as a function of conditioning voltage and analyzed with the global fit procedure and a two-component Boltzmann function (Fig. 26e). The first component of the half-maximal inactivation voltage (-93.5 ± 0.5 mV), V_{h1} , and the corresponding slope factor (5.98 ± 0.20 mV), k_h , for both components (V_{h1} and V_{h2}) were constrained for all variants.

Subsequently, V_{h2} and the fractional contributions of the component were fit individually. The mean V_{h2} and fractional contribution of the component for wild-type rNav1.4 was: -75.7 ± 0.6 mV and $5.0 \pm 3.4\%$ (n=5), for roNav1: -66.5 ± 0.4 mV and $11.7 \pm 1.7\%$ (n=5), for roNav2: -56.8 ± 0.7 mV, and $51.8 \pm 1.3\%$ (n=14), and for roNav2 under reducing conditions (1 mM TCEP): -62.7 ± 0.7 mV and $45.6 \pm 1.6\%$ (n=17). These results showed that fractions of channels that inactivated at relatively less negative voltage i.e., percentage fractional contributions of V_{h2} were increased in roNav1 and roNav2 compared to the wild-type rNav1.4 (Fig. 26e). roNav2 inactivation exhibited two half-maximal inactivation voltages, V_{h1} and V_{h2} , each contributed about 50% to the process. Fractions of roNav2 channels that exhibited a relatively less negative half-maximal inactivation voltage (V_{h2}) were decreased (about 6%) when measurements were performed with 1 mM TCEP in the patch pipette solution. Moreover, relatively larger fractions V_{h2} might indicate that roNav2 inactivates different from roNav1 and wild type.

Since V_h and k_h of channels were analyzed while channels were transiently expressed in presence of sodium selenate (300 nM), the influence of sodium selenate on voltage-dependence of inactivation of roNav1 and wild type was further investigated. Wild type and roNav1 were expressed in presence and absence of sodium selenate in the culture medium and measurements were performed by a procedure as described in this section earlier. The normalized peak current plotted versus the conditioning voltage was described with a Boltzmann function. As shown in Fig. 27, a Boltzmann function perfectly fit to the data and produced half-maximal inactivation voltage (V_h) for rNav1.4: -76 ± 1.92 mV (n=6, control) and -74 ± 1.85 mV (n=9, with 300 nM sodium selenate; P=0.46), roNav1: -71 ± 1.89 mV (n=9, control) and -67.7 ± 1.16 mV (n=6, with 300 nM sodium selenate; P=0.14) (Fig. 27d, left). Mean k_h for rNav1.4: 5.7 ± 0.21 mV (n=6, control) and 5.38 ± 0.14 mV (n=9, with 300 nM sodium selenate; P=0.2), for roNav1: 5.85 ± 0.48 (n=9, control) and 6.9 ± 0.53 (n=6, with 300 nM sodium selenate; P=0.17) (Fig. 27d, right). These results clearly indicate sodium selenate (300 nM) in the culture media does not affect the voltage-dependence of channel inactivation. Data clearly indicate that sodium selenate (300 nM) in the culture medium did not affect the voltage dependence of roNav1 and rNav1.4 inactivation.

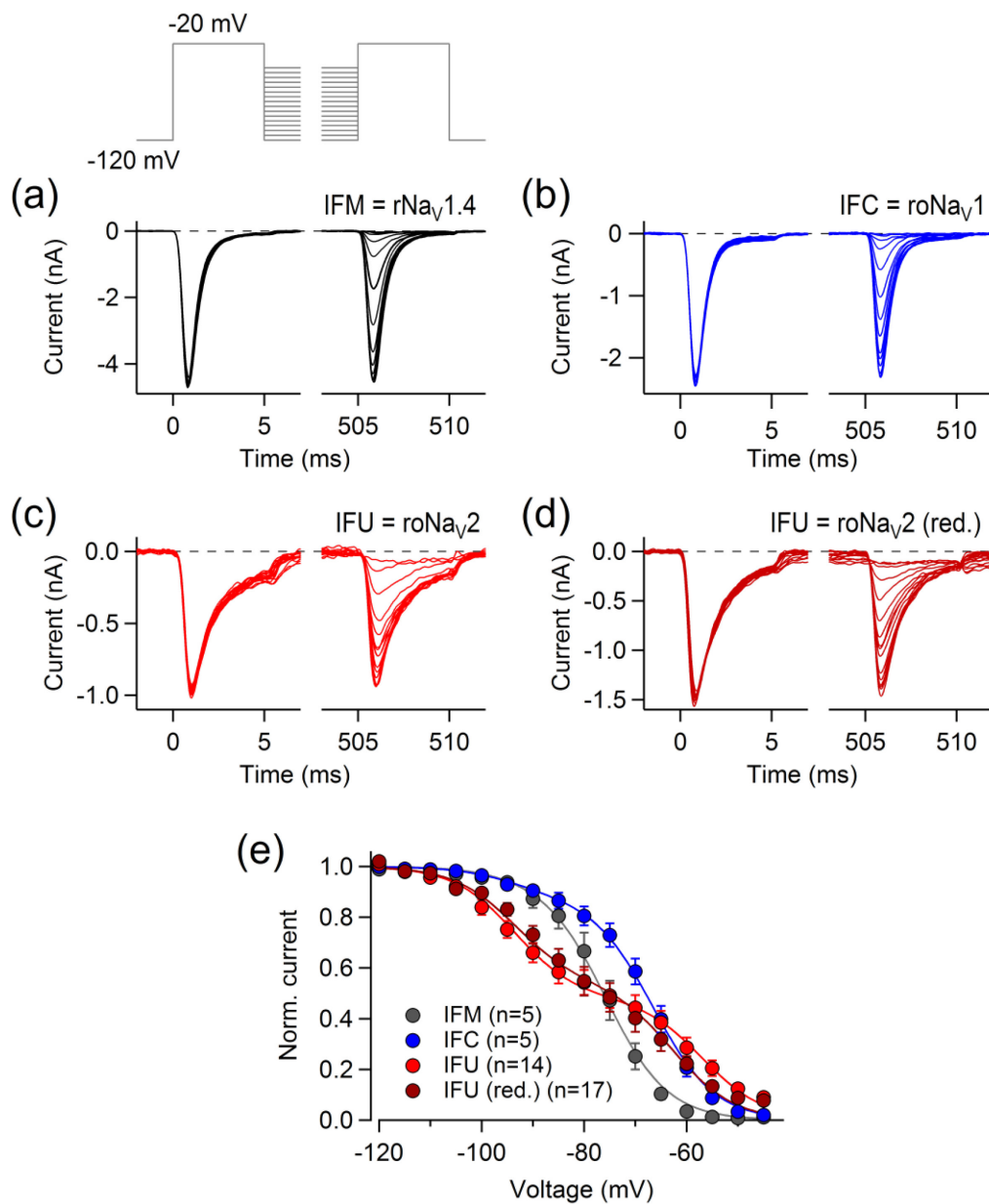


Figure 26: Voltage-dependence of inactivation. (a) Pulse protocol (top) and superimposed sample data for the assessment of the voltage dependence of inactivation of wild-type $rNav_{1.4}$; the interpulse intervals lasted 500 ms (bottom). (b-d) As in (a) (bottom), but for indicated channels. (e) Normalized peak current as a function of conditioning voltage with superimposed global fits according to a two-component Boltzmann function. Data in e are mean \pm s.e.m with n indicated in parentheses.

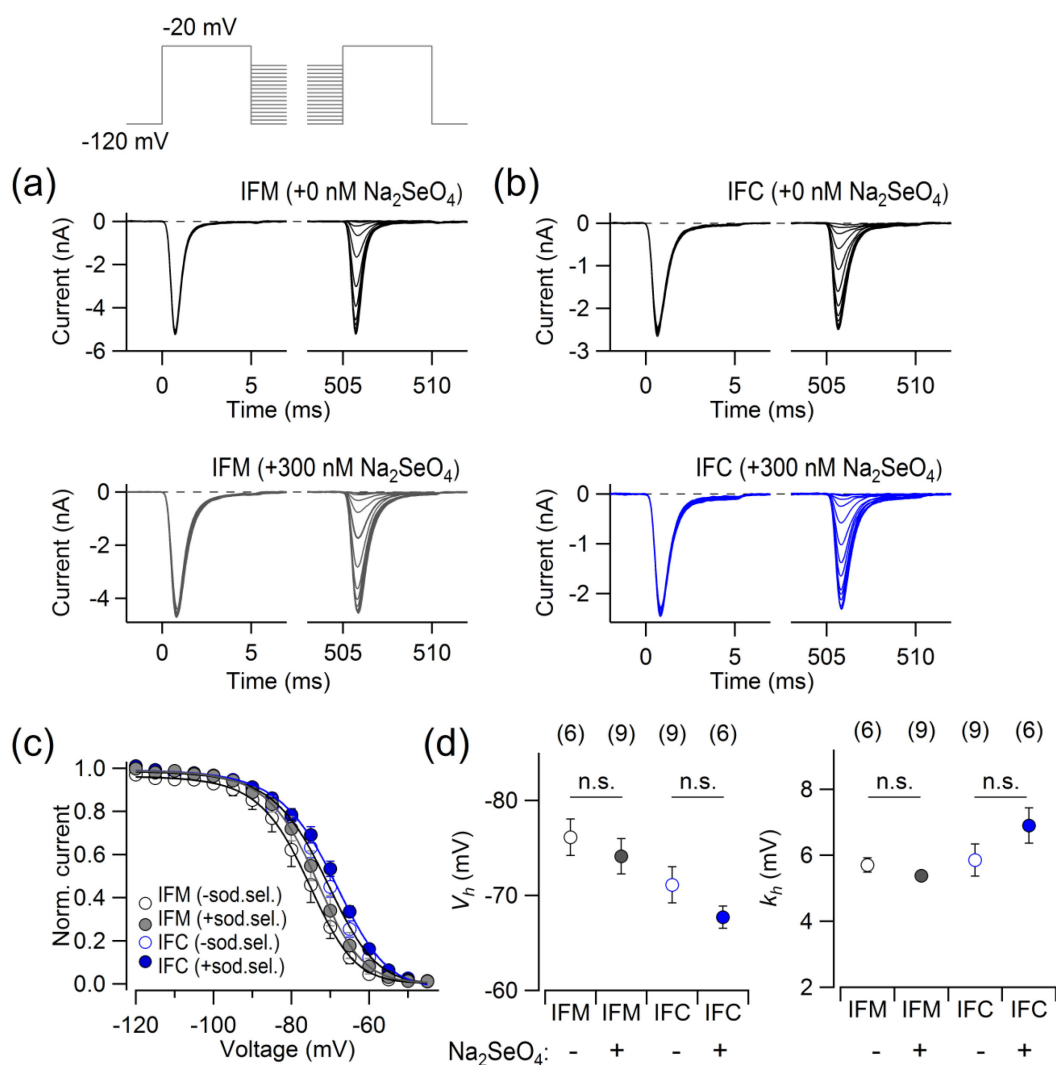


Figure 27: Influence of sodium selenate (300 nM) on voltage-dependence of inactivation. (a) Pulse protocol (top) and superimposed sample data for the assessment of the voltage dependence of inactivation of rNav1.4; the interpulse intervals lasted 500 ms (bottom). The presence and absence of sodium selenate in the cell culture is indicated. (b) As in a (bottom), but for roNav1. (c) Normalized current as the function of conditioning voltage with superimposed fits according to a Boltzmann function. (d) Mean V_h and mean k_h of indicated constructs. Presence (+) and absence (-) of sodium selenate in the cell culture media is shown. Data in c and d are mean \pm s.e.m (n is shown in parentheses). Statistical t-test: n.s., $P > 0.05$.

3.3.2.4. The time course of fractional recovery from inactivation

Transfected cells were depolarized to -20 mV for 10 ms from a holding potential of -100 mV to obtain a reference peak current. Subsequently, peak currents were measured at -20 mV from a holding potential of -100 mV in varying duration. The starting duration (0.2 ms) of depolarizing voltage was increased by a factor of 2 in every step until channels recover completely (Fig. 28). The peak currents monitored at varying duration of depolarizing pulse (-20 mV) were normalized with the reference peak and plotted against the time. Data were fit

with a double-exponential function and the time constant of recovery from inactivation was determined (Fig. 28e).

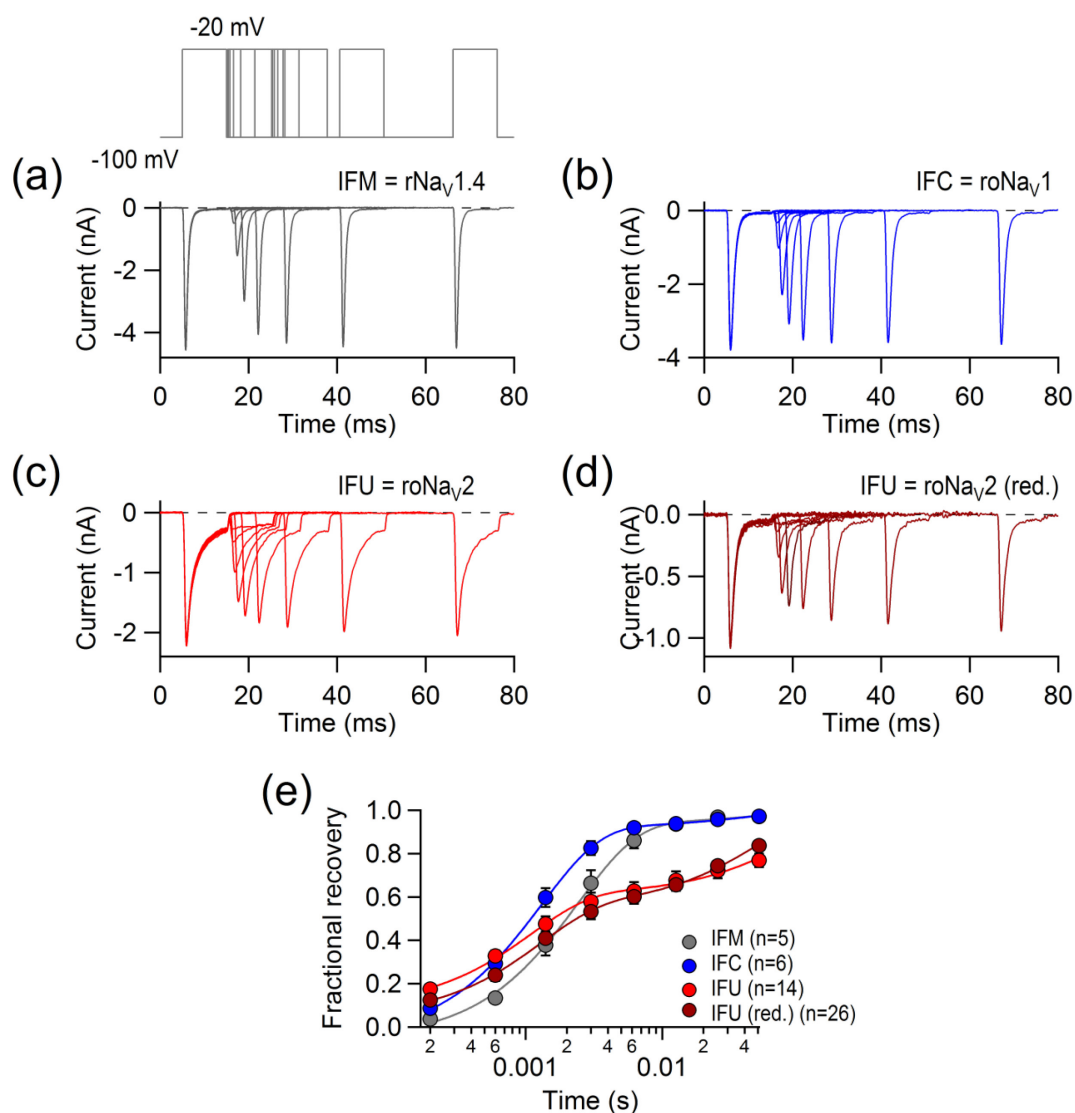


Figure 28: Fractional recovery from inactivation. (a) Pulse protocol (top) and sample current traces for the assessment of the time course of recovery from inactivation of rNav_v1.4 (bottom). (b-c) As in a, but for indicated constructs. (d) As in a, but for roNav_v2 in the presence of 1 mM TCEP in the patch pipette solution. (e) Fractional recovery as a function of the interpulse interval with superimposed double-exponential fits. Data are in mean \pm s.e.m. (n).

Fit of the data yielded two time constants and the fractional distribution of the fast component for each variant. Thus, for wild-type rNav_v1.4: 2.65 ± 0.27 ms, 96 ± 283 ms (94.2 ± 4.1 %, n=5), roNav_v1: 1.45 ± 0.12 ms, 59 ± 66 ms (93.2 ± 2.7 %, n=6), roNav_v2: 1.21 ± 0.13 ms, 92.8 ± 16.6 ms (56.4 ± 1.9 %, n=14), and roNav_v2 in reduced condition (1 mM TCEP): 1.34 ± 0.95 ms, 50.0 ± 3.8 ms (52.9 ± 1.4 %, n=26). Results showed that more than 90% of rNav_v1.4 and roNav_v1 channels recover from the inactivation with a rapid rate, while only about 50% of

roNav2 channels recover rapidly. Reduced condition marginally affects the recovery rate of roNav2 (Fig. 28e).

As illustrated in Fig. 29, sodium selenate (300 nM) in the cell culture media did not affect the rapid recovery of wild-type rNav1.4 and roNav1 from inactivation. Normalized peak currents as the function of time were appropriately fit with a single-exponential function and yielded the time constant of recovery from inactivation for each channel construct: rNav1.4: 2.5 ± 0.4 ms ($n=6$, control) and 2.4 ± 0.2 ms ($n=9$, with sodium selenate; $P=0.86$), and for roNav1: 1.6 ± 0.2 ms ($n=9$, control) and 1.5 ± 0.1 ms ($n=6$, with sodium selenate; $P=0.59$) (Fig. 29c,d).

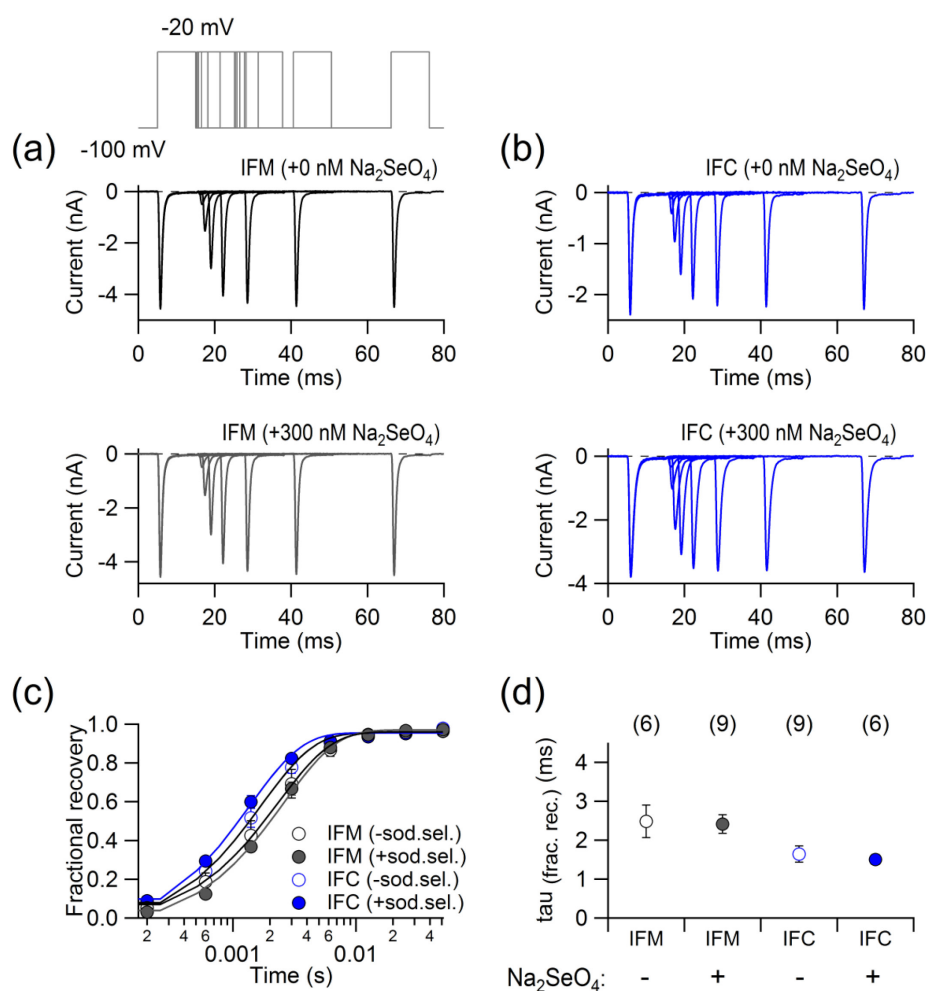


Figure 29: Influence of sodium selenate on fractional recovery. (a) Pulse protocol (top) and sample current traces for the assessment of the time course of fractional recovery of rNav1.4. The presence and absence of sodium selenate in the cell culture is indicated. (b) As in a, but for roNav1. (c) Fractional recovery as a function of the interpulse interval with a superimposed single-exponential fit of indicated channels. Presence or absence of sodium selenate (300 nM) in the cell culture is indicated. (d) Time course of fractional recovery of indicated constructs. Supplementation of sodium selenate in the cell culture is shown. Data are in mean \pm s.e.m. (n is indicated).

3.4. The response of roNav1 and roNav2 to endogenous redox stimuli

Varieties of RS are continuously produced in living cells as by-products of aerobic metabolism. To some extent, some of them act as signaling molecules whereas excessive production may have deleterious consequences. Endogenous RS concentration, chemical properties of RS, and the nature of microenvironment dictate RS functions in the living system. A precise spatio-temporal assessment of endogenous RS is clearly demanded to understand molecular mechanisms of RS-mediated cellular function.

Na⁺ channels are membrane proteins and an oxidation-mediated change in Na⁺ current can be monitored with high spatio-temporal resolution and accuracy. Thus, we hypothesized that the oxidation sensitivity of Na⁺ channel mutants with Cys (roNav1) and Sec (roNav2) might serve as smart tools to monitor membrane-delimited RS.

3.4.1. The response of roNav1 and roNav2 to basal redox status of HEK 293T cells

The oxidative modification(s) of amino-acid residues in the inactivation motif of Nav has a strong impact on the channel inactivation as it leads to a greater non-inactivated current component (Kassmann et al., 2008). Hence, the ratio of the non-inactivated current component and the peak current of the channel produces a ratiometric signal (R_I : $I_{\text{steady-state}}/I_{\text{peak}}$), which may allow monitoring the relative change in cellular RS levels.

To investigate the response of channels to the variable ambient intracellular milieu under control conditions, channel-expressing cells were grown under identical culture conditions. Transfected cells were depolarized to -20 mV for 20 ms from a holding voltage of -120 mV and the ratio (R_I) of the non-inactivating component at 5 ms after depolarization ($I_{5\text{ms}}$) and the peak current (I_P) was analyzed for wild type, roNav1, and roNav2 (Fig. 30a-c). The mean R_I with standard deviation (s.d.) assessed for wild-type rNav1.4: 0.0079 ± 0.0034 (n=20), roNav1: 0.024 ± 0.0062 (n=20; $P < 0.001$), and roNav2: 0.15 ± 0.068 (n=20; $P < 0.001$) (Fig. 30d) demonstrated that all channels exhibited variability in their R_I . The variability in R_I of roNav2 was about 16-fold larger than rNav1.4 and about 9-fold larger than roNav1. roNav1 exhibited about 2-fold greater variability in R_I in compared to the wild type. Notably, all channels showed variability in their early inactivation phase (current before ~ 5 ms), however, roNav1 and roNav2 showed greater variability in their steady-state inactivation ($I_{5\text{ms}}$) in compared to the wild type.

Further, a relative variability in R_I of channels (rNav1.4: 0.43, roNav1: 0.26, and roNav2: 0.45) under control condition indicated that the inactivation of channels might be sensitive to the variable intracellular milieu. The non-inactivating current component of roNav2 was diminished when measurements were performed in reduced condition (see

section 3.3.2.1), which indicates the variability in R_I of the channel might originate from the variable endogenous redox milieu under control condition.

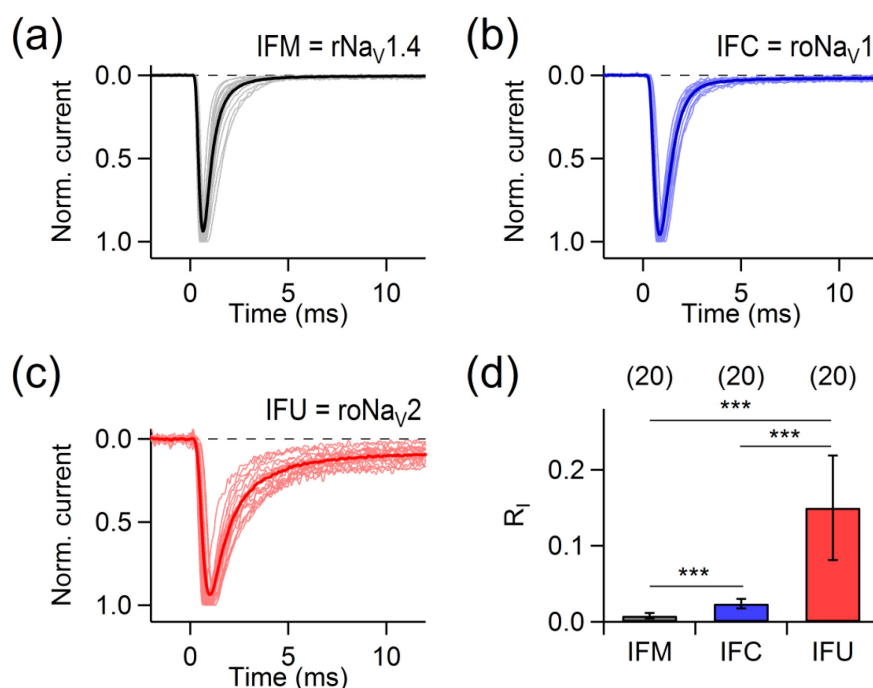


Figure 30: The inactivation of channel variants is sensitive to endogenous redox milieu. (a-c) Normalized current traces monitored at -20 mV from a holding voltage -120 mV of the indicated Nav channels expressed in HEK 293T cells. In each, 20 traces from different cells are superimposed (light); the thick traces indicate means. (b) Mean relative non-inactivated current 5 ms after depolarization to -20 mV, $R_I: I_5/I_p$. Data are mean \pm s.d. (n indicated in parentheses). Statistical t-test: ***, $P \leq 0.001$. (Modified from Ojha et al., 2017)

Additionally, redox-sensitive fluorescent proteins (rFPs), cytosolic roGFP2 (Dooley et al., 2004) and the GSH-dependent cytosolic redox sensor, Grx1-roGFP2 (Gutscher et al., 2008) indicated that cells cultured under control condition exhibited variable endogenous redox environment. Under control condition, the mean ratio of fluorescence (F_{400}/F_{470}) \pm s.d. was analyzed for roGFP2: 0.026 ± 0.0016 (n=20) and Grx1-roGFP2: 0.035 ± 0.0029 (n=20) (Fig. 31). The variability in fluorescence ratio of Grx1-roGFP2 was about 0.08, while it was 0.06 for roGFP2. The results indicate that the cells are heterogeneous with respect to the basal oxidation level.

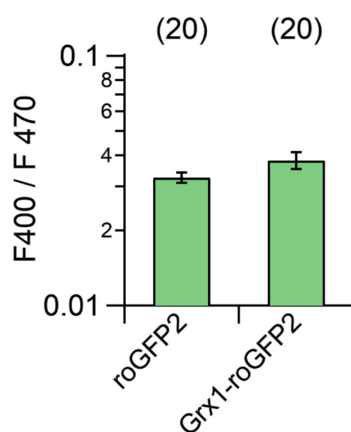


Figure 31: Mean fluorescence ratio (F400/F470) of roGFP2 and Grx1-roGFP2 measured from control cells. Data are mean \pm s.d. (n).

3.4.2. Detection of mitochondrial reactive oxygen species

It is evident that elevated glucose uptake by the cell produces excess mitochondrial reactive oxygen species (mtROS), such as superoxide (O_2^-) and hydrogen peroxide, which can contribute to clinical conditions, for instance, diabetes and cardiovascular risks (Li et al., 2013). Here, changes in intracellular RS by elevated glucose were monitored with roNav1 and roNav2 and the response of these channels were compared with the readouts of fluorescent redox reporters.

3.4.2.1. The response of mutant channels to mtROS

roNav1 and roNav2 expressing cells were cultured in Dulbecco's Modified Eagle's Medium (DMEM) and Ham's F-12 Nutrient Mixture containing 5.5 mM (low) and 25 mM glucose (high) to affect endogenous RS production. Transfected cells were depolarized to -20 mV for 20 ms from a holding voltage of -120 mV and the ratio (R_I : I_{10}/I_P) of the non-inactivating component at 10 ms after depolarization (I_{10}) and peak current (I_P) was determined for roNav1 and roNav2 expressed in the presence of low and high glucose. A mean R_I was analyzed for roNav1: 0.019 ± 0.0024 (n=13, with 5.5 mM glucose) and 0.018 ± 0.0011 (n=10, with 25 mM glucose; $P=0.65$); for roNav2: 0.10 ± 0.0059 (n=32, with 5.5 mM glucose) and 0.23 ± 0.018 (n=27, with 25 mM glucose; $P<0.001$) (Fig. 32b-c). Results demonstrated that the mean relative non-inactivating current fraction (R_I) of roNav2 was about 2-fold larger in high glucose (25 mM) compared to low glucose (5.5 mM), however, a variation of the glucose level did not affect R_I of roNav1. Treatment of cells with the mitochondrial uncoupler BAM15 (5 μ M) that does not depolarize the plasma membrane (Kenwood et al., 2014) reversed the increased R_I of roNav2 ($R_I=0.13 \pm 0.024$, n=23; $P<0.05$ versus vehicle control). DMSO (0.1 %) as a vehicle for BAM15 did not affect the response of roNav2 to high glucose ($R_I=0.25 \pm 0.049$, n=15, $P=0.93$ versus high glucose) (Fig. 32b). The

reversibility in R_I of roNav2 in the presence of BAM15 clearly indicated that the high-glucose-mediated increase in R_I of roNav2 appeared due to mtROS.

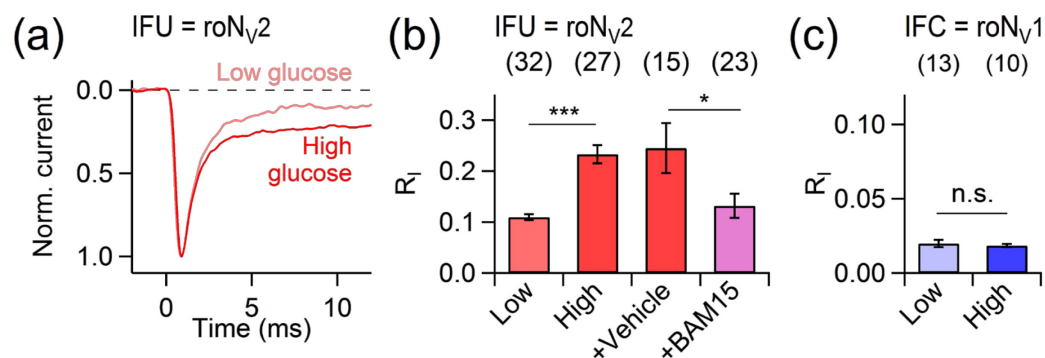


Figure 32: The response of roNav1 and roNav2 to elevated glucose uptake. (a) Superposition of two sample current traces at -20 mV from cells expressing roNav2, cultured in medium with low (5.5 mM) and high (25 mM) concentrations of glucose. (b) Mean R_I of roNav2 for low (light red) and high glucose (red); “+Vehicle” refers to the application of 0.1% DMSO in presence of high glucose, “+BAM15” refers to cells cultured in high-glucose medium in the presence of 5 μ M of the mitochondrial un-coupler, BAM15. (c) Mean R_I for roNav1 in response to low and high glucose conditions. Data in b and c are mean \pm s.e.m. with n indicated in parentheses. Statistical t-test with Bonferroni post hoc correction: ***, $P \leq 0.001$; *, $P \leq 0.05$; n.s., $P > 0.05$. (Ojha et al., 2017)

3.4.2.2. The response of fluorescent redox reporters to mtROS

roGFP2 and Grx1-roGFP2 expressing cells were grown in cell culture media containing 5.5 mM glucose (low) and 25 mM glucose (high) and the change in fluorescence ratio (F400/F470) of both sensors were analyzed to investigate redox changes mediated by elevated glucose. A means fluorescence ratio (F400/F470) was analyzed for roGFP2: 0.042 ± 0.0012 (n=21, with 5.5 mM glucose) and 0.039 ± 0.0018 (n=24, with 25 mM glucose, $P=0.12$); for Grx1-roGFP2: 0.039 ± 0.0017 (n=34, with 5.5 mM glucose) and 0.11 ± 0.0067 (n=27, with 25 mM glucose; $P < 0.001$) (Fig. 33a,b). Results showed that variations of the glucose level did not alter the signal of cytosolic roGFP2. However, fluorescence ratio of cytosolic Grx1-roGFP2 was about 3-fold higher in high glucose compared to low glucose. Further, treatment of cells with mitochondrial un-coupler, BAM15 (5 μ M), reversed the increased signal of Grx1-roGFP2 to low glucose level (0.068 ± 0.0032 , n=33; $P < 0.001$ versus high glucose) (Fig. 33a). The reversibility of the ratiometric signal of Grx1-roGFP2 in the presence of BAM15 indicated that elevated glucose-mediated production of excess mtROS disturbs cellular redox milieu and these changes were sensed by membrane proteins, such as ion channels.

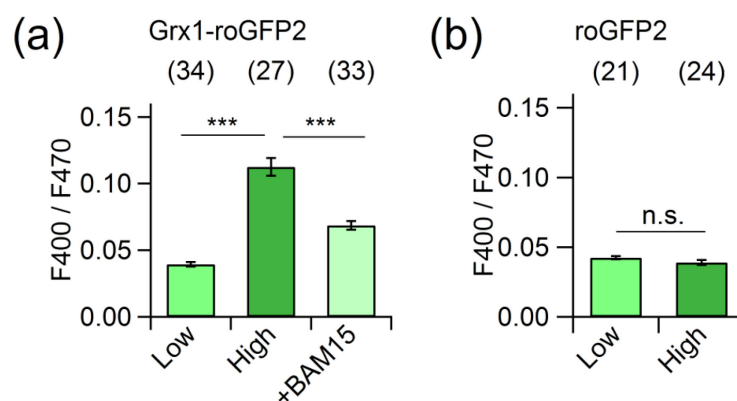


Figure 33: The response of fluorescent redox reporters to elevated glucose uptake. (a) Mean fluorescence ratios (400 nm/470 nm) of Grx1-roGFP2 expressed in cells treated with low (5.5 mM) and high (25 mM) glucose, “+BAM15” refers to cells cultured in high-glucose medium in the presence of 5 μ M of the mitochondrial uncoupler, BAM15. (e) Mean fluorescence ratios (400 nm/470 nm) of roGFP2 expressed in cells cultured in low and high glucose media. Data are mean \pm s.e.m. (n). Statistical t-test: ***, $P \leq 0.001$; n.s., $P > 0.05$. (Ojha et al., 2017)

3.5. The response of roNav1 and roNav2 to exogenous redox stimuli

Spatio-temporal monitoring of RS and understanding of the eventual role of a particular RS in cell physiology is extremely difficult. Interactions of a specific RS to varieties of other cellular RS and to antioxidant enzymes makes the situation extremely complex for investigating the precise role of an explicit RS in living cells. Therefore, extracellular application of stressor suits well to understand solely effect of a particular stressor in physiology or pathology (Stone & Yang, 2006). Here, we examined the potential usefulness of roNav1 and roNav2 in monitoring oxidative modification mediated by the extracellular stressors, chloramine T (ChT) and hydrogen peroxide (H_2O_2). The responses were compared with the sensitivity of redox-sensitive fluorescent proteins.

3.5.1. The response of roNav1 to chloramine T

Transfected cells were depolarized to -20 mV for 20 ms from a holding membrane voltage -120 mV, every 10 s. After control measurements for 100 s, 50 μ M ChT was extracellularly applied by exchanging the entire bath volume and inactivation loss of roNav1 was measured. Subsequently, a relative non-inactivating current fraction (R_I : I_s/I_p) of the channel was plotted as a function of time and was fit according to a single-exponential function to yield the time constant of R_I change. As illustrated in Fig. 34b, while the wild-type channel responded very slow with a mean time constant of R_I change: 1406 ± 33 s ($n=5$), roNav1 responded about 11-fold faster (128 ± 35 s, $n=4$) to 50- μ M ChT-induced chemical modifications.

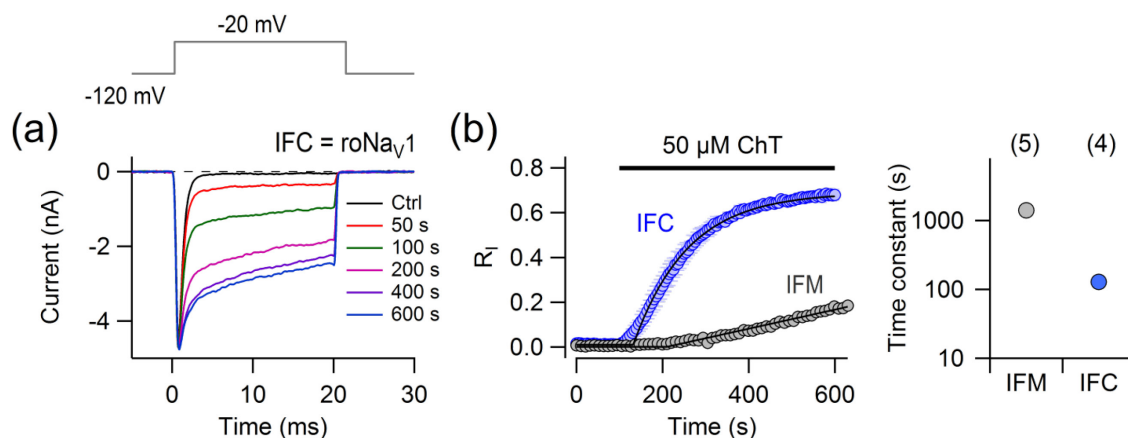


Figure 34: The response of roNav1 (IFC) and rNav1.4 (IFM) to chloramine T. (a) Pulse protocol (top). Superimposed current traces of roNav1 in response to extracellular application of 50 μ M ChT are shown at the indicated time point (bottom). (b) The mean relative non-inactivating current fraction (R_I) of indicated channels as the function of time and superimposed single-exponential fit (left). Mean time constant of change in R_I of indicated channels in response to 50 μ M ChT (right). Data in b are mean \pm s.e.m.(n).

As shown in Fig. 35a, inactivation of roNav1 was removed by short exposure to 5 μ M ChT, thereafter, the bath was washed with extracellular saline for about 1500 s that did not restore the inactivation of roNav1 and ChT-induced removal of inactivation remain persisted. However, extracellular application of saline containing 1 mM DTT completely restored the inactivation loss of roNav1. A single-exponential fit of the recovery phase yielded a time constant of complete inactivation recovery: 1043 ± 48 s ($n=3$) (Fig. 35b). Additionally, the response of roNav1 to 3 μ M ChT was monitored under control conditions and with the non-specific RS scavenger ascorbic acid (2 mM) supplemented with the patch pipette solution. In both conditions, the kinetics of inactivation loss was determined by a linear function (Fig. 35c). Thus, a mean slope was obtained for inactivation loss of roNav1 in response to 3 μ M ChT application under control condition ($70.3 \pm 1.16 \cdot 10^{-5}/s$, $n=7$) and in presence of intracellular 2 mM ascorbic acid ($7.74 \pm 0.44 \cdot 10^{-5}/s$, $n=5$). Results showed that intracellular supplement of ascorbic acid (2 mM) diminished the effect of extracellular applied 3 μ M ChT by 10-fold as the linear slope was changed by a factor of 0.110 ± 0.007 . Hence, a diminished inactivation removal of roNav1 in presence of intracellular ascorbic acid and a complete restoration of inactivation loss due to extracellular applied DTT, both confirmed that inactivation of roNav1 was responsive to ChT-induced redox processes.

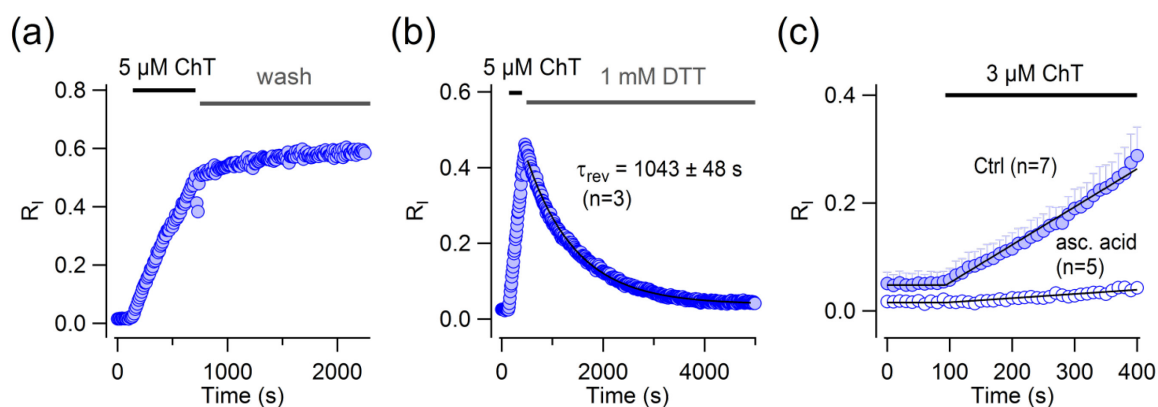


Figure 35: Reversibility of roNav1. (a) A representative experiment showing the ChT-induced inactivation removal of roNav1 persisted when ChT was washed out. (b) A representative experiment showing the ChT-induced inactivation removal was restored upon application of bath solution containing DTT (1 mM). A superimposed single-exponential fit (black line) is shown that yielded the indicated time constant of recovery upon DTT application. (c) Application of 3 μM ChT under control conditions and with 2 mM ascorbic acid supplemented to the pipette solution. The superimposed curves are linear functions starting at the beginning of ChT application. (Modified from Ojha et al., 2014).

3.5.2. Redox sensitivity comparison of roNav1 with roGFP2

The sensitivity of roNav1 and roGFP2 to ChT-induced redox changes was compared by co-expressing both in HEK 293 cells and measuring Na^+ currents in the whole-cell configuration in parallel to recording fluorescence of the same cell. The transfected cells were depolarized to -20 mV for 20 ms from a holding voltage -120 mV and the step was repeated every 1 s. Simultaneously, the same cell was illuminated with two wavelengths 400 nm and 475 nm, 20 ms each (Fig. 36a) and the response of roGFP2 and roNav1 to extracellular applied 50 μM ChT was monitored. Subsequently, ratiometric readouts of roNav1 ($R_i: I_{10}/I_p$) and roGFP2 ($rF: F_{400} / F_{475}$) were plotted as the function of time. Ratio changes within the initial 20 s upon stimulation with 50 μM ChT were fit with a linear function. Thus, a mean slope of ratios were determined for roNav1: $0.0177 \pm 0.0026 / \text{s}$ ($n=6$) and for roGFP2: $0.0016 \pm 0.0003 / \text{s}$ ($n=6$; $P=0.0015$) (Fig. 36b). Hence, the ratiometric RS-related signal derived from roNav1 responds about 10-times faster to ChT application than the roGFP2.

As illustrated in Fig. 36b, while the roNav1 signal was stable before the ChT (50 μM) application, roGFP2 signal was slightly increased. The overall dynamic range of roNav1 signal was about 0.8, while that of roGFP2 was only 0.2. Both signals saturated after about 100-200 s.

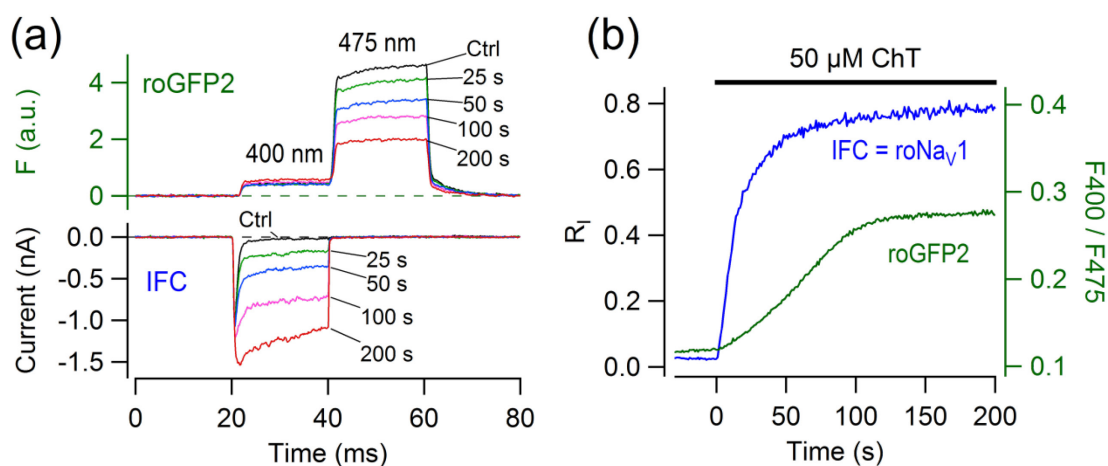


Figure 36: Comparison of roNav₁ (IFC) with roGFP2. (a) Raw data traces of single-cell fluorescence with excitation pulses at 400 and 475 nm (top) and current responses at -20 mV of the same cell (bottom) expressing roNav₁. Data were recorded before (Ctrl) and after application of 50 μ M ChT to the bath solution. Time of measurement is indicated. (b) Time courses of the loss of inactivation (blue) and the ratio F400/F475 (green) of roGFP2 fluorescence in response to 50- μ M ChT application. (Modified from Ojha et al., 2014).

3.5.3. The response of roNav₂ to chloramine T

Anticipating a high sensitivity of roNav₂ to redox modifications in compare to roNav₁, the response of roNav₂ to ChT concentrations at 3 μ M, 1 μ M, and 0.5 μ M were monitored. After monitoring a control current response for 100 s, ChT was acutely applied and changes in non-inactivating current fraction were monitored. Subsequently, a relative non-inactivating current fraction (R_I : I_{10}/I_p) was plotted as the function of time and fit according to a single-exponential function (Fig. 37a). Thus, a mean time constant of R_I change of roNav₂ was analyzed in response to ChT application at a concentration of 3 μ M: 222 ± 54 s ($n=10$), 1 μ M: 308 ± 58 s ($n=10$), and 0.5 μ M: 316 ± 88 s ($n=5$) (Fig. 37b). Results demonstrated that roNav₂ safely detects ChT at sub-micromolar concentration-induced modifications. The overall dynamic range of roNav₂ in detecting 3 μ M ChT-induced modification was about 0.4, while it was about 0.3 for 1 μ M and 0.5 μ M ChT.

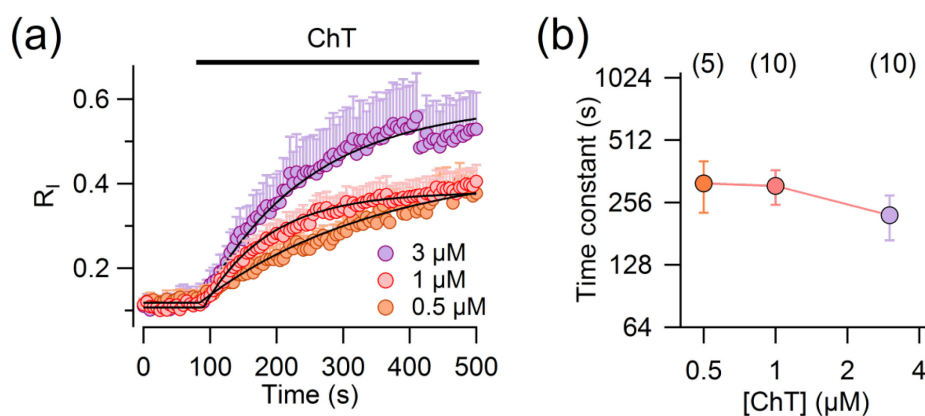


Figure 37: The response of roNav2 to chloramine T. (a) Superimposed single-exponential fit of mean relative non-inactivating current fraction (R_I : I_{10}/I_p) of roNav2 in response to indicated ChT concentrations. (b) The time constant of roNav2 response to indicated ChT concentrations. Data are mean \pm s.e.m. with n indicated in parentheses.

3.5.4. A comparison of RS-sensitivity of roNav1, roNav2, and roGFP2

The responses of roNav1, roNav2, and roGFP2 to small concentration (3 μ M and 1 μ M) of ChT-induced redox changes were investigated and the relative sensitivity of each construct was compared. After monitoring a control response of channels and roGFP2 for 100 s, ChT was acutely applied and change in ratiometric signal R_I for channels and F400/F470 for roGFP2 were monitored. The relative non-inactivating current fraction (R_I : I_{10}/I_p) of channels and the fluorescence ratio change (F400/F470) of roGFP2 were plotted as the function of time, later data were fit according to a single-exponential function to yield the time constant of responses. Since roGFP2 signal responded extremely slow to 3 μ M ChT, an extrapolated time constant of response was analyzed: 40705 ± 4440 s ($n=6$). roNav1 responded to 1 μ M and 3 μ M ChT with an extrapolated time constants of 22731 ± 1710 ($n=5$) and 2200 ± 408 s ($n=7$), respectively. Unlike roGFP2 and roNav1, roNav2 responded rapidly to ChT at 3 μ M (222 ± 54 , $n=10$) and 1 μ M (308 ± 58 , $n=10$) (Fig. 38b). While the oxidant ChT at 1 μ M and 3 μ M had a negligible effect on roNav1 and roGFP2 within 10 minutes, roNav2 responded rapidly and robustly. roNav2 responded about 10-fold faster ($P < 0.01$) to 3 μ M ChT compared to roNav1 (Fig. 38b).

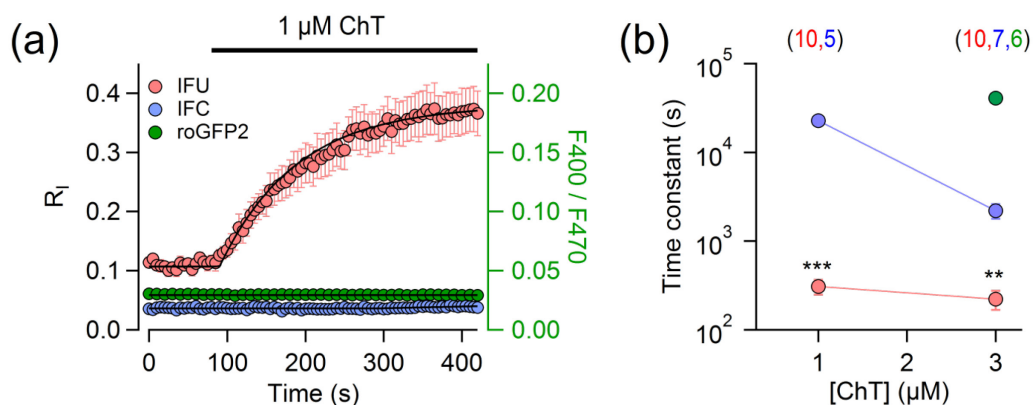


Figure 38: The response of roNav1 (IFC), roNav2 (IFU), and roGFP2 to ChT-induced redox changes. (a) Mean R_I (black Y-axis) of indicated channels and fluorescence ratio (F400/F470; green Y-axis) of roGFP2 plotted as the function of time in response to 1 μM ChT. A superimposed single-exponential fit is shown (black line). (b) Time constants of response to indicated ChT concentrations, roGFP2 (green), roNav1 (blue), and roNav2 (light red). Data are mean \pm s.e.m. (n indicated in parentheses). Statistical t-test: roNav1 vs roNav2: ***, $P \leq 0.001$ and **, $P \leq 0.01$.

3.5.5. Detection of hydrogen peroxide-mediated redox changes

Previous reports (Chance et al., 1979; Makino et al., 2004; Stone & Yang, 2006) indicated that the application of hydrogen peroxide (H_2O_2) in the experimental system is the most appropriate method to evaluate precise role of H_2O_2 against other cellular RS. H_2O_2 passes through the plasma membrane with a permeability coefficients ranges 0.01 to 0.7 cm/min (Chance et al., 1979; Makino et al., 2004) thereby the permeation of H_2O_2 is almost equal to the rate at which H_2O_2 metabolize in the cell by peroxidases and catalases (Stone & Yang, 2006). Therefore, a sensitive and rapid RS sensor is required to investigate the effect of extracellular H_2O_2 in the living cell immediately after its permeation into the cell. In account of that, the applicability of roNav1 and roNav2 in monitoring extracellular H_2O_2 mediated redox changes was investigated and the relative sensitivity of these channels was compared with roGFP2.

3.5.5.1. Monitoring of H_2O_2 mediated redox changes with roNav1, roNav2, and roGFP2

A relative sensitivity of roNav1, roNav2, and roGFP2 to H_2O_2 mediated redox changes were investigated at a constant temperature of 32 $^\circ\text{C}$. The ratiometric signal of channels (R_I) and roGFP2 (F400/F470) in response to extracellular application of H_2O_2 at concentration 1 μM , 10 μM , and 500 μM were measured and plotted as a function of time, later were fit with a single-exponential function to yield time constants of responses (Fig. 39). roNav1 responded extremely slow to the extracellular application of H_2O_2 , thus, an extrapolated time constant of

R_I change was analyzed in response to H_2O_2 at concentration $10 \mu M$: 13990 ± 1070 s ($n=3$) and $500 \mu M$: 3750 ± 91 s ($n=5$) (Fig. 39a, 40).

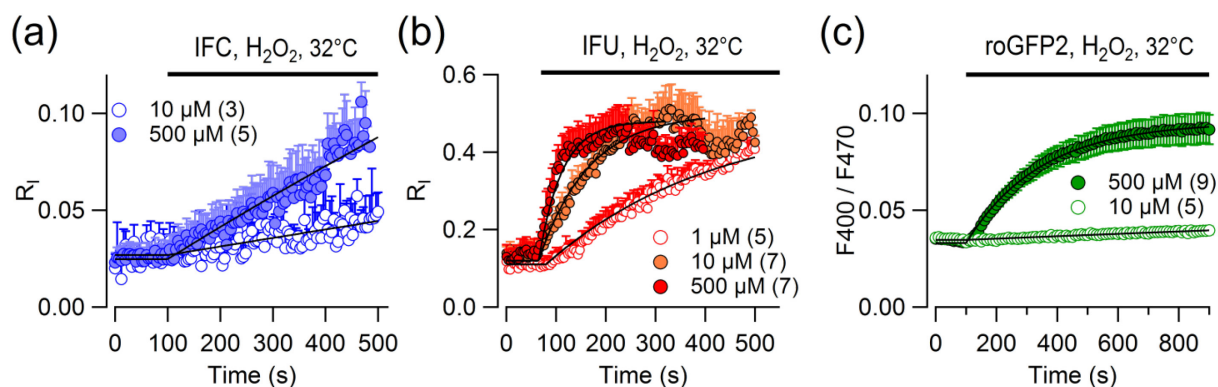


Figure 39: The response of roNav1 (IFC), roNav2 (IFU), and roGFP2 to hydrogen peroxide.

(a) Superimposed single-exponential fits (black) of mean relative non-inactivating current fraction (R_I) of roNav1 in response to the indicated concentration of H_2O_2 . (b) As in a, but for roNav2. (c) As in a, but for roGFP2 signal (F_{400}/F_{470}) in response to indicated H_2O_2 concentrations. The black bar indicates the continuous application of H_2O_2 at a constant temperature of $32^\circ C$. Data are mean \pm s.e.m. with n indicated in parentheses.

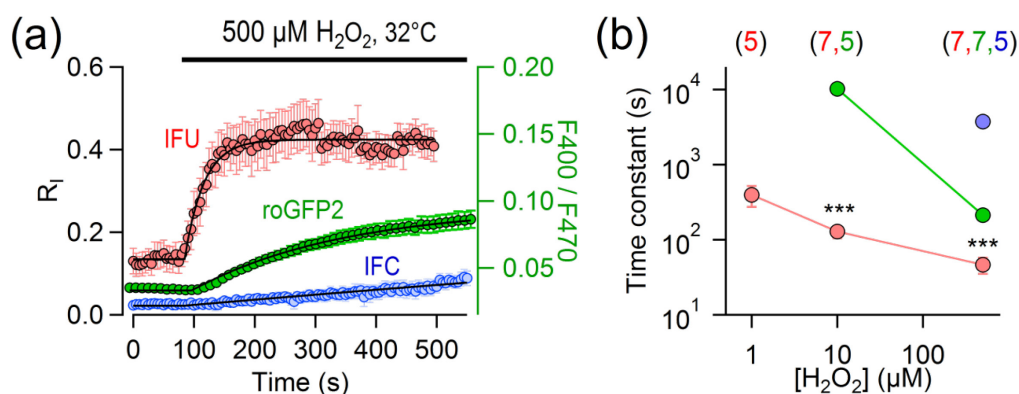


Figure 40: Sensitivity of channel variants and roGFP2 to H_2O_2 mediated ROS. (a) Change in mean relative non-inactivating current fraction (R_I , black Y-axis) of roNav1 (IFC) and roNav2 (IFU) and change in mean signal (F_{400}/F_{470} ; green Y-axis) of roGFP2 in response to $500 \mu M H_2O_2$. A superimposed single-exponential fit is shown (black). (b) Mean time constant of ratio change of channels (roNav1-blue, roNav2-light red) and roGFP2 (green) in response to indicated H_2O_2 concentration. All measurements were done at a constant temperature of $32^\circ C$. Statistical t-test: roNav2 versus roGFP2: ***, $P \leq 0.001$.

roNav2 responded rapidly and produced a mean time constant of R_I change in response to H_2O_2 at a concentration of $500 \mu M$: 47 ± 11 s ($n=7$), $10 \mu M$: 129 ± 23 s ($n=7$), and $1 \mu M$: 396 ± 122 s ($n=5$) (Fig. 39b, 40). The signal of roGFP2 was changed with a time constant 213 ± 10 s ($n=9$) and 10205 ± 311 s ($n=5$) in response to extracellular H_2O_2 at concentration $500 \mu M$ and $10 \mu M$, respectively (Fig. 39c, 40). Results demonstrated that roNav2 responded

about 5-fold faster ($P < 0.001$) to extracellular H_2O_2 at $500 \mu\text{M}$ in compared to roGFP2. The overall dynamic range of ratio change of roNav2 was about 0.45, while it was about 0.06 for roNav1 and roGFP2 in response to $500 \mu\text{M}$ extracellular H_2O_2 .

3.5.5.2. Reversibility of roNav2 from H_2O_2 mediated redox modifications

Extracellular $500 \mu\text{M}$ H_2O_2 was acutely applied to roNav2 expressing cells for 450 s using a glass application pipette at a constant temperature of $30 \text{ }^\circ\text{C}$ and non-inactivating current fraction (R_i) was monitored. After monitoring R_i for 450 s, application of H_2O_2 was turned off. As illustrated in Fig. 41, roNav2 responded very quickly to $500 \mu\text{M}$ H_2O_2 with a time constant of $65 \pm 15 \text{ s}$ ($n=4$). About 50% of inactivation removal of roNav2 was restored with a time constant of $110 \pm 14 \text{ s}$ ($n=3$) when the application was turned off. Restoration of inactivation removal without externally provided any reducing agent indicated that roNav2 is self-capable in being partially reversed.

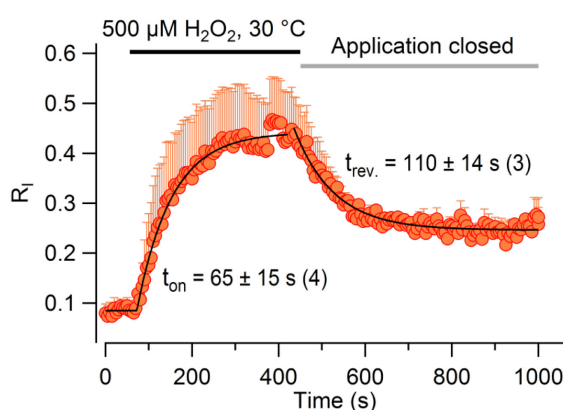


Figure 41: Reversibility of roNav2. Mean change in R_i (I_{10}/I_p) of roNav2 as the function of time in response to $500 \mu\text{M}$ H_2O_2 . The application was closed at 450 s and the reversal of R_i is shown. A superimposed single-exponential fit (black) is shown. The time constant (mean \pm s.e.m.) of response is indicated. Experiments were performed at a constant temperature of $30 \text{ }^\circ\text{C}$.

3.5.6. The response of roNav1 and fluorescent redox reporters to heme degradation products

Heme, a protoporphyrin ring system with a centrally bound iron, functions as a prosthetic group in hemoglobin and is critical for oxygen transport. Heme degradation is a highly regulated process that occurs in spleen and liver. First order heme degradation products constitute carbon monoxide (CO), iron ion (Fe^{2+}), and biliverdin (Maines, 1988; Nagababu & Rifkind, 2004). Subsequently, biliverdin degrades to produce bilirubin, which further degrades to forms third-order heme degradation products, called bilirubin oxidation end-products (BOXes). BOXes exist in two isoforms, namely Z-BOX A and Z-BOX B, which

differ by the position of the methyl and vinyl groups (Clark & Pyne-Geithman, 2005; Kranc et al., 2000; Pyne-Geithman et al., 2005). Several evidences suggest that HDPs (heme degradation products), such as CO and BOXes, play role in certain physiological and pathophysiological functions (Amersi et al., 2002; Clark & Pyne-Geithman, 2005; Wu & Wang, 2005). However, HDPs' production, distribution, and the mechanism behind their involvement in either physiology or pathophysiology are not clear yet. In this context, we investigated the functional role of CO and BOXes in redox processes employing roNav1, roGFP2, and Grx1-roGFP2.

3.5.6.1. The response of roNav1 and roGFP2 to carbon monoxide

Carbon monoxide (CO) is one of the first-order heme degradation products. To understand the concentration-dependent role of CO in cell biology, its controlled release is required because excess CO produces lethal consequences. Chemically synthesized CO-releasing molecules (CORMs), such as CORM-2 (Tricarbonyldichloro-ruthenium(II) dimer) may resolve this issue (Motterlini et al., 2002). Therefore, CORM-2 was used to investigate the functional role of CO in redox processes employing roNav1 and roGFP2.

roNav1 expressing cells were depolarized to -20 mV for 20 ms from a holding membrane potential -120 mV, every 5 s and current responses were monitored. After control current measurements for 100 s, 50 μ M CORM-2 was extracellularly applied for 200 s that produced a rapid block of peak current (about 50 %) of the channel. Wild-type rNav1.4 showed a similar response, but the current block was smaller (about 30%) than to as it was in roNav1 (Fig. 42c). Extracellular application of 50 μ M CORM-2 appreciably affects the relative non-inactivating current fraction of channels, but produced a rapid current block.

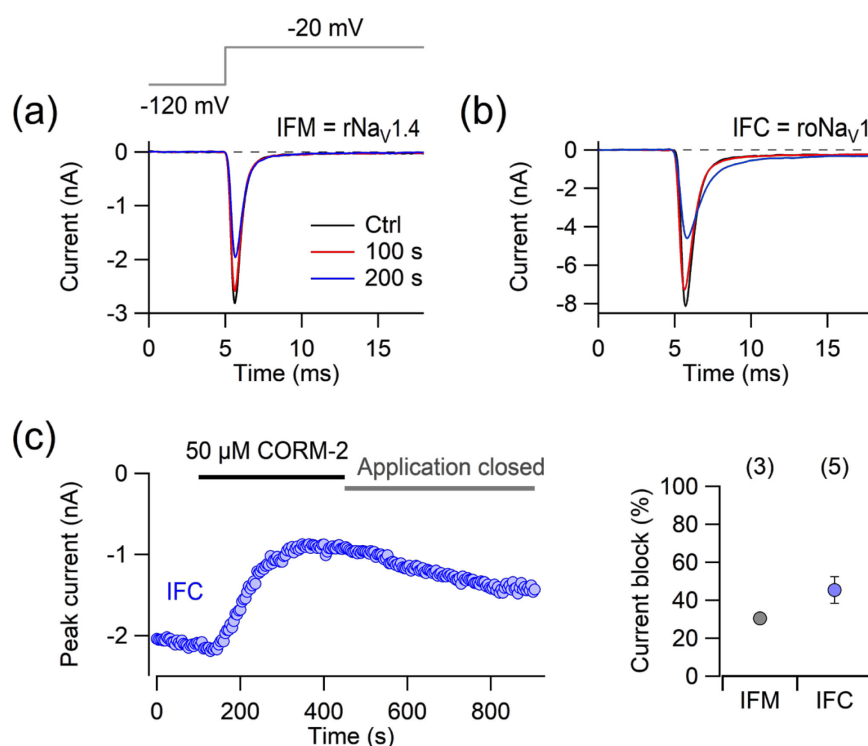


Figure 42: The response of wild-type rNav_v1.4 and roNav_v1 to CORM-2. (a) Pulse protocol (top). Represented current traces of peak current block of wild-type channel in response to extracellular application of 50 μM CORM-2 at the indicated time. (b) As in a, but for roNav_v1. (c) A representative current block of roNav_v1 as the function of time. The application of 50 μM CORM2 is indicated by the black bar. A percentage block of peak current monitored 200 s after the application of 50 μM CORM-2 for the indicated channel (right). Data in panel c (right) are mean ± s.e.m. (n).

The response of 50 μM CORM-2 was also examined with roGFP2 and Grx1-roGFP2. After monitoring a control fluorescence signal (F400/F470) for 100 s, cells were exposed to extracellular 50 μM CORM-2 for 500 s. As illustrated in Fig. 43a, no change in the fluorescence ratio of either fluorescent construct was observed in response to 50 μM CORM-2. When 50 μM H₂O₂ was applied to roGFP2 expressing cells before and after the application of 50 μM CORM-2, fluorescence ratios of roGFP2 were increased in response to 50 μM H₂O₂, while no change in the ratio was observed during the application of 50 μM CORM-2 (Fig. 43b,c). The results showed that 50 μM CORM-2 does not oxidatively modify roGFP2 indicating 50 μM CORM-2 has no role in modifying cellular redox status.

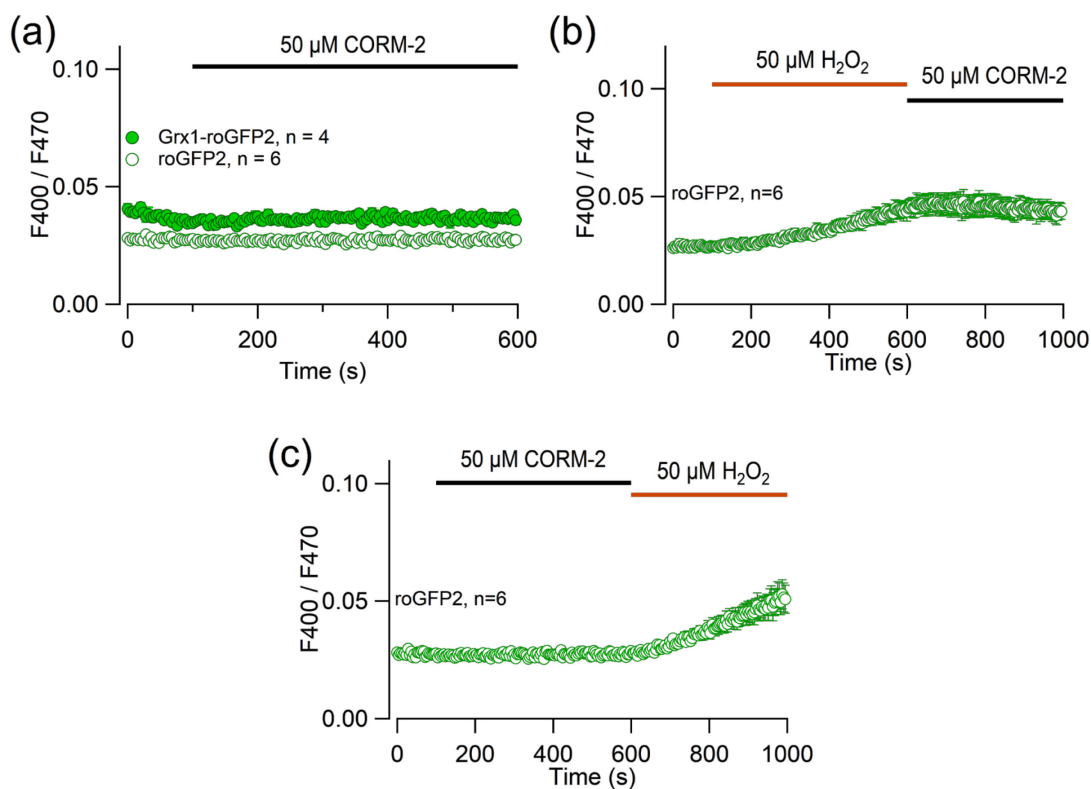


Figure 43: The response of fluorescent redox reporters to CORM-2. (a) Fluorescence ratio (F400/F470) of indicated reporters in response to 50 μM CORM-2 plotted as the function of time. (b-c) The fluorescence signal of roGFP2 as the function of time in response to extracellular application of indicated stressors. Data are mean \pm s.e.m. (n).

3.5.6.2. The response of roGFP2 and Grx1-roGFP2 to bilirubin oxidation end-products

roGFP2 and Grx1-roGFP2 were used to investigate a possible immediate and long-term influences of two isomeric forms of bilirubin oxidation end-products (BOXes), namely Z-BOX A and Z-BOX B on the redox state of HEK 293T and HepG2 cells.

As shown in Fig. 44, roGFP2 expressed in HEK 293T cells did not respond to acutely applied Z-BOX A and Z-BOX B at 100 μM , while Grx1-roGFP2 responded slowly to both isomeric forms of BOXes. Changes in fluorescence signal of Grx1-roGFP2 in response to BOXes were analyzed with a linear function. Grx1-roGFP2 responded slowly to 100 μM Z-BOX A and Z-BOX B with a slope of $0.000117 \pm 2.3\text{e-}06$ (n=7) and $0.000213 \pm 2.9\text{e-}06$ (n=8), respectively. However, it responded very quickly to 100 nM H_2O_2 with a slope of 0.0086 ± 0.000228 (n=5) (Fig. 44d).

It was reasoned that HepG2 cells might be more appropriate expression system to investigate the role of BOXes in redox process because the liver is one of the important sites of heme degradation processes. Therefore, experiments were further performed with HepG2 cells expressing Grx1-roGFP2. Grx1-roGFP2 expressed in HepG2 cells responded to Z-BOX

A (100 μM) with a slope of $0.0001857 \pm 5.6\text{e-}06$ ($n=7$) and to Z-BOX B (100 μM) with a slope of $0.000157 \pm 1.3\text{e-}05$ ($n=8$). Application of 100 nM and 100 μM H_2O_2 as a control yielded a mean slope $0.000163 \pm 3.7\text{e-}06$ ($n=9$) and 0.009 ± 0.000135 ($n=8$), respectively (Fig. 44c,d).

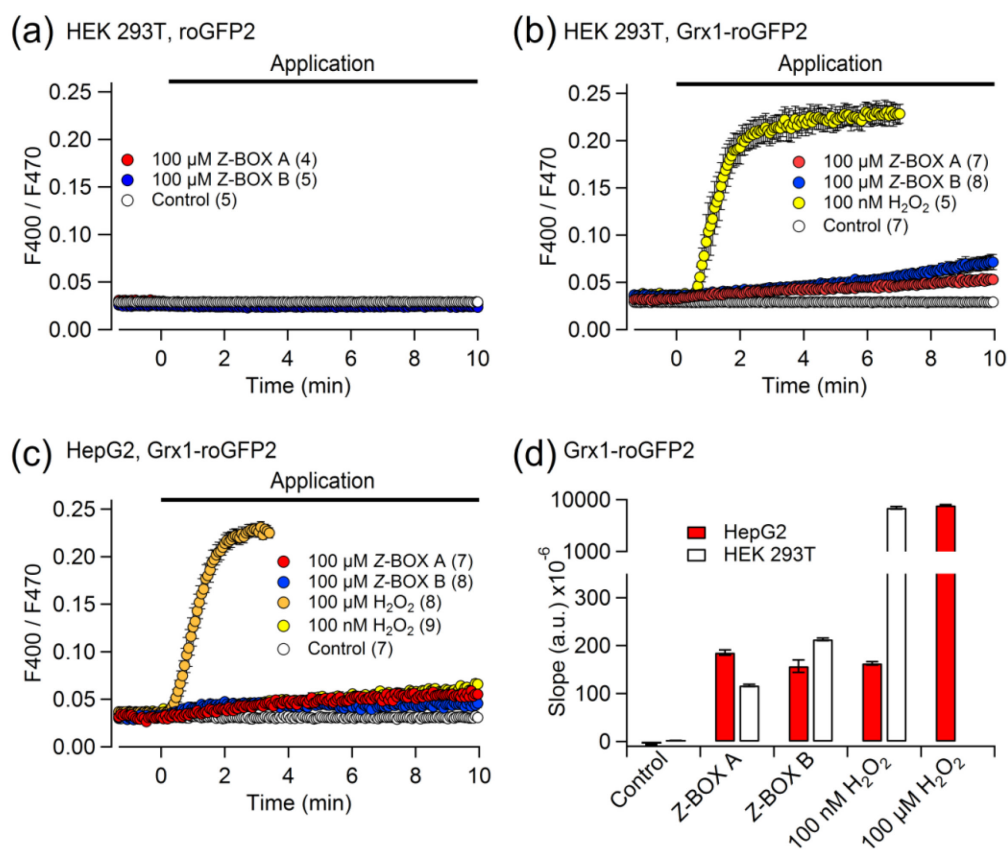


Figure 44: The response of fluorescent redox reporters to BOXes. (a) Mean fluorescent ratio (400/470 nm) as a function of time monitored from roGFP2 expressing HEK 293T cells in response to 100 μM Z-BOX A, 100 μM Z-BOX B, and bath control. (b) As in a, but for Grx1-roGFP2. Ratiometric signal of Grx1-roGFP2 in response to 100 nM H_2O_2 is also shown. (c) As in b, but for Grx1-roGFP2 expressing HepG2 cells. (d) Maximal slope of fluorescence ratio change induced by indicated applications for HepG2 (red) and HEK 293T cells (white bars). Data are mean \pm s.e.m. with n indicated in parentheses. (Seidel et al., 2017)

The influence of both isomers of BOXes on the redox status of HepG2 cells was similar to as it was observed in HEK 293T cells. However, both cells responded differently to H_2O_2 . While 100 nM H_2O_2 has only a small effect on the Grx1-roGFP2 signal in HepG2 cells (comparable to that of 100 μM BOXes), 100 nM H_2O_2 profoundly affected the redox state in HEK 293T cells (Fig. 44b-d). For the induction of a similar response in HepG2 cells, an about 1000-fold higher concentration of H_2O_2 might be needed. The data demonstrated that either BOXes affect the Grx1-roGFP2 or they are affecting the glutathione redox system by a mechanism different to that employed by H_2O_2 .

Grx1-roGFP2 expressing HepG2 cells were incubated at 37 °C with BOXes (Z-BOX A and Z-BOX B) for 1 hour before performing single-cell fluorescence measurements in order to investigate the long-lasting influence of BOXes on the cellular redox status. As a control, H₂O₂ was applied to the culture. A ratiometric fluorescence readout of Grx1-roGFP2 was analyzed for vehicle control: 0.048 ± 0.001 (n=46), 100 nM H₂O₂: 0.049 ± 0.00062 (n=82; P<0.001), 100 μM H₂O₂: 0.084 ± 0.0017 (n=60; P<0.001), Z-BOX A (100 μM): 0.068 ± 0.0012 (n=51; P<0.001), and for Z-BOX B (100 μM): 0.061 ± 0.001 (n=52; P<0.001). As illustrated in Fig. 45, Z-BOX-A and Z-BOX-B at 100 μM significantly increased the fluorescent ratio, which is an indicator of disulfide-bond formation in Grx1-roGFP2, with respect to vehicle control. Thus, accumulation of BOXes in the living system may affect the cellular redox status.

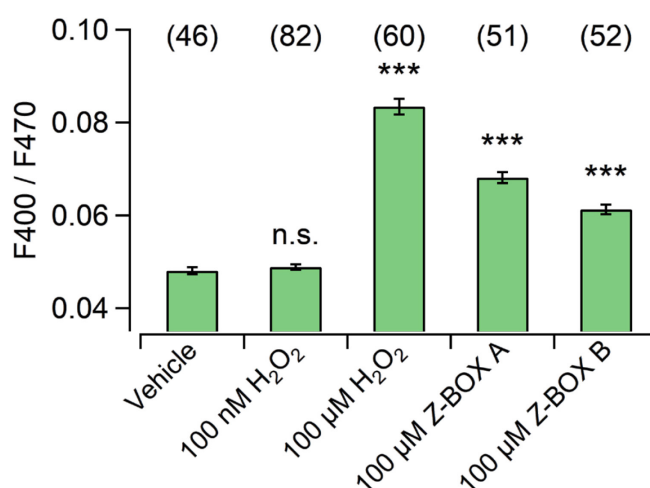


Figure 45: BOXes and intracellular redox status. Mean fluorescent ratio F400/F470 of Grx1-roGFP2 expressed in HepG2 cells. Before measuring the single-cell fluorescence, the cells were incubated at 37 °C for one hour with vehicle (0.25% DMSO), 100 nM H₂O₂, 100 μM H₂O₂, 100 μM Z-BOX-A, and 100 μM Z-BOX-B. Data are mean \pm s.e.m. with the number of cells indicated in parentheses. Two-sided Student's t-test with respect to vehicle control, followed by post-hoc Bonferroni correction for multiple comparisons: n.s., P>0.05; ***, P<0.001. (Seidel et al., 2017)

3.5.7. The response of roNav1 to photo-activated KillerRed-induced ROS

KillerRed (KR) is a genetically encoded photosensitizer that produces ROS, mainly O₂⁻ via a type I reaction along with profound self-photo-bleaching upon green light (520-590 nm) irradiation (Liao et al., 1994; Bulina et al., 2005; Wojtovich & Foster, 2014). Since KR is fully genetically encoded, it can be expressed directly in target cells, both individually and in fusion with a target protein to investigate the eventual role of RS in spatio-temporally controlled manner (Bulina et al., 2005; Wojtovich & Foster, 2014).

Herein, we monitored and compared the response of roNav1 to cytoplasmic and membrane-delimited RS generated upon the photo-activation of cytoplasmic KR (Cyt-KR) and membrane-localized KR, respectively. KR fused with $\beta 1$ subunit of Nav, Nav $\beta 1$ -KR, was used to generate membrane-delimited RS (Fig. 46).

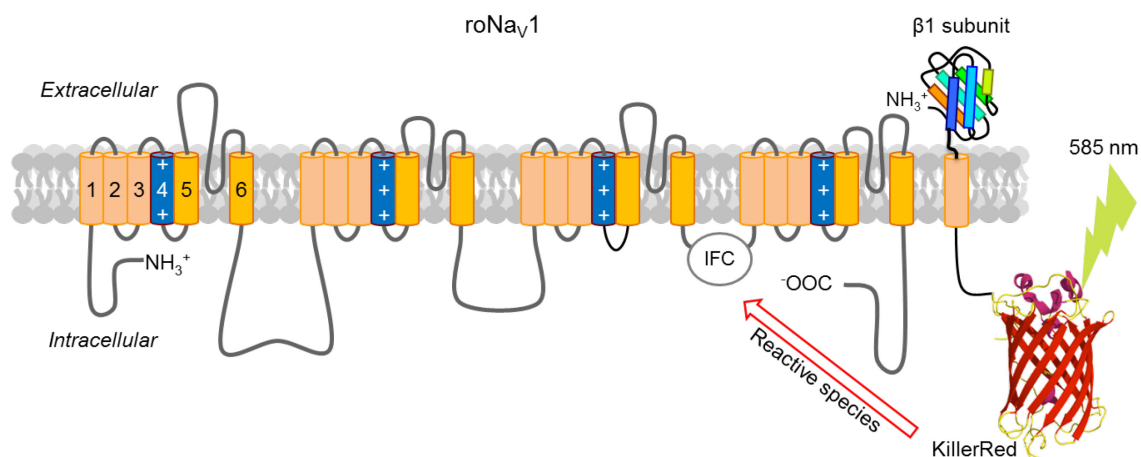


Figure 46: Schematic presentation of membrane-delimited ROS production. KillerRed fused with $\beta 1$ subunit of Nav ($\text{Nav}\beta 1$ -KR) is localized in the cell membrane. KillerRed targeted to cell membrane produce membrane-delimited ROS upon green-light irradiation (585 nm). Sensing of membrane-delimited RS with roNav1 is illustrated.

Cells expressing Cyt-KR and Nav $\beta 1$ -KR were illuminated with green light (585 nm), which produced a progressive loss of roNav1 inactivation (Fig. 47). A relative change in non-inactivating current fraction ($R_I: I_{10}/I_p$) as the function of time was fit with a single-exponential fit that yielded a time constant of R_I change upon photo-activation of Cyt-KR: 1790 ± 775 s ($n=4$) and Nav $\beta 1$ -KR: 116 ± 21 s ($n=4$; $P=0.74$) (Fig. 47b,c). Photo-activation of Nav $\beta 1$ -KR and Cyt-KR produced the overall dynamic change of about 0.9 and 0.5 in R_I of roNav1, respectively. Hence, the dynamic change in R_I of roNav1 was about 2-fold higher for photo-activated Nav $\beta 1$ -KR induced RS compared to Cyt-KR. However, the time constant of R_I change of roNav1 in both cases was similar.

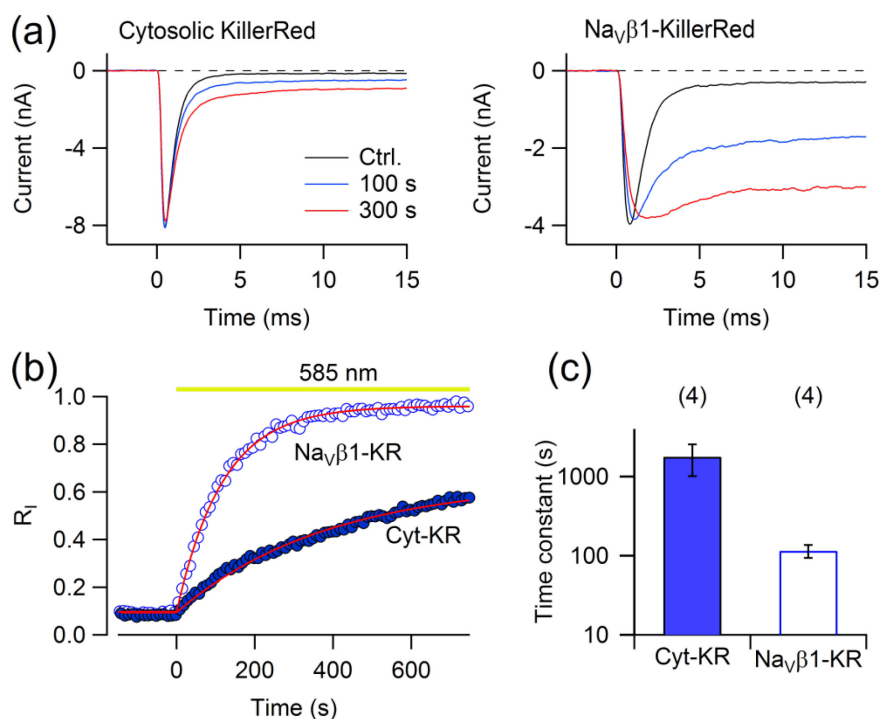


Figure 47: The response of roNav1 to photo-activated KR-induced ROS. (a) Representative current traces at -10 mV for roNav1 co-expressed with cytosolic KR (left) and Nav β 1-KR (right) before (Ctrl) and 100 s and 300 s after 585 nm light illumination. (b) A relative non-inactivating current fraction (R_i) of roNav1 in response to ROS produced by photo-activated cytosolic KR and Nav β 1-KR as the function of time and a superimposed single-exponential fit (red) are shown. The green bar indicates continuous illumination of 585 nm light. (c) Time constants of R_i change in response to photo-activation of indicated KR constructs. Data in c are mean \pm s.e.m. (n).

3.5.8. The response of roNav1 and roNav2 to visible-light induced reactive species

Redox-sensitive green fluorescent proteins, such as roGFP2 and Grx-roGFP2, or synthetic optical reporters are very useful and convenient tools for monitoring cellular RS precisely in spatio-temporal fashion. However, their application is limited to situations where the excitation light itself is not a confounding factor. It is evident that irradiated light that is used to read out the fluorescence signal and/or excited fluorescent proteins may generate RS, initiate photochemical reactions, and disturb cellular redox homeostasis (Dixit & Cyr, 2003; Edwards & Silva, 2001; Eichler et al., 2005; Hockberger et al., 1999; Lavi et al., 2003). Thus, light-independent detection of RS in single cells may be desirable. In account of that, the usefulness of roNav1 and roNav2 to monitor light-induced RS and/or chemical modifications in an epifluorescence setting was examined.

3.5.8.1. Detection of visible-light induced reactive species with roNav1

Channel expressing cells were placed into the focus of a 20x dry objective of an inverted microscope and illuminated with a 100-W mercury lamp for epifluorescence excitation. After several control recordings at -10 mV for 20 ms from a holding voltage of -120 mV, every 10 s in the dark, the light was turned on and the loss of inactivation was monitored. Excitation through a GFP filter set (BP 450–490, FT 510), i.e. stimulating with blue light (8.3 mW objective output measured at 470 nm), resulted in the rapid progressive loss of roNav1 inactivation, while the effect in the wild type was much smaller (Fig. 48a,b).

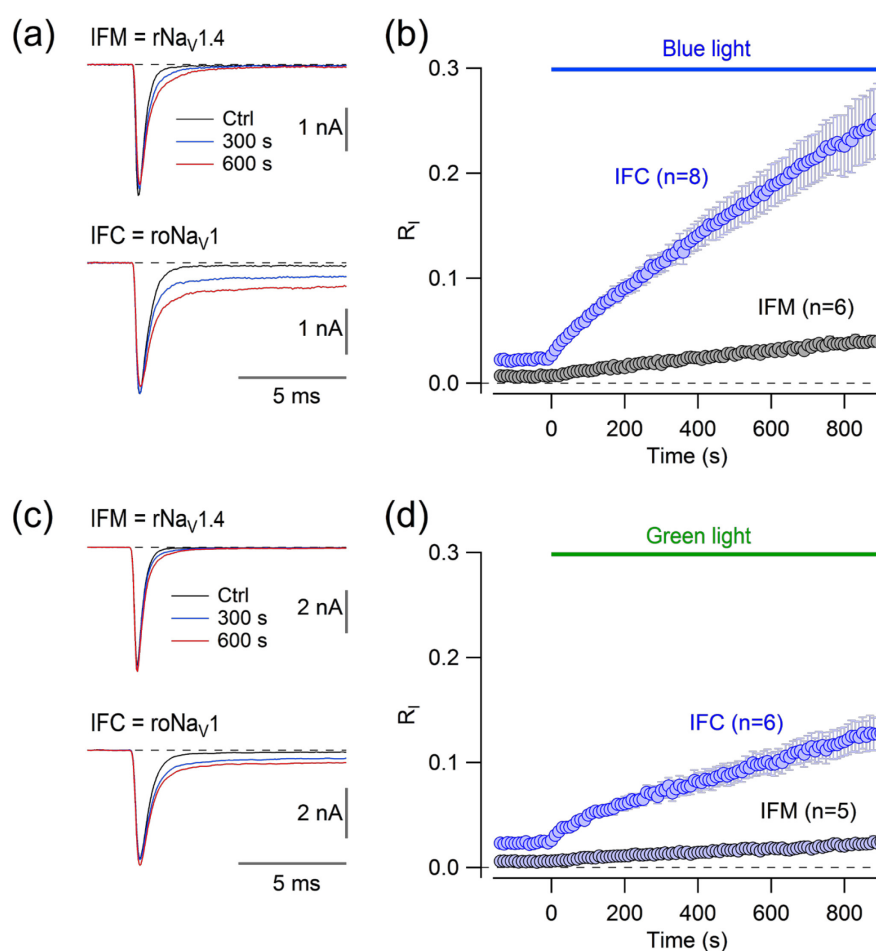


Figure 48: Photodamage induced by illumination typically employed in epifluorescence experiments. (a) Raw data traces in response to depolarizations to -10 mV for the wild type (top) and roNav1 (bottom) before (Ctrl) and 300 s and 600 s after epifluorescence excitation light was turned on. 100-W mercury lamp, BP 450-490, FT 510, 20x dry objective (NA=0.30). (b) Inactivation removal during blue-light exposure for indicated constructs. (c,d) Similar to a and b, but for green light irradiation, BP 510-560, FT 580. Data are mean \pm s.e.m. (n is shown in parentheses). (Ojha et al., 2014)

Moreover, epifluorescence excitation of cells with green light (BP 510–560, FT 580; 3.2 mW objective output measured at 535 nm) even removed the inactivation of roNav1,

while only marginal effects were observed in the wild type. The overall dynamic range of R_i change of roNav1 was about 0.25 and 0.1 whereas dynamic range of R_i change of wild-type rNav1.4 was about 0.04 and 0.02 in response to blue light and green-light induced RS, respectively. Hence, roNav1 can serve as a useful tool for detecting RS generated by cell exposure to light. The sensitivity of roNav1 is high enough to even monitor functional changes induced by RS originating from green light (510–560 nm).

3.5.8.2. Detection of blue-light induced reactive species with roNav2

roNav2 expressing cells were placed into the focus of plan-apochromat 63x oil immersion objective (NA=1.4) of an inverted microscope with a 150-W xenon lamp for epifluorescence excitation. After control recordings in the dark, blue light (470 nm, 0.5 mW at microscope objective) was turned on and currents in response to trains of depolarizing pulse -20 mV from a holding potential of -120 mV was monitored (Fig. 49a). Illumination of cells with blue light (470 nm) resulted in progressive loss of the channel inactivation (Fig. 49b). A single-exponential fit of relative change in non-inactivating current fractions (R_i : I_{i0}/I_p) as the function of time yielded a mean time constant for roNav2: 0.377 ± 0.042 s ($n=27$; $P<0.001$ versus wild type), roNav1: 549 ± 112 s ($n=6$; $P<0.001$ versus wild type), and wild-type Nav1.4: 5010 ± 610 s ($n=6$) (Fig. 49c). The time constant of channel response to blue light showed that roNav2 responded about 1,500-fold and 13,000-fold faster to blue light-induced RS compared to roNav1 and wild type, respectively. It is also conceivable that the rapid change in inactivation properties of roNav2 may be associated with light-induced chemical modifications of Sec residue located in the inactivation motif of the channel.

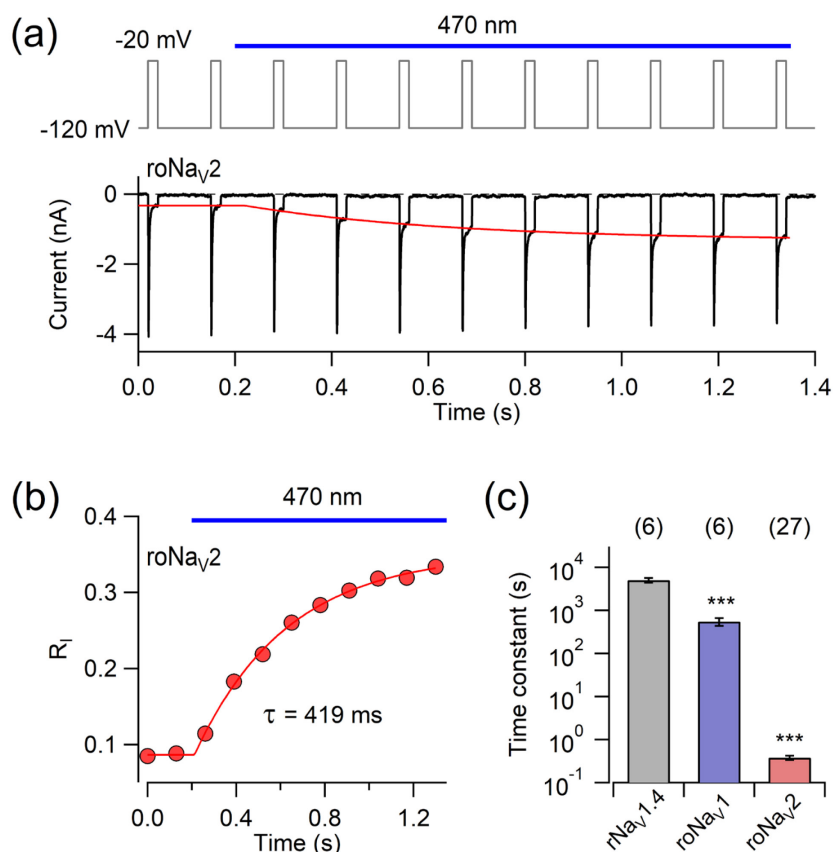


Figure 49: The response of roNav2 to photo-damage induced by blue light. (a) Current recording (bottom) from roNav2 in response to a train of depolarizing pulses to -20 mV from a holding potential of -120 mV (top). The blue bar marks continuous illumination of the cell with 470-nm light (0.5 mW at objective) via a plan-apochromat 63x/1.4 oil immersion objective. The red curve superimposed to the current traces illustrates a data fit of the time course of light-induced loss of channel inactivation. (b) Mean time course of light-induced loss of inactivation (increase in R_I) of roNav2 and a superimposed single-exponential fit (red line). (c) Mean time constants of 470-nm light-induced loss of inactivation for indicated channels. Data are mean \pm s.e.m. with number of cells indicated in parentheses. Statistical t-test, wild type vs. roNav1 and roNav2: ***, $P \leq 0.001$. (Ojha et al., 2017)

3.5.8.3. Reversibility of roNav2 from light-induced chemical modification

The loss of roNav2 inactivation on 1 s blue (470 nm) light-irradiation completely restored when the measurements were performed in the dark. As illustrated in Fig. 50, while roNav2 removed its inactivation (R_I increased) in response to 470-nm light with a time constant of 0.377 ± 0.042 s ($n=27$), loss of inactivation further completely restored in dark with a time constant of 106 ± 16 s ($n=8$). The onset of the sensor response to 470-nm light and the time course of reversibility was similar when measurements performed in the perforated-patch configuration using 5 μ M escin in the patch pipette solution (onset: 0.53 ± 0.09 , $n=7$, reversibility: 114 ± 33 s, $n=4$; $P=0.16$, 0.82 versus whole-cell), and the whole-cell configuration (Fig. 50b).

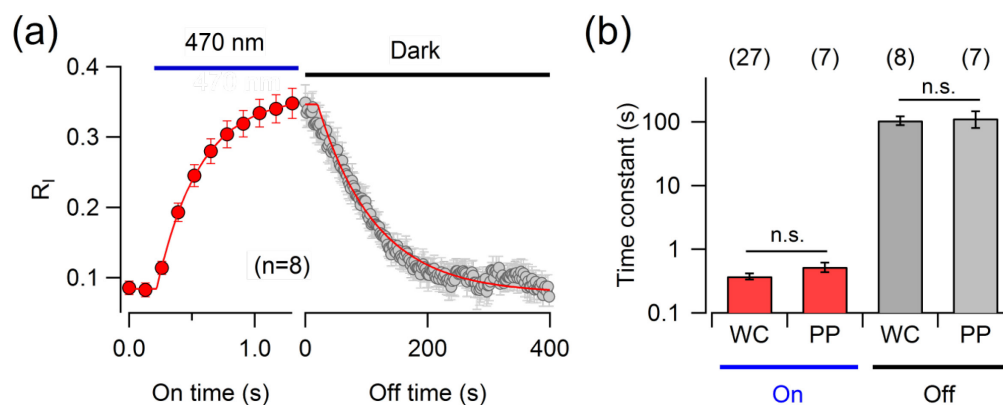


Figure 50: Reversibility of roNav2 form blue-light induced modification. (a) A mean time course of blue-light (470 nm) induced loss of inactivation (red circles) and subsequent recovery in the dark (gray circles) with superimposed single-exponential fits (red line). The blue bar indicates continuous illumination with 470 nm, the black bar marks recovery in the dark. (b) Mean time constants of light-induced loss of inactivation (“On”) and recovery in the dark (“Off”) comparing experiments performed in whole-cell mode (“WC”) and perforated-patch mode (“PP”). Data are mean \pm s.e.m., number of cells indicated in parentheses. Statistical t-test: n.s., $P > 0.05$. (Modified from Ojha et al., 2017).

3.5.8.4. The response of roGFP2 variants to blue-light irradiation

Cells expressing roGFP2 and its variants containing a single Cys at position 147, a single Sec at position 147, Sec:Cys at position 147:204, and Grx1-roGFP2 were excited with blue light using a 150-W xenon lamp by placing cells into the focus of plan-apochromat 63x oil immersion objective (NA=1.4) of an inverted microscope. After measuring control fluorescence ratio at 400 nm and 470 nm, each wavelength for 10 ms, every 10 s, transfected cells were subjected to 470-nm light and the ratiometric readout of each construct was monitored. Subsequently, measurements were continued, but with 25 s step interval to allow restoration in fluorescence change. Change in fluorescence ratio was plotted as the function of time and was fit with a single-exponential function. Thus, a mean time constant of onset response was analyzed for eGFP_S147C:Q204 = 877 ± 18 s (n=5), eGFP_S147U:Q204 = 830 ± 14 s (n=5), eGFP_S147C:Q204C (roGFP2) = 561 ± 37 s (n=4), eGFP_S147U:Q204C = 5 ± 0.5 s (n=4), and Grx1-roGFP2 = 42 ± 4 s (n=6).

As shown in Fig. 51, only two constructs among all, i.e. eGFP_S147U:Q204C and Grx1-roGFP2 showed reversibility from blue light-induced modification with a time course of 158 ± 11 s and 69 ± 3 s, respectively. Fluorescent variants that showed extremely slow reversibility were characterized with an extrapolated time constant: eGFP_S147C:Q204 = 20514 ± 10900 s, roGFP2 = 7026 ± 600 s. eGFP_S147U:Q204 did not show reversibility.

Results clearly showed that roGFP2 responded to blue-light (470 nm) induced RS about as fast as roNav1 (Fig. 51b,f, and 49c). However, eGFP mutant 147U-204C showed a fast reaction upon blue light illumination that was fully reversible, and hence, comes close to the performance of roNav2 (Fig. 51e,f, and 49c). Furthermore, all variants containing either a Cys or a Sec were modified during the blue-light illumination indicating the similar situation might be true for cellular proteins.

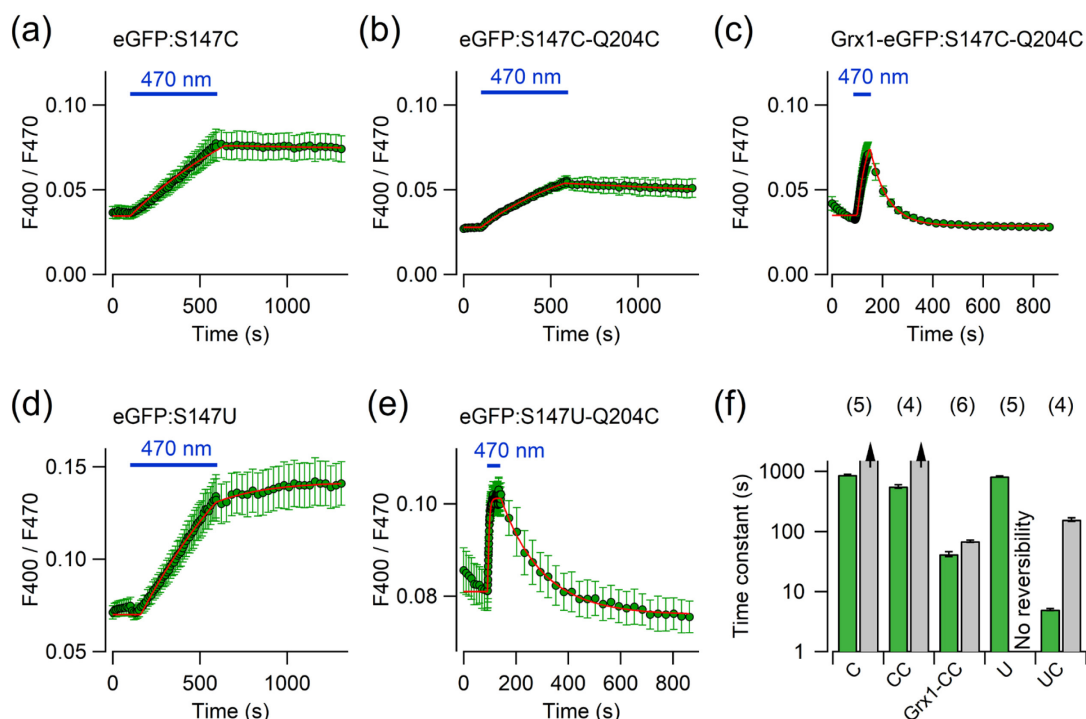


Figure 51: Blue light-induced modifications of eGFP-based fluorescence proteins. Time courses of the F400/F470 fluorescence ratios of the indicated eGFP-based proteins expressed in HEK 293T cells with blue-light stimulation via a 63x (NA=1.4) objective indicated by the blue bars. (a) eGFP_S147C:Q204, (b) roGFP2 (eGFP_S147C:Q204C), (c) Grx1-roGFP2 (Grx1 fused to eGFP_S147C:Q204C), (d) eGFP_S147U:Q204, and (e) eGFP_S147U:Q204C. The superimposed red curves are single-exponential fits during and after the light exposure. (f) Time constants of fluorescence ratio (F400/F470) change (green bars) and reversibility (gray bars) of indicated constructs. C indicates eGFP with a single Cys at 147, CC indicates eGFP with Cys at 147 and 204, Grx1-CC indicates Grx1-roGFP2, U indicates eGFP with a single Sec at 147, and UC indicates eGFP with Sec at 147 and Cys at 204. Data are mean \pm s.e.m. (n). (Modified from Ojha et al., 2017)

3.6. Gated RS sensitivity of roNav1 and roNav2

An RS sensor that can be turned on and off at will is required to infer about the dynamics of RS distribution and lifetime. Ion channels are molecular switches par excellence, in particular, voltage-gated sodium channels that open and close in response to changes in membrane voltage in the millisecond range. At resting membrane potential, inactivation

motif (IFM) of Nav is expected to be in the cytosol, while the motif makes firm contact with the channel protein during long depolarize condition, i.e. inactivated state. Therefore, it was hypothesized that RS-sensitive motif of roNav1 (IFC) and roNav2 (IFU) can be protected from RS attack when channels attain inactivated state. Therefore, experimental protocols were designed to test for the 'state dependence' of channels' RS sensitivity.

3.6.1. Gated RS sensitivity of roNav1

Co-expressing roNav1 and roGFP2 cells were depolarized to -20 mV for 20 ms, every 2 s from a holding potential -120 mV. After measuring a parallel control response of roNav1 and roGFP2 for 100 s, cells were subjected to 400-nm light and assayed for the ratiometric RS-related signal. While the resting holding potential was -120 mV, blue light (400 nm) resulted in a progressive loss of inactivation, and along with that, an RS-signal was detected by roGFP2. During an episode with a holding potential of -20 mV, i.e. roNav1 was inactivated and unavailable for measurements, while roGFP2 proceeded to become modified. Resuming a holding potential back to -120 mV indicated that roNav1 was effectively protected from modification during the inactivated state (-20 mV episode) (Fig. 52). Similar experiments were performed in the perforated-patch configuration by using escin (5 μ M) in the patch pipette solution as a perforating reagent, thereby preserving the cytosol during measurements, produced same outcome (Fig. 53). Results obtained in both cases, whole-cell and perforated-patch configuration showed that light-induced loss of channel inactivation was depended on the channel state; roNav1 was modified with blue light (400 nm) when the channel was in resting condition (-120 mV), while no modification was observed during inactivated state.

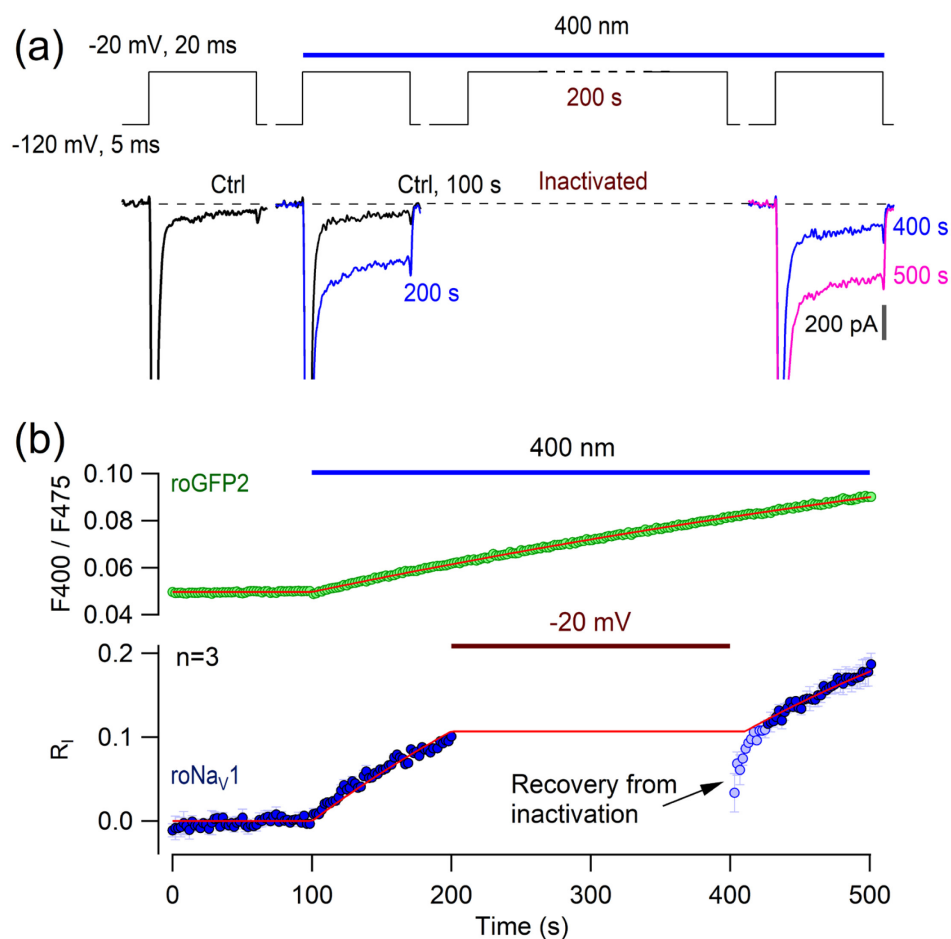


Figure 52: State dependence of roNav_v1 modification. (a) Parallel measurements of roNav_v1 and roGFP2 were performed in 4 episodes as indicated in pulse protocol. 1st episode (control): cell was depolarized to -20 mV from a holding voltage -120 mV, every 2 s. 2nd episode: as in the 1st episode, but the cell was subjected to 400 nm light. 3rd episode: holding potential was set to -20 mV for 100 s to inactivate the channel and 400 nm light was remained turned on. 4th episode: holding voltage set back to -120 mV for 2 s to ensure full recovery from inactivation later as in 2nd episode. A representative current response in response to pulse protocol at indicated time (bottom). (b) Loss of channel inactivation (bottom) and roGFP2 signal (top) in response to illuminating a cell with 400 nm light (blue bar). Superimposed red curves indicate mono-exponential time courses. (Modified from Ojha et al., 2014)

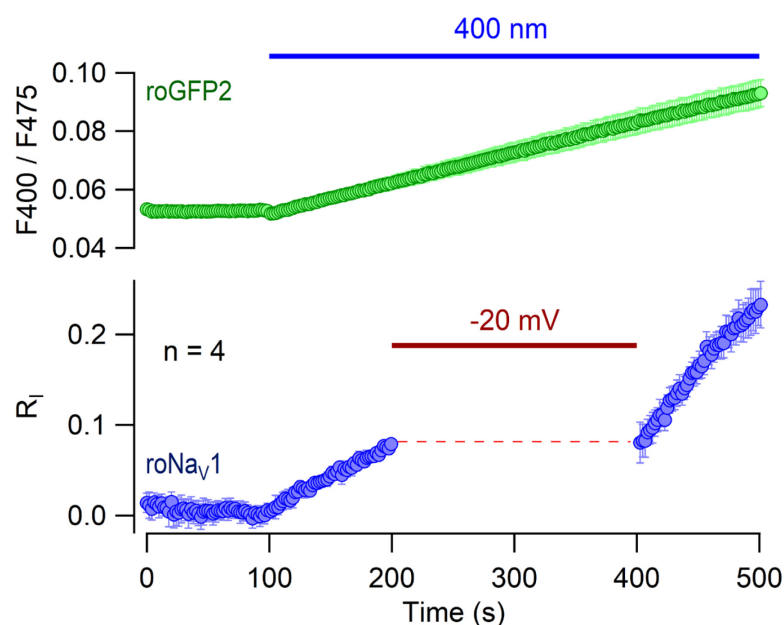


Figure 53: State dependence of roNav1 modification under physiological conditions. Loss of roNav1 inactivation (bottom) and roGFP2 signal (top) in response to illuminating cells with 400 nm light (blue bar) in the perforated patch configuration using 5 μ M escin in the patch pipette solution. In the episode indicated by the red bar, the holding potential was set to -20 mV in order to inactivate the channels. roNav1 were measured with repetitive pulses to -20 mV, while roGFP2 was read out with 20 ms pulses to 400/465 nm. (Ojha et al., 2014)

The ‘state dependence’ of roNav1’s RS sensitivity was also examined for chloramine T challenges and RS generated via light excited Lucifer Yellow (LY) and KillerRed (KR). Loss of roNav1 inactivation proceeded with a time constant of 230 s in response to 10 μ M ChT when the channel was in resting state, i.e. membrane voltage was -120 mV, and test pulses were measured every 15.6 s. However, the time constant increased to 486 s when the experimental protocol contained 10 s episodes at -50 mV to inactivate most of the channels (Fig. 54). In a separate experiment, we loaded the cell via the patch pipette with Lucifer Yellow, a commonly used fluorescent dye that produces RS upon irradiation (Higure et al., 2003; Kasmann et al., 2008) and stimulated with blue light (Fig. 55a-c). Besides that, we expressed the genetically encoded photosensitizer KillerRed (Bulina et al., 2006; Wojtovich & Foster, 2014) together with roNav1 in HEK 293 cells and stimulated RS production with green light (Fig. 55a,d). In both cases, we assayed the incremental loss of roNav1 inactivation depending on whether the light pulse was given during the resting state (-120 mV) or during an inactivation episode (-50 mV) (Fig. 55). These results confirmed that roNav1 exhibits properties of a gateable RS-sensitive sensor that can be protected from RS reactions by switching the channel into an inactivated state.

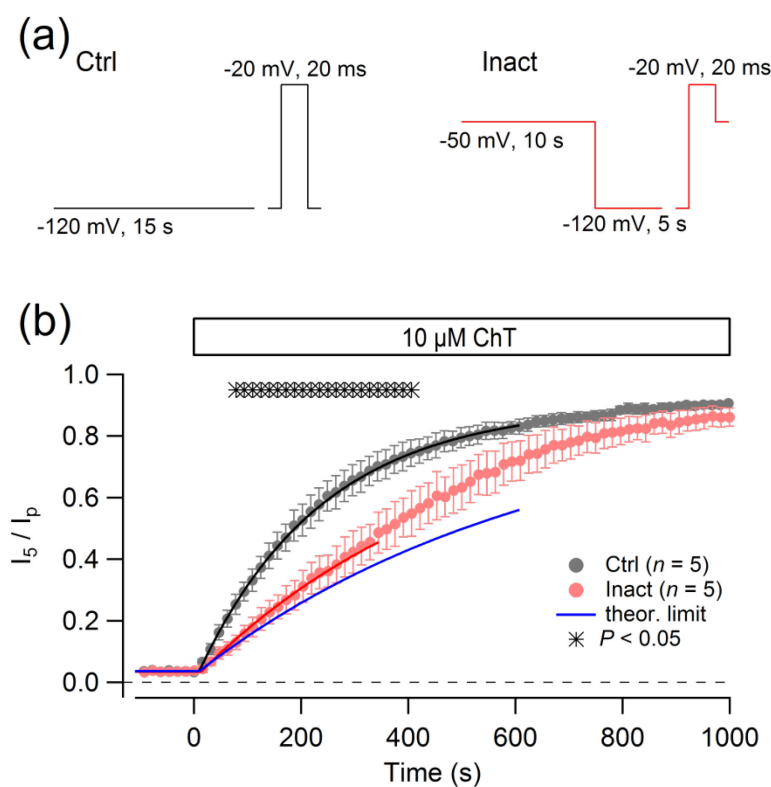


Figure 54: State dependence of roNav1 modification. (a) Pulse protocols used to test for a state dependence of RS-induced loss of inactivation. In the left condition (Ctrl), 20-ms depolarizations to -20 mV were elicited every 15 s with a constant holding voltage of -120 mV. In the protocol on the right (Inact), the first 10 s of the holding period was at -50 mV to inactivate the channels, followed by a 5-s period at -120 mV to ensure full recovery from inactivation before the test pulse to -20 mV was elicited. (b) Time courses of loss of inactivation upon application of 10- μ M chloramine T (ChT) for the control protocol (Ctrl) and the inactivation protocol (Inact). Error bars denote s.e.m. values of $n=5$ cells each. Also indicated is the statistical evaluation (asterisks, two-sided t-test with unequal variances) of the differences between both groups as a function of time. Superimposed on the mean data are single-exponential fits with a limiting ratio of 0.9 to estimate the initial slope of inactivation loss. Ctrl: $\tau = 232 \pm 5.8$ s; Inact: $\tau = 496 \pm 25$ s. The blue curve is a prediction of the time course of modification assuming full protection of the IFC (inactivation) motif during the period of channel inactivation. (Ojha et al., 2014)

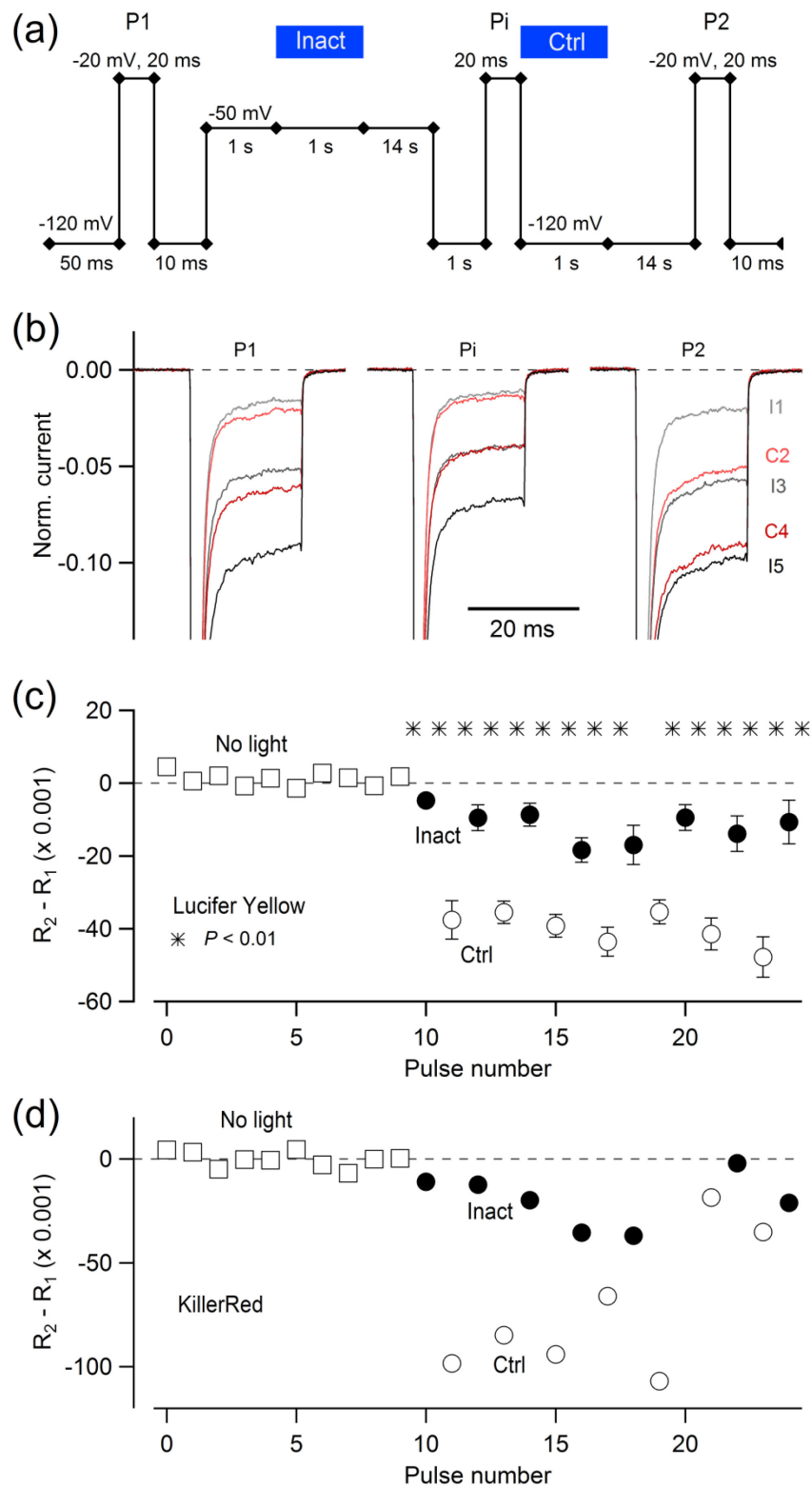


Figure 55: State dependence of roNav1 probed with light-induced RS. (a) Schematic pulse protocol used to measure Na^+ currents. There are three test depolarizations at -20 mV: P1 before an inactivation episode, Pi after the inactivation episode to test for recovery from inactivation, and P2 after an episode at the holding potential of -120 mV. This protocol was repeated at an interval of about 35 s. RS production was either stimulated by irradiation of Lucifer Yellow (100 μM) loaded into the cell via the patch pipette (b, c) or by irradiating cells expressing the cytosolic KillerRed protein (d). (b) Superimposed current traces from the protocol shown in (a). After establishing a whole-cell configuration and ensuring proper loading of the cell with LY, the protocol was applied 10

times without light. After that, the light stimulation (blue bars in a) alternated from pulse to pulse, yielding traces with light stimulation during inactivation (I1, I3, I5, gray), and traces with light stimulation when the channel was in a resting state (C2, C4, red). (c) The inactivation index was measured for P1 and P2, and the difference of inactivation index (R2-R1) was plotted as a function of pulse number. Symbols denote the kind of light stimulation: no light (open squares), light during channel inactivation (filled circles), light at holding voltage (open circles). Error bars denote s.e.m. values for $n = 9$ experiments. Asterisks denote $P \leq 0.01$ of t-test for successive data points, clearly indicating that loss of inactivation is significantly greater when the light pulse was given while the cells were at holding voltage. Note that this even is a conservative estimate because the time between the light pulse and P2, i.e. the interval during which RS can affect roNav1, was about twice as long when the light was given during the inactivation episode. Taking the average of the first three pulses each (i.e., $n = 27$ each) (not considering the very first I1 pulse), we obtain: control, $\Delta R = 3.74 \pm 0.22\%$; inact., $\Delta R = 1.22 \pm 0.20\%$, P (t-test) = $3.6 \cdot 10^{-11}$. (d) A similar experiment as in (c), but with co-expression of roNav1 and cytosolic KillerRed. During light pulses, the cell was irradiated with green light liberating RS from KillerRed. The differential loss of inactivation also clearly indicates that roNav1 is protected in its inactivated state for RS arising from KillerRed. (Ojha et al., 2014).

Dynamics of intracellular RS monitored with roNav1

Due to the rapid response time of roNav1 and its independence on light, it can be useful in studying distribution and lifetime of RS triggered by the light pulse. To demonstrate this option, we liberated RS from cell-loaded Lucifer Yellow with brief (600 μ s) light flashes. We showed that upon brief (600 μ s) flash-light-illumination of cells loaded with Lucifer Yellow, real-time modification of roNav1 produces two-time constants: one about 10 ms and the other on the order of seconds. This infers that LY upon blue-light illumination liberates at least two major species of reactive components with respective mean lifetime (Fig. 56). The result shows that roNav1 is suited to monitor the lifetime of different light-induced reactive species components acting at the plasma membrane.

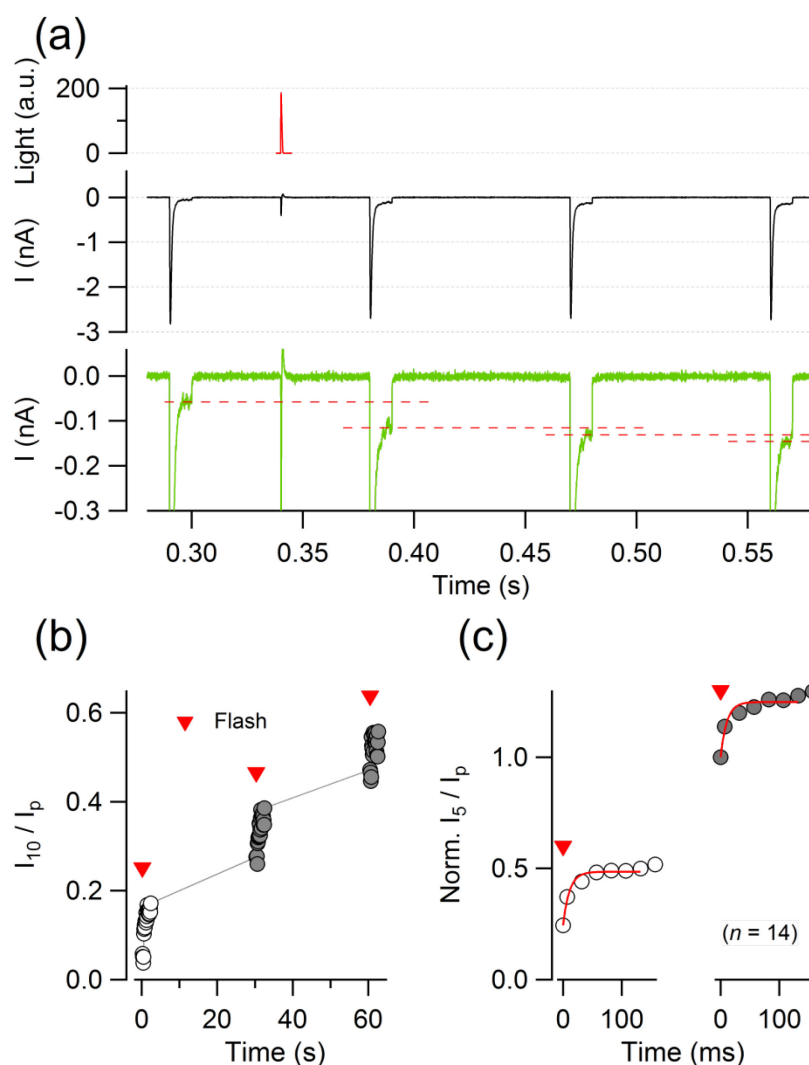


Figure 56: Kinetics of roNav1 modification by light-induced RS generation. (a) (top) recording of a light flash stimulation applied to liberate RS from Lucifer Yellow. (middle) current trace with 10-ms depolarizations to activate roNav1 every 80 ms, indicating that the flash applied between the first and the second depolarization shown in this panel only slightly reduced the peak current amplitude. (bottom) the same data after scaling by a factor of 10 in order to visualize the degree of non-inactivating current. The horizontal dashed lines indicate such current levels and the progressive loss of inactivation from one pulse to the next clearly showing that a great fraction of inactivation loss has happened in the first pulse after the flash, i.e. in less than 40 ms. (b) The degree of inactivation removal as a function of time on a longer time scale showing the results of three subsequent trains of depolarizations (each data point refers to one depolarizing pulse) in which a light flash was given for each train after the third depolarization (indicated by red inverted triangles). This time course shows a very rapid initial loss of inactivation (ms range) followed by a slower process with a time constant of more than 1 s. (c) Average time course of flashlight induced loss of inactivation for two successive trains of 5-ms depolarizations at an interval of 25 ms. The data are normalized to the inactivation index obtained before the second light flash. The superimposed red curves are single-exponential fits yielding time constants of 11.0 ± 2.2 ms for the first and 10.7 ± 3.2 ms for the second train; the corresponding amplitudes were 0.251 ± 0.008 and 0.248 ± 0.012 , respectively. (Ojha et al., 2014).

3.6.2. Gated RS sensitivity of roNav2

Since roNav1 worked as a switchable sensor, roNav2's state dependence of RS sensitivity was evaluated. roNav2 expressing cells were depolarized to -20 mV for 20 ms from a holding potential -120 mV. Subsequently, holding potential was kept constant at -120 mV for next 300 ms followed by a depolarization at -20 mV for 20 ms (Fig 57a, upper). Irradiation of light pulse of 470-nm for 300 ms while the membrane voltage was clamped to -120 mV resulted in inactivation loss of roNav2 (Fig. 57a, lower). Brief light pulses resulted in a cumulative loss of inactivation, which follows an exponential function when only the illuminated episodes were considered (Fig 57b). In further experiments, cells were depolarized to -20 mV from a holding potential -120 mV for 320 ms thereby channels become inactivated; subsequently, membrane potential was changed to -120 mV for 100 ms to recover channel from inactivation, later followed by a depolarization at -20 mV for 20 ms (Fig. 57c, upper). Blue light (470 nm) irradiation while the channel was in inactivated state (-20 mV) did not affect relative non-inactivating current fractions of roNav2 (Fig 57c-lower, d). The results clearly indicate that light-induced loss of inactivation of roNav2 depends on the channel state. Therefore, roNav2 exhibited a state dependence for RS sensitivity. roNav2 can be protected from light-induced RS/chemical modification by means of electrical membrane potential, and hence, can serve as a switchable or gateable RS sensor.

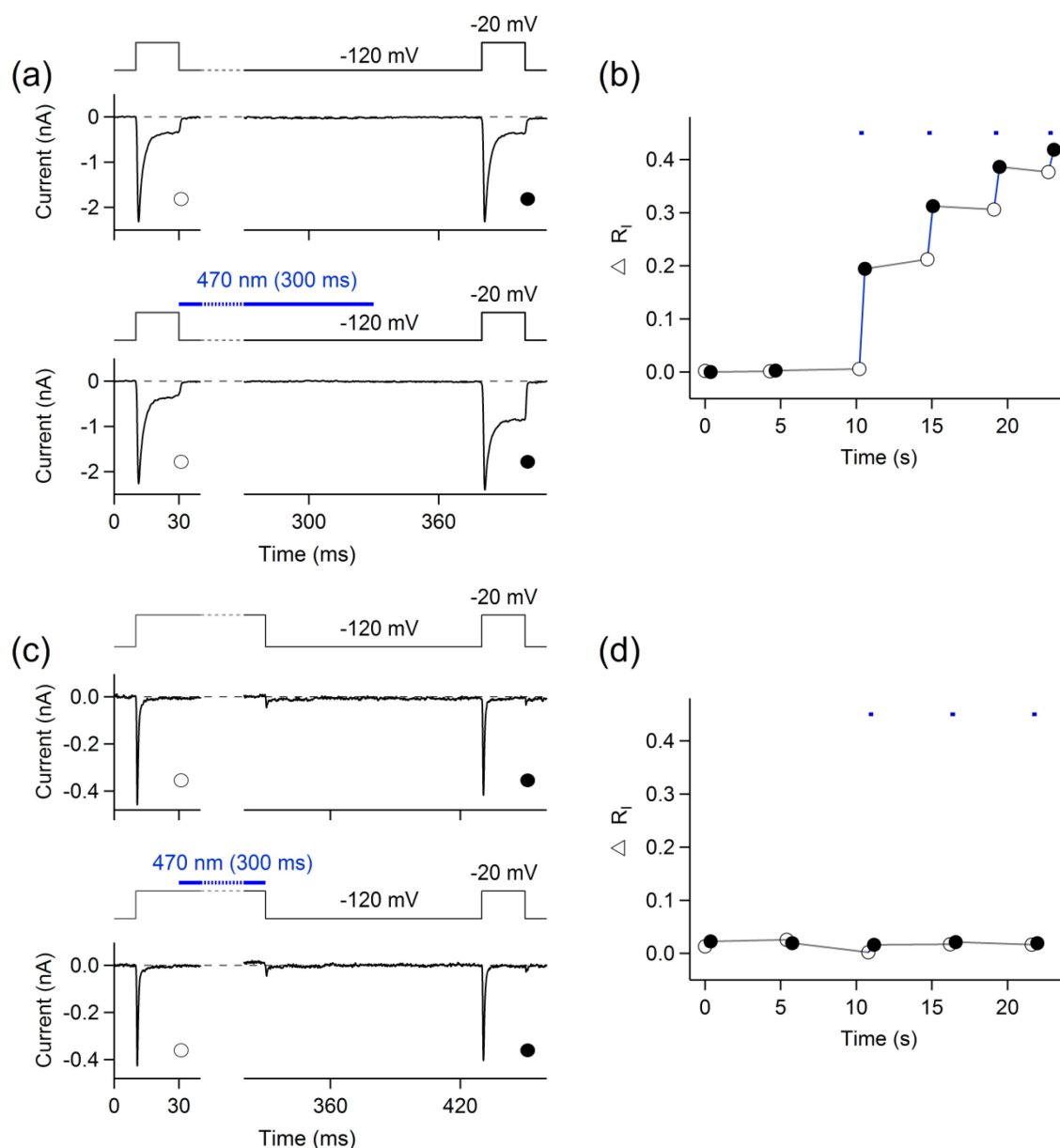


Figure 57: Inactivation protects roNav2 from modification. (a) Two successive current traces from roNav2 expressed in HEK 293T cells measured with the pulse protocol shown in the top panel. For the first trace, no light was on; for the second trace, the 470-nm light was on between the control and the test pulse as indicated by the blue bar. The interval between the first and the second pulse was about 5 s. (b) Relative change in non-inactivating current (ΔR_I) from the experiment shown in (a) and successive sweeps as a function of real-time; white symbols refer to the control pulses, black symbols to the test pulses, blue lines connect consecutive control and test pulses. Episodes of 300-ms blue light exposure are indicated by the blue symbols at the top and manifest in strong increases of R_I in the subsequent pulses. (c) Similar current recordings as in a, but the blue-light pulse was given while the channel was kept in an inactivated (closed) state by holding the membrane voltage at -20 mV. (d) As in b, but for the data from c. (Ojha et al., 2017)

4. Discussion

4.1. Challenges in monitoring cellular reactive species

Cellular reactive species (RS) play important roles in vital physiological functions, while excess RS contribute to the development of clinical conditions and aging (Datta et al., 2000; Finkel, 2011; Holmström & Finkel, 2014; Thannickal & Fanburg, 2000). The understanding of molecular mechanisms by which RS function in either physiology or pathology requires precise information of cellular RS, such as their real-time generation and spatial distribution. Thus, there is a deliberate demand of tools that can capture and quantify RS in the living cell or tissues with adequate sensitivity. Increasing evidences suggest that monitoring of cellular RS is problematic even more than it was realized before because of the varied chemical nature of different RS, variable spatio-temporal distribution, interactions with other RS and with various antioxidants existing *in vivo* (Gomes et al., 2005; Kalyanaraman et al., 2012; Sharma et al., 2012). Moreover, even at toxic concentration, certain short-lived RS remain present in so small concentration that their detection or quantification becomes extremely challenging (Valgimigli et al., 2001). Thus, a rapid and sensitive RS sensor is desired to capture short-lived cellular RS existing in small concentrations.

Various methods, such as enzymatic assays (Flohe, 1984), electron paramagnetic resonance (EPR) spectroscopy (Valgimigli et al., 2001), nuclear magnetic resonance, and mass spectroscopy (Luo et al., 2005; Wright et al., 2002) have been employed since long time to investigate RS signals and related consequences in cells or tissues. Whereas all these approaches revealed several aspects of cellular RS, said methods involve cell lysis, analytical separation, and the performance of measurements under artificial conditions that make methods prone to artifacts (Bulina et al., 2005; Dixit et al., 2003; Gutscher et al., 2008; Murphy et al., 2011). Further, the reasonable argument arises that if the oxidative damage is involved in the onset of a disease, then antioxidant therapy must cure or delay the progression of that disease. However, the antioxidant therapy has not been successful so far in treating diseases that are associated with oxidative stress (Galli et al., 2002; Halliwell & Whiteman, 2004; Steinberg & Witztum, 2002). It is, therefore, necessary to be able to measure cellular RS with high accuracy to establish the precise role of cellular RS in physiology and pathophysiology.

4.2. Detection of cellular reactive species with fluorescent reporters: advantages and limitations

Development of redox-sensitive genetic variants of green fluorescent protein (GFP) has opened a new window for real-time RS detection in intact living cells and revolutionized the redox research. Genetically encoded redox-sensitive green fluorescent proteins, e.g., roGFP2 (Dooley et al., 2004) and variants, e.g., Grx1-roGFP2 (Gutscher et al., 2008), received much attention for studying RS signaling in living cells. roGFP2 (wild-type GFP with mutations C48S, S65T, S147C, and Q204C) reports real-time dynamic changes in the cellular redox environment in a ratiometric manner (Dooley et al., 2004). Two surface-exposed cysteines of roGFP2 that are located at positions 147 and 204 on adjacent β -strands close to the chromophore form a disulfide-bridge in response to oxidation. The formation of a disulfide-bridge results to the spectral shifts of roGFP2 near 400 nm and 490 nm (Dooley et al., 2004; Meyer & Dick, 2010). Since roGFP2 is a ratiometric fluorescence redox sensor, it overcomes artifacts that arise due to photo-bleaching (Dooley et al., 2004; Gutscher et al., 2008; Meyer & Dick, 2010). Although the usefulness of roGFP2 in detecting physiologically relevant RS signals is limited by the slow kinetic response to cellular oxidation, a fusion of human glutaredoxin-1 to roGFP2 remarkably increased the sensitivity of roGFP2 to short- and long-lived cellular redox signals (Gutscher et al., 2008; Hansen et al., 2006). Since roGFP2 and its variants are genetically encoded, they can be targeted to a specific subcellular site in the cell. Hence, genetically encoded fluorescent redox reporters are undoubtedly very useful tools that allow monitoring of cellular RS precisely in a spatio-temporal manner and promise to overcome some limitations of conventional redox measurements.

Moreover, the adequate yield of genetically encoded fluorescent reporters in various cell types adds an important property of such reporters in investigating redox related functions of several biological stressors of unknown functions. For example, assay of third-order heme degradation products, i.e. BOXes, with Grx1-roGFP2 expressing HEK 293T and HepG2 cells showed the importance of genetically encoded fluorescent reporters in revealing redox related functions of BOXes. Grx1-roGFP2 expressed in HEK 293T and HepG2 cells indicate that BOXes may modify cytosolic glutathione, but the rate of modification of cytosolic glutathione is different in both cell types (Seidel et al., 2017). In both cell types, BOXes initiate disulfide bond formation in Grx1-roGFP2 that indicates glutathione redox potential shifts to a more oxidized state when cells are exposed to BOXes (Seidel et al., 2017). Grx1-roGFP2 responds differently to the same concentration of hydrogen peroxide and BOXes, which suggests that BOXes may differently interact with cellular glutathione system. Additionally, Seidel et al. (2017) showed that BOXes do not increase lipid

peroxidation but interact with glutathione. Hence, a clear picture that illustrates how BOXes affect cellular redox homeostasis is still not clear and to establish the precise role of BOXes in redox regulation, further study is required. Nevertheless, assay of BOXes employing Grx1-roGFP2 unraveled redox-related functional aspects of BOXes.

Despite several advantages of genetically encoded fluorescent redox reporters, the photonic exposure to read-out the state of these reporters makes the technique prone to artifacts because photonic illumination to the cell itself and/or excited fluorescent probes may modify the cellular environment (Bulina et al., 2005; Editorial, *Nat. Meth.*, 2013; Edward & Silva, 2001; Greenbaum et al., 2000; Niwa et al., 1996). Such photonic artifacts are infrequently considered in life science research (Editorial, *Nat. Meth.*, 2013), thus, cellular RS detection requires alternative/additional tools that can be employed in a non-photonic fashion.

4.3. Development of non-photonic alternatives to fluorescent redox reporters

A previous report (Kassmann et al., 2008) showed that the inactivation of wild-type rat Nav1.4 is susceptible to oxidative modification mainly due the presence of methionine in the inactivation motif (IFM). Oxidative modification of methionine within the IFM motif (e.g., the formation of methionine sulfoxide by addition of oxygen to the sulfur atom of methionine) results in a marked loss of channel inactivation (Kassmann et al., 2008; Kim et al., 2014). Anticipating a greater oxidation sensitivity of cysteine and selenocysteine compared to methionine, in order to increase the oxidation sensitivity of channel inactivation, we genetically engineered two rNav1.4 mutants namely roNav1 (reduction-oxidation sensitive voltage-gated Na⁺ channel1; rNav1.4 mutant IFC), and roNav2 (reduction-oxidation sensitive voltage-gated Na⁺ channel2; rNav1.4 mutant IFU), as plausible alternatives to fluorescent redox reporters. These channel variants indicate real-time dynamic changes in the cellular redox milieu based on the oxidative modification of a single Cys (roNav1) or a single Sec (roNav2) located in the inactivation motif. Both channel variants, roNav1 and roNav2, progressively lose their inactivation in response to oxidative modification, the degree of RS-mediated channel modification is measured as a ratiometric signal from the degree of inactivation, thus, yield a concentration independent parameter allowing for absolute calibration.

roNav1 was selected among several rNav channel mutants containing either additional methionine (Met) or cysteine residues (Cys) in the inactivation motif because roNav1 exhibits functional properties close to the wild type and exhibits relatively small non-inactivating residual current under control conditions compared to other channel mutants with additional

Met or Cys. This close resemblance to the channel properties infers that replacement of Cys for Met in the IFM motif only has a minor impact on the stability of inactivation domain at its receptor site.

It is noteworthy that the introduction of additional Met in the inactivation motif of the wild type (IFM) increases the susceptibility of inactivation to oxidative modification. Channel variants with additional Met residues, e.g., MFM and MMM, exhibit greater oxidation sensitivity than the wild type, and thus suits well to study Met-directed oxidative processes. Previous evidences suggest that methionine oxidation play important roles in certain physiological functions, such as cytoplasmic translocation of the cytochrome (Godoy et al., 2009), cellular protein phosphorylation (Hardin et al., 2009), functional modulation of ion channels (Hoshi & Heinemann, 2001), and leukocyte migration (Sroussi et al., 2007). However, excess methionine oxidation produces pathophysiological consequences, such as reperfusion injury (Chan, 1996), and rheumatoid arthritis (Chidwick et al. 1991). Although several attempts have been made to monitor real-time methionine oxidation in order to understand functional consequences (Guan et al., 2003; Oien et al., 2009; Sen et al., 2017), said channel mutants with additional Met may also help to better understand those functional consequences of methionine oxidation that are still overlooked due to the lack of appropriate detection tools.

Since cysteine is well-recognized for the ease of its oxidation in biological samples compared to methionine (Kim et al., 2014; Lavine, 1947; Vogt, 1995), roNav1 exhibits relatively greater oxidation sensitivity than Nav channel mutants with additional Met residues. Aiming for even improving the redox sensitivity of roNav1, in order to also detect minor physiologically relevant changes in cellular redox levels, we genetically engineered roNav2 by inserting a selenocysteine into the inactivation motif (IFM1305U) of the wild-type channel. roNav2 is the first reported seleno- Na^+ channel protein that is adequately expressed in a heterologous expression system. Although significant efforts have been made since over more than two decades to understand the complex molecular machinery involved in producing recombinant selenoproteins in a eukaryotic expression system, it is not yet completely understood at the molecular detail. Selenium supplement and co-expression of certain trans-acting factors, such as SelA, SelB, and SelC, favor the production of selenoproteins in cultured mammalian cells (Gursinsky et al., 2008; Hondal, 2009; Small-Howard et al., 2006). The type of SECIS element and its placement after the stop codon are two additional deciding factors for the adequate expression of the Sec-containing protein in heterologous expression systems (Gursinsky et al., 2008; Krol, 2002). Applied to voltage-gated Na^+ channels in HEK 293T cells, even in the absence of mentioned trans-acting factors,

a SECIS element from human selenoprotein N and supplementation of the cell culture medium with 300 nM sodium selenate as a selenium donor was sufficient to yield measurable Na^+ current. roNav2 therefore demonstrates the use of Sec insertion as a powerful tool for increasing the experimental realm when studying structure-function relationships of ion channels.

Further, the adequate yield of roNav2 in cultured mammalian cells demonstrates the importance of selection of SECIS element, its distance from the stop codon, and the requirement of selenium supplement for the expression of selenoproteins in heterologous systems. The mutation in selenoproteins has long been reported in various clinical conditions, such as disorders of endocrine, skeletal muscles, and cardiovascular systems (Gonzalez-Flores et al., 2013; Schmidt et al., 2012), vigorous investigation of such disorders has not done so far due to small expression or no yield of selenoproteins in heterologous systems. Hence, the explicit treatment of selenoprotein-associated disorders is largely unknown. Genetically engineered roNav2 and its satisfactory expression yield in HEK 293T cells may shed some light on factors affecting Sec incorporation in proteins. Understanding of the mechanism and determining factors of selenoprotein production could allow the development of clinically relevant molecules that may modulate selenoprotein production in patients suffered from selenoprotein-associated disorders. Additionally, heterologous expression of proteins containing non-standard amino acids has become a frequently used technique for investigating unique structural and functional properties of enzymes and proteins (Gonzalez-Flores et al., 2013; Hondal, 2005; Stone and Yang, 2006). In this context, a successful Sec incorporation, as it was shown for roNav2, may provide functional insight of several selenoproteins of unknown functions.

Notably, insertion of a Sec in the inactivation motif of the Nav channel affects inactivation properties, mainly the half-maximal inactivation voltage and the time constant of fractional recovery. Thus, the introduction of a single Sec in place of a methionine in the IFM motif has a significant impact on the stability of inactivation domain at its receptor site. It can be speculated that Sec located in the inactivation motif of the channel may disturb the conformational organization of the inactivation motif. Further research is required to understand how a single Sec located in the inactivation domain affects functional properties of the channel.

4.4. Comparison of channel-based RS sensors with fluorescent redox reporters

Like fluorescent redox reporters, i.e. roGFP2 and Grx1-roGFP2, channel-based RS sensors yield real-time ratiometric signals in response to the dynamic change in the cellular redox

milieu. In a quantitative comparison, roNav1 and roGFP2 signals measured from the same cell in response to various extracellular stressors yield similar results. However, roNav1 displays a greater dynamic range in its ratiometric readout. Like previously described for the roGFP2 sensitivity to oxidative stressors, the sensitivity of roNav1 to small concentrations of extracellularly applied RS stressors is limited by the slow reaction kinetics of Cys oxidation (Cannon & Remington, 2006; Gutscher et al., 2008; Hansen et al., 2006). roNav2 can safely monitor redox changes induced by stressors in sub-micromolar concentration ranges. A relative greater oxidation sensitivity of roNav2 compared to roNav1 and roGFP2 arises due to the presence of Sec in its inactivation motif (Arnér, 2010; Hatfield et al., 2014). A relative higher oxidation sensitivity of roNav2 is physiologically relevant because it can capture short-lived RS immediately after its generations in the living cell. Hence, roNav2 can indicate small fluctuations in redox homeostasis. Nevertheless, roNav1 will be appropriate for monitoring long-lived RS and their consequences.

A higher oxidation sensitivity of a Sec-based (roNav2) compared to Cys-based RS sensor (e.g., roNav1 and roGFP2) is anticipated by the strong nucleophilicity of Sec. At physiological pH, Sec is probably deprotonated and more reactive; the pKa of selenol/selenate of free Sec is about 5.2, the pKa of the thiol/thiolate in free Cys, however, is 8.3 (Arnér, 2010; Stone & Yang, 2006). Although pKa values of the free amino acid are experimentally determined in the aqueous solution, the situation may be completely different when amino acids, such as Cys and Sec, are present in a protein structure (Arnér, 2010; Toppo et al., 2009; Wessjohann et al., 2007). Additionally, the cellular environment and the presence of proximal amino acid in the protein structure influence the chemical reactivity of a particular amino acid (García-Santamarina et al., 2014). Quantum chemical calculations suggest that the reactivity of Cys and Sec to H₂O₂ in aqueous solution is almost similar, however, the reactivity of the Sec is greater when it is located in enzymes, for instance in glutathione peroxidase (Cardey & Enescu, 2007). This indicates that the molecular environment along with the pKa value may strongly determine the sensitivity of Sec, and that appears also to be true at the location of the inactivation motif of roNav2 channels.

Previous reports (Halliwell & Whiteman, 2004; Shay & Wright, 2002) suggest that the cell culture procedure affects endogenous RS, roNav2 and Grx1-roGFP2 are capable in distinguishing endogenous RS differences. Moreover, roNav2 and Grx1-roGFP2 can also capture minor differences in intracellular RS induced by glucose supplemented in cell culture media, while roGFP2 and roNav1 fail to report these changes. The human Grx1 accelerates the rate of disulfide bond formation in roGFP2 thereby Grx1-roGFP2 exhibits greater redox sensitivity compared to roGFP2 (Gutscher et al., 2008), while the performance of roNav2 is

based on the oxidative modification of a single amino-acid residue, Sec. The performance of roNav2 comparable to Grx1-roGFP2 to oxidative modifications illustrates the worthwhile application of Sec as a powerful RS sensing element.

In a qualitative comparison of measured signals from channel-based RS sensors (roNav1 and roNav2) and fluorescent sensors (roGFP2 and Grx1-roGFP2), channel-based RS sensors produce noisier signals than that of fluorescent reporters during RS quantification. As previously described for channel signals (Ojha et al., 2014), peak Na⁺ currents are part of the measurement thereby the signal cannot be averaged as much as, for example, fluorescence episodes of 10-20 ms. Moreover, channel signals are formed by approximately 1000-10,000 channel proteins only and, thus, are subject to greater statistical fluctuations (non-stationary channel noise).

4.5. Advantages of channel-based RS sensors

The strongest argument for the use of channel-based RS sensors in RS sensing comes from the potential photo-toxicity of blue light required to elicit signals of roGFP2 and its variants. As shown in Fig. 51 and 58, redox measurements using fluorescent reporters may exhibit light-induced artifacts because endogenous photosensitizers and photo-activated fluorescent reporters upon visible-light irradiation either produce RS or modify cellular milieu (Edwards & Silva, 2001; Eichler et al., 2005; King et al., 2004; Editorial, Nat. Meth., 2013). Additionally, the effects on cell membrane components induced by seemingly non-destructive short-time exposure of visible light are not yet fully explored.

Since measurements using channel-based RS sensors do not require light, they can be used to study phototoxic effects. As illustrated in Fig. 48 and 49, inactivation properties of channels were substantially affected when cells were subjected to blue and green light. Altered inactivation properties of channels upon blue/green light illumination may indicate that structure and function of the membrane or cytoplasmic proteins, which contain either Cys or Sec residue(s), may be modified when cells are subjected to light. Functional modifications of Cys/Sec rich membrane or cytoplasmic proteins may depend on wavelength, intensity, and exposure time of the light. Both channel-based RS sensors, roNav1 and roNav2, respond to blue-light-induced chemical modification, roNav2 responds about 1,500-fold faster to blue-light compared with roNav1. Thus, it can be speculated that the rate of light-induced modification of cellular/membrane proteins will also depend on structural elements of the protein when cells are subjected to the light of a particular wavelength and intensity for the particular duration of time. Noticeably, the rapid response of roNav2 to small doses of blue light is completely reversed in the dark. A relative higher sensitivity of roNav2

to blue-light-induced RS compared to roNav1 and rapid recovery in the dark is anticipated by a high nucleophilicity and electrophilicity of selenium in Sec compared with sulfur in Cys (Ruggles et al., 2011). While a relatively higher sensitivity of roNav2 to blue light is beneficial because immediate chemical modification induced by light irradiation can be monitored rapidly, a potential drawback could be the exquisite sensitivity because the sensor itself is driven into saturation with even short light exposures.

Further, as illustrated in section 3.5.8.4, the change in fluorescence ratio of all fluorescent variants upon blue-light irradiation inferred that blue-light either chemically modify these fluorescent proteins or produces light-induced RS. This evidence clearly showed that RS measurements using fluorescent probes will inherently suffer from the light-mediated artifacts. Moreover, the light independence of channel-based RS sensors is an advantageous feature whenever excitation light would interfere with other light-sensitive components as shown in Fig. 47 where roNav1 responds to photo-activated KillerRed induced RS.

Due to the rapid response time of channel-based RS sensors and their independence on light, they can be useful in studying distribution and lifetime of RS triggered by the light pulse. As described in section 3.6, types of reactive species with respective mean lifetime can be assessed by the real-time oxidative modifications of channel-based RS sensors. Importantly, the activity of channel-based RS sensors can be controlled by means of electrical membrane potential, thus, they can be sent into a hibernating state by depolarizing the membrane for longer duration and the condition so-called inactivation. In the inactivated state, the relevant oxidation-sensitive element of the channel, i.e. Cys (roNav1) and Sec (roNav2), apparently becomes protected from RS attack. As shown in Fig. 52, 54, 55, and 57, roNav1 and roNav2 remain effectively protected from light-induced RS when channels were in inactivated state. This was not only true for light-induced RS but also for chloramine T challenges and RS generated via light excited Lucifer Yellow and KillerRed (Ojha et al., 2014). In all cases, incremental loss of channel inactivation in response to RS depends on whether the channel was in a resting state or in an inactivated state confirms that RS sensitivity of channel sensor to oxidative modification could be controlled by means of changing electrical membrane potential. Hence, by designing of tailored pulse protocols one can thus read-out channel-based RS sensors only at specific intervals and protect them from RS-mediated destruction otherwise.

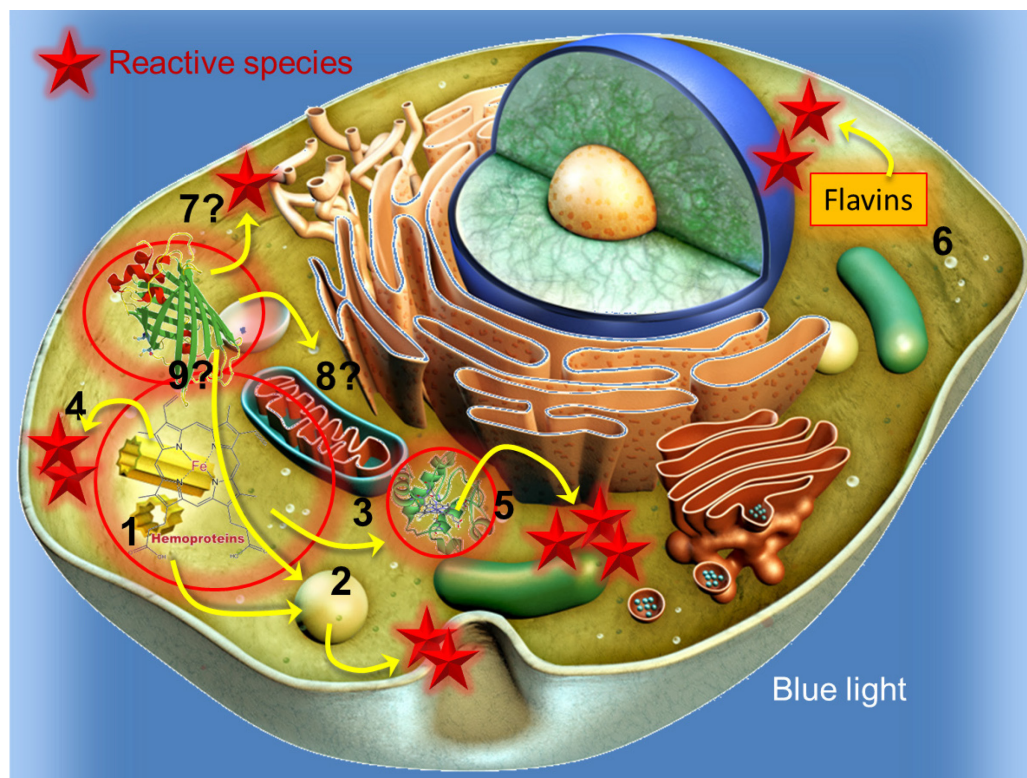


Figure 58: Visible-light-induced modifications of cellular milieu. Possible modifications in the living cell upon visible light, for instance blue-light, illumination are illustrated. Each numeral depicts a presumable modification in the cell upon visible light illumination. Upon light illumination: 1. Cytochromes or hemoproteins may become photosensitized. 2. Photosensitized cytochromes may transfer their energy to the neighboring non-sensitized cellular component(s) and thus, non-sensitized component(s) may get functionally modify and/or produce RS. 3. A photosensitized cytochrome may transfer energy to other types of cytochromes. 4. Photosensitized cytochromes can induce RS. 5. Different types of cytochromes and/or tryptophan-rich proteins may become photosensitized either by excited light or by getting suitable energy from neighboring cytochromes. 6. Flavins produce RS. 7. Photobleaching of fluorescent reporters may produce RS. 8. Excited fluorescent reporters may alter glutathione homeostasis or another cellular redox couple. 9. Excited fluorescent reporters may transfer their energy to the non-photo-sensitized cellular component. Question marks indicate consequences of excited fluorescent reporters in the living cell require thorough examination. Red stars indicate reactive species.

(The cell picture is modified from: <https://ciiid.washington.edu/content/signaling-human-cell-transgenics>).

A very important advantage of channel-based RS sensors is that the recorded signals come from a site right at the interface of membrane protein and cytosol; hence, signals of the channel-based RS sensors represent a chemical process occurring exactly at the plasma membrane. This is a very important aspect if membrane-delimited processes are to be studied, while the spatial resolution of membrane-targeted fluorescent proteins, such as roGFP2, is diffraction limited and thus will not provide a clean membrane-delimited signal

and is confounded by background fluorescence arising from the proteins close but not inside the plasma membrane. Additionally, measurements with the channel-based RS sensors in the cell-attached configuration will give access to the status of sensors positioned under the pipette tip of about 1 μM diameter.

4.6. Cysteine and selenocysteine as oxidation sensing elements in channel-based RS sensors

Cellular RS chemically react with biomolecules and/or synthetic redox indicators and form oxidation end product(s) as unique chemical ‘fingerprint’ that indicate the cellular redox status (Halliwell & Gutteridge, 1999; Shulaev et al., 2006). Qualitative and quantitative assay of end-products reflect the degree of cellular oxidation.

Cysteine residues are present in the catalytic active site of several enzymes, such as thioredoxin and glutathione, and play important role in sensing cellular redox status (Berndt et al., 2006), which indicate cysteine can serve as a redox-sensing element in RS-sensing probes. Based on the oxidative modification of two surface-exposed cysteines (147C and 204C), genetically encoded roGFP2 reports the dynamic change in the redox milieu. Cysteine forms a disulfide bond (-S-S-) with adjacent cysteine in the presence of oxidants and thus, yields a cysteine dimer, i.e. cystine. The cysteine/cystine, i.e. thiol/disulfide couple indicates the oxidative state of the cell and functions in cellular redox switching (Jonnes et al., 2004). Since the formation of cystine is an indicative parameter of oxidation, the formation of a disulfide bridge between 147C and 204C of roGFP2 indicates the relative change in the cellular redox environment (Fig. 59). The formation of a disulfide bridge produces structural rearrangements of roGFP2 that is reflected by a shift in the excitation spectrum.

Whereas roGFP2 has no specificity for a particular redox couple and responds too slowly to endogenous redox changes, Grx1-roGFP2 has very high specificity and sensitivity for the GSH/GSSG redox couple (Gutscher et al., 2008; Meyer & Dick, 2010). Grx1 particularly interacts with glutathione (Björnberg et al., 2006; Gutscher et al., 2008; Meyer & Dick, 2010). During cellular oxidation, the nucleophilic Cys (C23) of Grx1 explicitly reacts with oxidized glutathione (GSSG) and forms a mixed Grx1-glutathione disulfide intermediate. Subsequently, one of the two cysteines of roGFP2 becomes S-glutathionylated, later rearrangements lead to the formation of internal disulfide bridge (C147–C204) in roGFP2 (Bhaskar et al., 2014; Meyer & Dick, 2010). As illustrated in Fig. 59b, the three consecutive steps of thiol-disulfide exchange in Grx1-roGFP2 are fully reversible in presence of reduced glutathione.

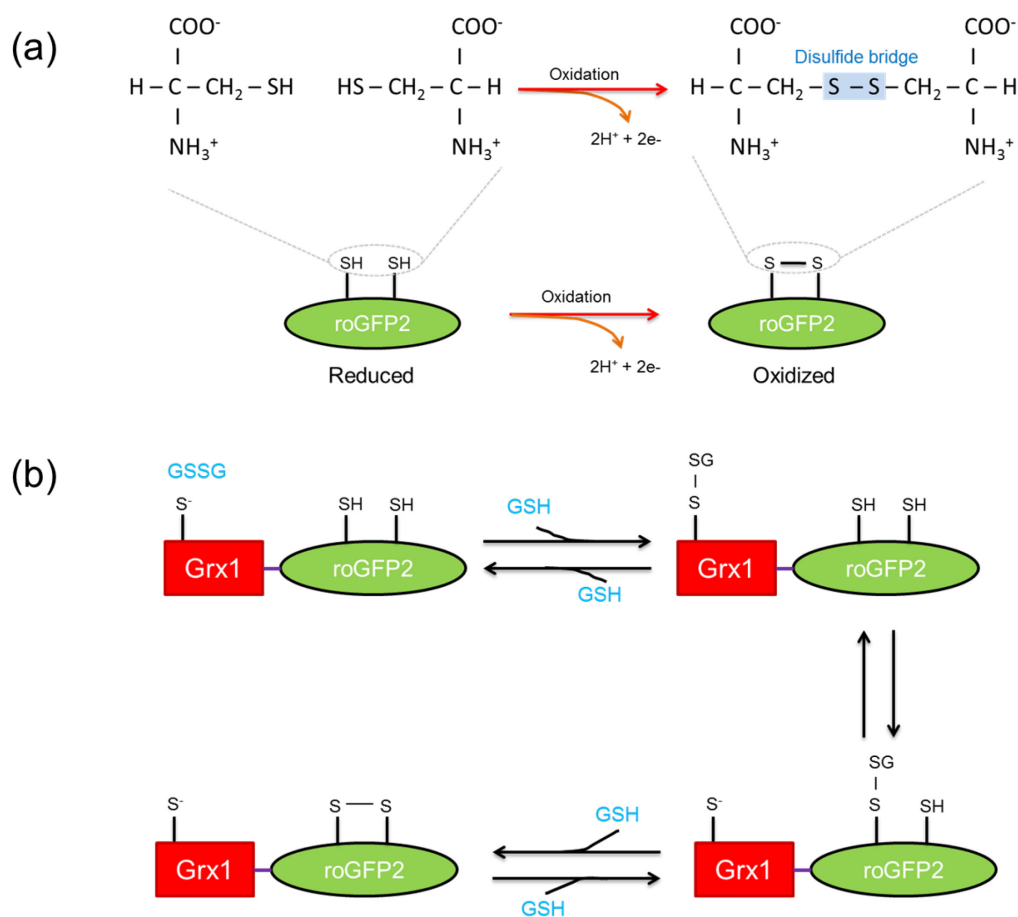


Figure 59: Principle of cysteine-based redox sensors. (a) Molecular mechanism of the roGFP2 biosensor. Two cysteines (147C and 204C) of roGFP2 form a disulfide bridge with each other in response to oxidation. The thiol group of two adjacent cysteines loses one hydrogen atom to form a disulfide bond. The thiols (-SH) indicate a reduced state, while a disulfide bridge (-S-S-) indicates an oxidized state. (b) Molecular mechanism of the Grx1-roGFP2 biosensor. First step: the nucleophilic cysteine (C23) of Grx1 particularly reacts with oxidized glutathione (GSSG) and a mixed Grx1-glutathione disulfide intermediate is formed. Second step: Grx1-glutathione disulfide intermediate reacts with one of the two thiols of roGFP2 to form glutathionylated roGFP2. Third step: glutathionylated roGFP2 rearranges to form a disulfide bridge between 147C and 204C of roGFP2. All steps are fully reversible in presence of reduced GSH. (Scheme adapted and modified from Bhaskar et al., 2014; Meyer & Dick, 2010).

Further, it can be presumed that the molecular mechanism of channel-based RS sensors is very much like roGFP2 for indicating dynamic changes in the redox milieu. Similar response kinetics of roGFP2 and roNav1 to oxidative modification indicates cysteine located in the inactivation motif of the roNav1 may also find a Cys as a binding partner from a cytoplasmic protein or an intracellular loop of the sensor and forms a disulfide bridge to become immobilized (Fig. 60 and 61). Formation of a disulfide bridge may produce a conformational change in the inactivation motif of the channel; thereby the channel pore does

not occlude appropriately, and hence, the relative fraction of the non-inactivating current of roNav1 increases with time.

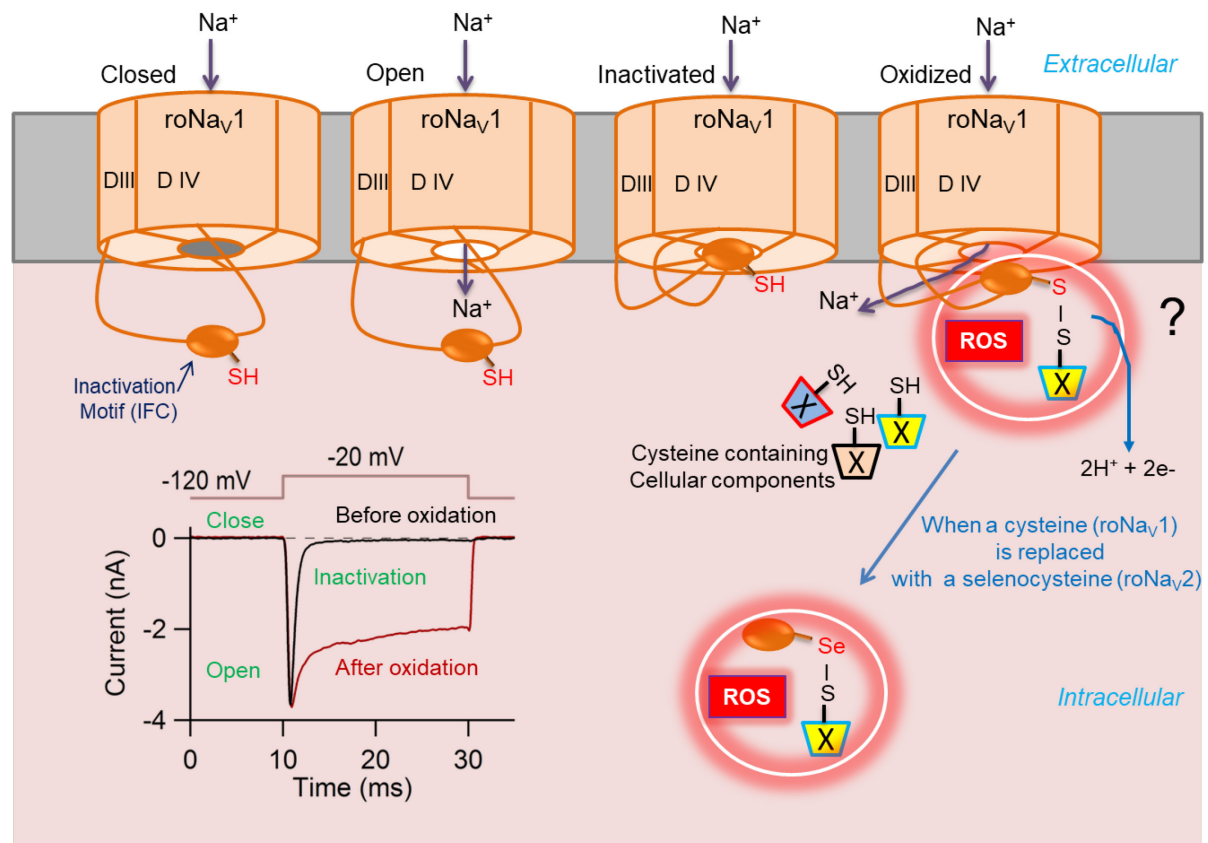


Figure 60: Molecular mechanism of channel-based RS sensors. Different states of membrane-localized roNav1 are shown. At very negative potential (e.g., -120 mV) or resting membrane potential, channel gate remains closed and, thus, permeation of Na^+ ions into the cell via the channel pore is not possible. The inactivation motif (IFC) of roNav1 remains in the cytosol during the closed state of the channel. The channel opens in response to membrane depolarization (e.g., -20 mV) and a transient inward Na^+ current is produced due to the movement of Na^+ into the cell. Upon sustained depolarization, the channel pore is occluded by the inactivation motif (IFC) and inward Na^+ current is terminated. During oxidation, cysteine located in the inactivation motif of the roNav1 may form a disulfide-bridge (-S-S-) between nearby cysteine of cytosolic proteins; modification of the inactivation motif affects the inactivation kinetics and produces greater fractions of non-inactivating current over time. roNav2 may exhibit a mechanism similar to roNav1 for RS sensing but forms a selenium-sulfur bond (-Se-S-). The question mark indicates the requirement of further examination. roNav1 current responses before and after oxidation are shown in the left-lower panel.

As described in section 3.5.8.4, the response kinetics of roNav2 similar to eGFP mutant 147U:204C to blue-light-induced modification indicates that the Sec residue in the channel's inactivation motif may also find a Cys as a binding partner from a cytoplasmic protein or an intracellular loop of the sensor and forms selenium-sulfur bond (-Se-S-) to become immobilized (also see Fig. 60 and 61). It is also conceivable that the rapid change in

inactivation properties of roNav2 might be associated with a lasting chemical modification or a short-lived photonic alteration of the Sec residues as reported for certain proteins that contain a diselenide bond (Ji et al., 2014). Additionally, unlike roGFP2, roNav2 and eGFP mutant 147U:204C reversed in the dark from blue-light-induced modification, which can be explained by a relatively weaker bond strength of selenium-sulfur bond (Se-S bond length=2.2 Å) in roNav2 and eGFP mutant 147U:204C compared to disulfide bond (S-S bond length=2.0 Å) in roGFP2 (Hondal et al., 2013). Since RS fluxes are often associated with physiological and pathophysiological consequences, reversibility of roNav2 makes it very useful tool for investigating the consequences of cellular RS over time.

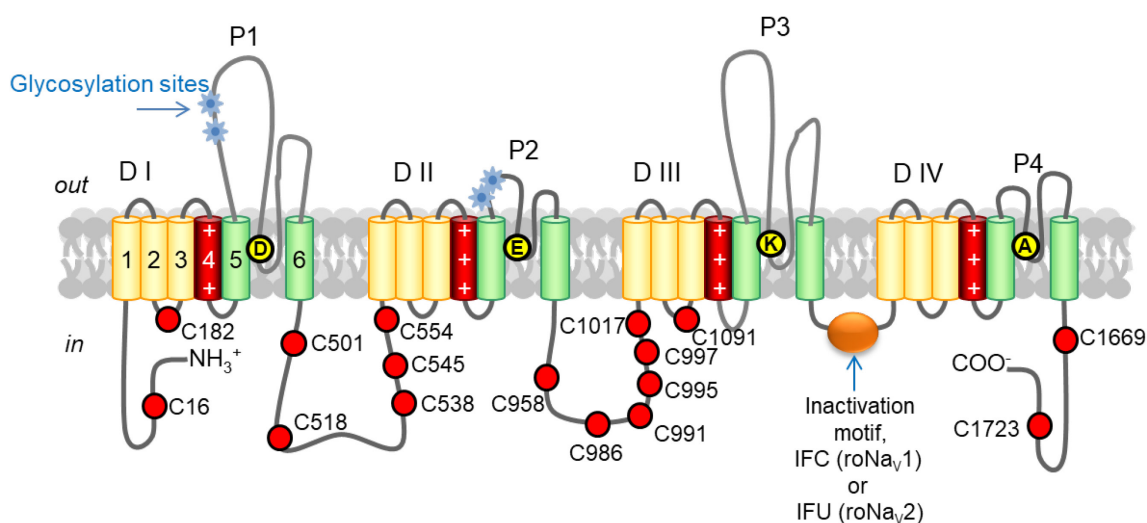


Figure 61: Transmembrane topology of channel-based RS sensors. The cartoon illustrates the rat Nav1.4 channel equipped with a cysteine (roNav1) or a selenocysteine (roNav2) in the inactivation motif. Cysteines located in intracellular loops of the channel-based RS sensor (roNav1/roNav2) are indicated. Indicated positions of cysteines are based on the rat skeletal muscle Nav1.4. During oxidation, a cysteine (roNav1) or a selenocysteine (roNav2) located in the inactivation motif might form a disulfide-bridge with any one of the indicated cysteine located in intracellular loops of the channel.

Since human glutaredoxin-1 specifically interacts with glutathione and it accelerates the formation of a disulfide-bridge in roGFP2 (Björnberg et al., 2006; Gutscher et al., 2008; Meyer & Dick, 2010), the presence of human Grx1 in the proximity of the inactivation motif may increase the oxidation sensitivity of roNav1. As shown in Fig. 62, the sensitivity of roNav1 can be increased by either fusing Grx1 to roNav1 or co-expressing membrane localized Grx1 with roNav1. Exhibiting a molecular mechanism similar to Grx1-roGFP2, proposed Grx1-roNav1 may report real-time dynamic changes in a glutathione couple with high sensitivity and in a non-photonic fashion.

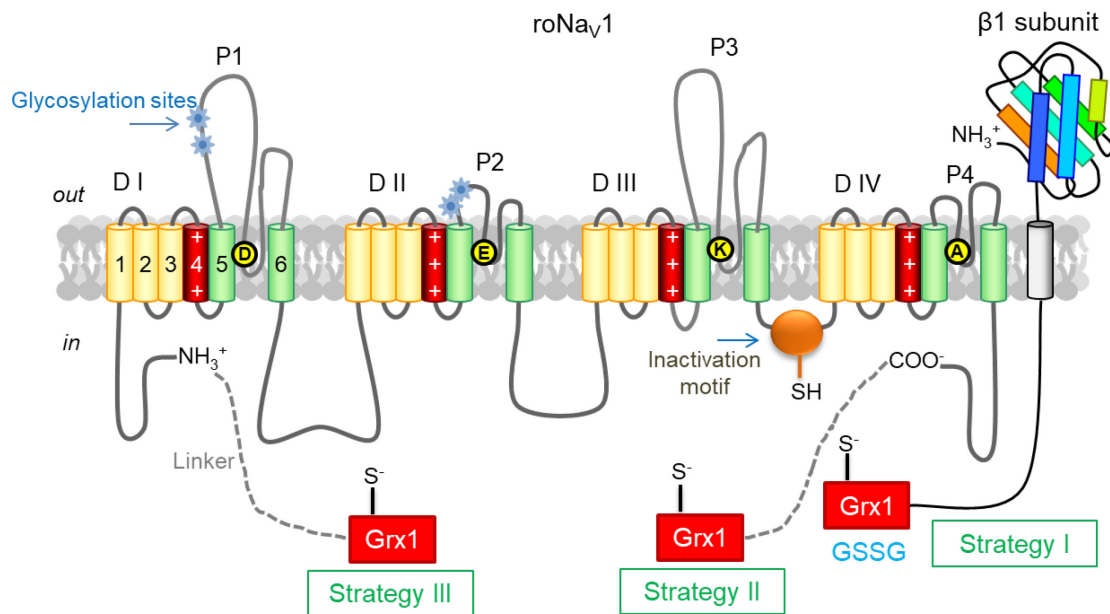


Figure 62: Strategies to develop Grx1-roNav1. Since it was presumed that the thiol located in the inactivation motif (IFC) of roNav1 forms a disulfide-bridge with neighboring cysteine of cellular proteins during oxidation, the introduction of human glutaredoxin-1 (Grx1) in the proximity of the inactivation motif of the channel may accelerate the formation of a disulfide bond. Grx1 can be placed in the proximity of the inactivation motif of the roNav1 by three strategies: strategy I – co-expression of Grx1 fused $\beta 1$ subunit of Na_v with roNav1, strategy II – fusion of Grx1 with the C-terminus of roNav1 with and without a linker, and strategy III – fusion of Grx1 with the N-terminus of roNav1 with and without a linker.

4.7. Limitations of channel-based RS sensors

Channel-based RS sensors may have some disadvantages, such as the requirement of performing patch-clamp experiments on single cells. This involves complicated experimental procedures and requirements of a complete patch-clamp electrophysiology setup. Additionally, the process of patching a cell needs a tight contact between the patch pipette and the cell, and application of pulse protocol essential to read-out channel-based RS sensors may have an impact on the cellular RS signaling. Moreover, the cell will progressively lose its reducing power in long recording sessions in patch-clamp whole-cell configuration. However, the performance of experiments with perforated patch methods, where electrical access to the cell interior is mediated by a perforating agent (e.g., escin), and thus retaining most of the cytosolic components of the cell, can be an alternative approach to whole-cell methods. Notably, roNav2 does not require very long recording sessions because of its rapid response rate and high sensitivity to redox modification. Therefore, measurements performed in whole-cell mode and perforated-mode do not affect the sensor readout as exemplified for blue-light-induced RS/chemical modification in section 3.5.8.3. Furthermore, the response of

channels to any particular redox pair has not yet been examined; channel-based RS sensors are seemingly non-specific and report overall changes in redox milieu.

Since real-time dynamic change in the cellular redox environment is indicated by relative fractions of the non-inactivating current of channel-based RS sensors, the applicability of channel-based RS sensors is limited where stressor itself interferes with channel's activity as it was seen for CORM-2. Since CORM-2 rapidly blocks peak currents of channel-based RS sensors, its redox-related functions cannot be assessed by channel-based RS sensors. Fluorescent reporters are very useful tools for studying redox-related signals, if any, arising from such types of chemical species. The molecular mechanism by which CORM-2 blocks peak current and affect functional properties of channel-based RS sensors and wild-type rNav1.4 requires further research.

All the techniques/methods of RS measurements have some pitfalls and advantages. Thus, it is very important to think cautiously about the working methodology and factors that confound the method before choosing a particular method of RS detection. It is therefore important to employ two or more techniques/methods for RS detection to avoid wrong interpretation of the results (Dikalov et al., 2007; Meyer & Dick, 2010). In accordance to that, channel-based RS sensors as non-photonic variants can be combined with other sensors, particularly fluorescent probes of RS determination in living cells for accurate interpretation.

5. Conclusions

We have developed two RS sensing tools, roNav1 and roNav2, based on rat Nav1.4 (SCN4A) for monitoring membrane-delimited reactive species in a non-photonic and ratiometric fashion. Oxidative modification of a single cysteine (roNav1) and a single selenocysteine (roNav2) in the inactivation motif of channel-based RS sensors results in a marked loss of inactivation that can be monitored by repeatedly recording currents mediated by channels on a real-time scale with high precision. The degree of inactivation loss yields a ratiometric signal (steady-state current / peak current) that allows real-time monitoring of concentration-dependent redox modifications delimited to the cell membrane.

The sensitivity of channel-based RS sensors to light-induced chemical modifications makes them very useful tools for testing the quality of photonic experiments in life science research. Moreover, these channel-based RS sensors are appropriately suited for single-molecule measurements and they can be employed for complex kinetic analysis, such as the dynamics and lifetime of RS in single living cells.

Notably, roNav2 is the first reported seleno- Na^+ channel, i.e. a voltage-gated Na^+ channel protein containing selenocysteine, which was adequately expressed in a heterologous expression system. The unprecedented high sensitivity of roNav2 to oxidative modifications demonstrated the power of recombinant selenoproteins as sensitive sensors for redox processes.

Putting the present study in a nutshell, channel-based RS sensors (roNav1 and roNav2) are not only rapid, sensitive, ratiometric, and light independent membrane-based RS sensors but also gateable (switchable) by the membrane voltage, allowing for complex experimental settings in which membrane-delimited occurrence of reactive species has to be monitored.

6. References

- Aggarwal, S. K., & MacKinnon, R.** (1996). Contribution of the S4 to K⁺ channel. *Neuron*, **16** (6), 1169-1177.
- Alberts, B., Johnson, A., Lewis, J., Raff, M., Roberts, K., & Walter, P.** (2002). Ion channels and the electrical properties of membranes. *Molecular Biology of the Cell*. 4th edition. New York: Garland Science.
- Ambrozova, G., Pekarova, M., & Lojek, A.** (2010). Effect of polyunsaturated fatty acids on the reactive oxygen and nitrogen species production by raw 264.7 macrophages. *European journal of nutrition*, **49** (3), 133-139.
- Amersi, F., Shen, X. D., Anselmo, D., Melinek, J., Iyer, S., Southard, D. J., Katori, M., Volk, H.D., Busuttill, R.W., Buelow, R., & Kupiec-Weglinski, J. W.** (2002). Ex vivo exposure to carbon monoxide prevents hepatic ischemia/reperfusion injury through p38 MAP kinase pathway. *Hepatology*, **35**(4), 815-823.
- Arnér, E. S.** (2010). Selenoproteins - what unique properties can arise with selenocysteine in place of cysteine? *Experimental cell research*, **316** (8), 1296-1303.
- Balsler, J. R.** (2002). Inherited sodium channelopathies: models for acquired arrhythmias?. *American Journal of Physiology-Heart and Circulatory Physiology*, **282**(4), H1175-H1180.
- Bayir, H.** (2005). Reactive oxygen species. *Critical care medicine*, **33** (12 Suppl), S498-S501.
- Beckmann, J. S., Ye, Y. Z., Anderson, P. G., Chen, J., Accavitti, M. A., Tarpey, M. M., & White, C. R.** (1994). Extensive nitration of protein tyrosines in human atherosclerosis detected by immunohistochemistry. *Biological Chemistry Hoppe-Seyler*, **375** (2), 81-88.
- Berndt, C., Lillig, C. H., & Holmgren, A.** (2007). Thiol-based mechanisms of the thioredoxin and glutaredoxin systems: implications for diseases in the cardiovascular system. *American Journal of Physiology-Heart and Circulatory Physiology*, **292**(3), H1227-H1236.
- Bhaskar, A., Chawla, M., Mehta, M., Parikh, P., Chandra, P., Bhave, D., Kumar, D., Carroll, K.S., & Singh, A.** (2014). Reengineering redox sensitive GFP to measure mycothiol redox potential of *Mycobacterium tuberculosis* during infection. *PLoS pathogens*, **10**(1), e1003902.
- Björnberg, O., Østergaard, H., & Winther, J. R.** (2006). Mechanistic insight provided by glutaredoxin within a fusion to redox-sensitive yellow fluorescent protein. *Biochemistry*, **45**(7), 2362-2371.
- Bogeski, I., & Barbara, A. N.** (2014). Redox regulation of ion channels. *Antioxidants & Redox Signaling*, **21**(6), 859-862
- Bogeski, I., Kappl, R., Kummerow, C., Gulaboski, R., Hoth, M., & Niemeyer, B. A.** (2011). Redox regulation of calcium ion channels: chemical and physiological aspects. *Cell calcium*, **50** (5), 407-423.
- Brackenbury, W. J., & Isom, L. L.** (2011). Na⁺ channel β subunits: overachievers of the ion channel family. *Frontiers in pharmacology*, **2**, 53.
- Brand, M. D.** (2010). The sites and topology of mitochondrial superoxide production. *Experimental gerontology*, **45** (7), 466-472.
- Briehl, M. M.** (2015). Oxygen in human health from life to death-An approach to teaching redox biology and signaling to graduate and medical students. *Redox biology*, **5**, 124-139.
- Bulina, M. E., Chudakov, D. M., Britanova, O. V., Yanushevich, Y. G., Staroverov, D. B., Chepurnykh, T. V., Merzlyak, E.M., Shkrob, M.A., Lukyanov, S., & Lukyanov, K. A.** (2006). A genetically encoded photosensitizer. *Nature biotechnology*, **24**(1), 95-99.

- Butz, E. A., Hostager, B. S., & Southern, P. J.** (1994). Macrophages in mice acutely infected with lymphocytic choriomeningitis virus are primed for nitric oxide synthesis. *Microbial pathogenesis*, **16**(4), 283-295.
- Cai, Z., & Yan, L. J.** (2013). Protein oxidative modifications: beneficial roles in disease and health. *Journal of Biochemical and Pharmacological Research*, **1** (1), 15.
- Cannon, M. B., & Remington, S. J.** (2006). Re-engineering redox-sensitive green fluorescent protein for improved response rate. *Protein science*, **15**(1), 45-57.
- Cannon, S. C.** (2000). Spectrum of sodium channel disturbances in the nondystrophic myotonias and periodic paralyses. *Kidney international*, **57**(3), 772-779.
- Catterall, W. A.** (1984). The molecular basis of neuronal excitability. *Science*, **223**, 653-662.
- Catterall, W. A.** (2000). From ionic currents to molecular mechanisms: the structure and function of voltage-gated sodium channels. *Neuron*, **26**(1), 13-25.
- Catterall, W. A.** (2010). Ion channel voltage sensors: structure, function, and pathophysiology. *Neuron*, **67** (6), 915-928.
- Catterall, W. A.** (2014). Structure and function of voltage-gated sodium channels at atomic resolution. *Experimental physiology*, **99**(1), 35-51.
- Chan, P. H.** (1996). Role of oxidants in ischemic brain damage. *Stroke*, **27**(6), 1124-1129.
- Chance, B., Sies, H., & Boveris, A.** (1979). Hydroperoxide metabolism in mammalian organs. *Physiological reviews*, **59**(3), 527-605.
- Chandy, K. G.** (1991). Simplified gene nomenclature. *Nature*, **352**(6330), 26.
- Chen, J., Avdonin, V., Ciorba, M.A., Heinemann, S.H., & Hoshi, T.** (2000). Acceleration of P / C-type inactivation in voltage-gated K⁺ channels by methionine oxidation. *Biophysical journal*, **78**(1), 174-187.
- Chidwick, K., Winyard, P. G., Zhang, Z., Farrell, A. J., & Blake, D. R.** (1991). Inactivation of the elastase inhibitory activity of alpha 1 antitrypsin in fresh samples of synovial fluid from patients with rheumatoid arthritis. *Annals of the rheumatic diseases*, **50**(12), 915-916.
- Ciorba, M.A., Heinemann, S.H., Weissbach, H., Brot, N., & Hoshi, T.** (1999). Regulation of voltage-dependent K⁺ channels by methionine oxidation: effect of nitric oxide and vitamin C. *FEBS letters*, **442**(1), 48-52.
- Clark, J. F., & Pyne-Geithman, G.** (2005). Vascular smooth muscle function: the physiology and pathology of vasoconstriction. *Pathophysiology*, **12**(1), 35-45.
- Creighton, T. E.** (1993). Proteins: structures and molecular properties. *Macmillan*.
- Cunningham, M. L., Krinsky, N. I., Giovanazzi, S. M., & Peak, M. J.** (1985). Superoxide anion is generated from cellular metabolites by solar radiation and its components. *Journal of free radicals in biology & medicine*, **1**(5-6), 381-385.
- D'Autréaux, B., & Toledano, M. B.** (2007). ROS as signalling molecules: mechanisms that generate specificity in ROS homeostasis. *Nature reviews. Molecular cell biology*, **8**(10), 813.
- Desaphy, J. F., De Luca, A., Imbrici, P., & Camerino, D. C.** (1998). Modification by ageing of the tetrodotoxin-sensitive sodium channels in rat skeletal muscle fibres. *Biochimica et Biophysica Acta (BBA)-Biomembranes*, **1373**(1), 37-46.
- Dexter, D. T., Holley, A. E., flitter, W. D., Slater, T. F., Wells, F. R., Daniel, S. E., Lees, A. J., Jenner, P., & Marsden, C. D.** (1994). Increased levels of lipid hydroperoxides in the Parkinsonian substantia nigra: on HPLC and ESR study. *Movement Disorders*, **9**(1), 92-97.

- Dickinson, B. C., & Chang, C. J.** (2011). Chemistry and biology of reactive oxygen species in signaling or stress responses. *Nature chemical biology*, **7**(8), 504-511.
- Dixit, R., & Cyr, R.** (2003). Cell damage and reactive oxygen species production induced by fluorescence microscopy: effect on mitosis and guidelines for non-invasive fluorescence microscopy. *The Plant Journal*, **36**(2), 280-290.
- Dixon, S. J., & Stockwell, B. R.**, (2014). The role of iron and reactive oxygen species in cell death. *Nature chemical biology*, **10**(1), 9-17.
- Dooley, C.** (2006). Green fluorescence protein based indicators of dynamic redox changes and reactive oxygen species. *PhD thesis*. University of California, San Diego, USA.
- Dooley, C. T., Dore, T. M., Hanson, G. T., Jackson, W. C., Remington, S. J., & Tsien, R. Y.** (2004). Imaging dynamic redox changes in mammalian cells with green fluorescent protein indicators. *Journal of Biological Chemistry*, **279**(21), 22284-22293.
- Drazic, A., & Winter, J.** (2014). The physiological role of reversible methionine oxidation. *Biochimica et Biophysica Acta (BBA) Proteins and Proteomics*, **1844**(8), 1367-1382.
- Eaholtz, G., Colvin, A., Leonard, D., Taylor, C., & Catterall, W. A.** (1999). Block of brain sodium channels by peptide mimetics of the isoleucine, phenylalanine, and methionine (IFM) motif from the inactivation gate. *The Journal of general physiology*, **113**(2), 279-294.
- Editorial.** (2013). Artifacts of light. The dangers of phototoxicity in fluorescence experiments are too often ignored. *Nature methods*, **10**, 1135.
- Edwards, A. M., & Silva, E.** (2001). Effect of visible light on selected enzymes, vitamins and amino acids. *Journal of Photochemistry and Photobiology B: Biology*, **63**(1), 126-131.
- Eichler, M., Lavi, R., Shainberg, A., & Lubart, R.** (2005). Flavins are source of visible-light-induced free radical formation in cells. *Lasers in surgery and medicine*, **37**(4), 314-319.
- Elliott, S. J., Kunze, D. L., & Schilling, W. P.** (1991). Oxidant stress alters ion gradients and decreases membrane potential in cultured pulmonary artery endothelial cells (CPAS). *The FEBS journal*, **5**, A656-A656.
- Ertel, S. I., Ertel, E. A., & Clozel, J. P.** (1997). T-type Ca²⁺ channels and pharmacological blockade: potential pathophysiological relevance. *Cardiovascular Drugs and Therapy*, **11**(6), 723-739.
- Escayg, A., MacDonald, B. T., Meisler, M. H., Baulac, S., Huberfeld, G., An-Gourfinkel, I., Brice, A., LeGuern, E., Moulard, B., Chaigne, D., Malafosse, A., & Buresi, C.** (2000). Mutations of SCN1A, encoding a neuronal sodium channel, in two families with GEFS+ 2. *Nature genetics*, **24**(4), 343.
- Evans, J. R., & Bielefeldt, K.** (2000). Regulation of sodium currents through oxidation and reduction of thiol residues. *Neuroscience*, **101**(1), 229-236.
- Favre, I., Moczydlowski, E., & Schild, L.** (1996). On the structural basis for ionic selectivity between Na⁺, K⁺, and Ca²⁺ in the voltage-gated sodium channel. *Biophysical journal*, **71**(6), 3110-3125.
- Fedorova, M., Kuleva, N., & Hoffmann, R.** (2009). Reversible and irreversible modifications of skeletal muscle proteins in a rat model of acute oxidative stress. *Biochimica et Biophysica Acta (BBA)-Molecular Basis of Disease*, **1792**(12), 1185-1193.
- Fisher, A. B.** (2009). Redox signaling across cell membranes. *Antioxidants & redox signaling*, **11**(6), 1349-1356.
- Frank, H. Y., & Catterall, W. A.** (2003). Overview of the voltage-gated sodium channel family. *Genome biology*, **4**(3), 207.

- García-Santamarina, S., Boronat, S., & Hidalgo, E.** (2014). Reversible cysteine oxidation in hydrogen peroxide sensing and signal transduction. *Biochemistry*, **53**(16), 2560-2580.
- Ghosh, M. K., Mukhopadhyay, M., & Chatterjee, I. B.** (1997). NADPH-initiated cytochrome P450-dependent free iron-independent microsomal lipid peroxidation: specific prevention by ascorbic acid. *Molecular and cellular biochemistry*, **166**(1), 35-44.
- Godley, B. F., Shamsi, F. A., Liang, F. Q., Jarrett, S. G., Davies, S., & Boulton, M.** (2005). Blue light induces mitochondrial DNA damage and free radical production in epithelial cells. *Journal of Biological Chemistry*, **280**(22), 21061-21066.
- Godoy, L. C., Muñoz-Pinedo, C., Castro, L., Cardaci, S., Schonhoff, C. M., King, M., To'rtora, V., Marin, M., Miao, Q., Jiang, J. F., Kapralov, A., Jemmerson, R., Silkstone, G. G., Patel, J. N., Evans, J. E., Wilson, M. T., Green, D. R., Kagan, V. E., Radi, R., & Mannick, J. B.** (2009). Disruption of the M80-Fe ligation stimulates the translocation of cytochrome c to the cytoplasm and nucleus in nonapoptotic cells. *Proceedings of the National Academy of Sciences*, **106**(8), 2653-2658.
- Goldin, A. L.** (1999). Diversity of Mammalian Voltage-Gated Sodium Channels. *Annals of the New York Academy of Sciences*, **868**(1), 38-50.
- Goldin, A. L.** (2002). Evolution of voltage-gated Na⁺ channels. *Journal of Experimental Biology*, **205**(5), 575-584.
- Goldin, A. L.** (2003). Mechanisms of sodium channel inactivation. *Current opinion in neurobiology*, **13**(3), 284-290.
- Goldin, A. L., Barchi, R. L., Caldwell, J. H., Hofmann, F., Howe, J. R., Hunter, J. C., & Noda, M.** (2000). Nomenclature of voltage-gated sodium channels. *Neuron*, **28**(2), 365-368.
- Gomes, A., Fernandes, E., & Lima, J. L.** (2005). Fluorescence probes used for detection of reactive oxygen species. *Journal of biochemical and biophysical methods*, **65**(2), 45-80.
- Gonzalez, D. R., Treuer, A., Sun, Q. A., Stamler, J. S., & Hare, J. M.** (2009). S-Nitrosylation of cardiac ion channels. *Journal of cardiovascular pharmacology*, **54**(3), 188.
- Gonzalez-Flores, J. N., Shetty, S. P., Dubey, A., & Copeland, P. R.** (2013). The molecular biology of selenocysteine. *Biomolecular concepts*, **4**(4), 349-365.
- Goto, H., Yang, B., Petersen, D., Pepper, K. A., Alfaro, P. A., Kohn, D. B., & Reynolds, C. P.** (2003). Transduction of green fluorescent protein increased oxidative stress and enhanced sensitivity to cytotoxic drugs in neuroblastoma cell lines. *Molecular cancer therapeutics*, **2**(9), 911-917.
- Greenbaum, L., Rothmann, C., Lavie, R., & Malik, Z.** (2000). Green fluorescent protein photobleaching: a model for protein damage by endogenous and exogenous singlet oxygen. *Biological chemistry*, **381**(12), 1251-1258.
- Groeger, G., Quiney, C., & Cotter, T. G.** (2009). Hydrogen peroxide as a cell survival signaling molecule. *Antioxidants & redox signaling*, **11**(11), 2655-2671.
- Guan, Z., Yates, N. A., & Bakhtiar, R.** (2003). Detection and characterization of methionine oxidation in peptides by collision-induced dissociation and electron capture dissociation. *Journal of the American Society for Mass Spectrometry*, **14**(6), 605-613.
- Gutscher, M., Pauleau, A. L., Marty, L., Brach, T., Wabnitz, G. H., Samstag, Y., Meyer, A. J., & Dick, T. P.** (2008). Real-time imaging of the intracellular glutathione redox potential. *Nature methods*, **5**(6), 553-559.
- Hajieva, P., Bayatti, N., Granold, M., Behl, C., & Moosmann, B.** (2015). Membrane protein oxidation causes neuronal degeneration. *Journal of Neurochemistry*, **133**(3), 352-367.
- Halliwell, B.** (2001). Free radicals and other reactive species in disease. *Encyclopedia of Life Sciences*, 1-7.

- Halliwell, B.** (2006). Reactive species and antioxidants. Redox biology is a fundamental theme of aerobic life. *Plant physiology*, **141**(2), 312-322.
- Halliwell, B., & Gutteridge, J.** (1984). Oxygen toxicity, oxygen radicals, transition metals and disease. *Biochemical journal*, **219**(1), 1.
- Hardin, S. C., Larue, C. T., Oh, M. H., Jain, V., & Huber, S. C.** (2009). Coupling oxidative signals to protein phosphorylation via methionine oxidation in Arabidopsis. *Biochemical Journal*, **422**(2), 305-312.
- Heinemann, S. H., Terlau, H., Stühmer, W., Imoto, K., & Numa, S.** (1992). Calcium channel characteristics conferred on the sodium channel by single mutations. *Nature*, **356**(6368), 441.
- Hensley, K., Butterfield, D. A., Hall, N., Cole, P., Subramaniam, R., Mark, R., & Aksenova, M.** (1996). Reactive Oxygen Species as Causal Agents in the Neurotoxicity of the Alzheimer's Disease-Associated Amyloid Beta Peptides. *Annals of the New York Academy of Sciences*, **786**(1), 120-134.
- Hentze, M. W., Muckenthaler, M. U., Galy, B., & Camaschella, C.** (2010). Two to tango: regulation of mammalian iron metabolism. *Cell*, **142**(1), 24-38.
- Figure, Y., Katayama, Y., Takeuchi, K., Ohtubo, Y., & Yoshii, K.** (2003). Lucifer Yellow Slows Voltage-Gated Na⁺ Current Inactivation in a Light-Dependent Manner in Mice. *The Journal of physiology*, **550**(1), 159-167.
- Hille, B.** (2001). Ion channels of excitable membranes. Sunderland, MA: Sinauer.
- Hockberger, P. E., Skimina, T. A., Centonze, V. E., Lavin, C., Chu, S., Dadras, S., Reddy, J. K., & White, J. G.** (1999). Activation of flavin-containing oxidases underlies light-induced production of H₂O₂ in mammalian cells. *Proceedings of the National Academy of Sciences*, **96**(11), 6255-6260.
- Hondal, R. J.** (2005). Incorporation of selenocysteine into proteins using peptide ligation. *Protein and peptide letters*, **12**(8), 757-764.
- Hondal, R. J., & Ruggles, E. L.** (2011). Differing views of the role of selenium in thioredoxin reductase. *Amino acids*, **41**(1), 73-89.
- Hondal, R. J., Marino, S. M., & Gladyshev, V. N.** (2013). Selenocysteine in thiol/disulfide-like exchange reactions. *Antioxidants & redox signaling*, **18**(13), 1675-1689.
- Hool, L. C., & Corry, B.** (2007). Redox control of calcium channels: from mechanisms to therapeutic opportunities. *Antioxidants & Redox Signaling*, **9**(4), 409-435.
- Hoshi, T., & Heinemann, S. H.** (2001). Regulation of cell function by methionine oxidation and reduction. *The Journal of Physiology*, **531**(1), 1-11.
- Huber, R. E., & Criddle, R. S.** (1967). Comparison of the chemical properties of selenocysteine and selenocystine with their sulfur analogs. *Archives of Biochemistry and Biophysics*, **122**(1), 164-173.
- Huguenard, J. R.** (1996). Low-threshold calcium currents in central nervous system neurons. *Annual review of physiology*, **58**(1), 329-348.
- Isom, L. L., De Jongh, K. S., Patton, D. E., Reber, B. F. X., Offord, J., Charbonneau, H., & Catterall, W. A.** (1992). Primary Structure and Functional Expression of the β 1 Subunit of the Rat Brain Sodium Channel. *Science*, 839-842.
- Isom, L. L., Ragsdale, D. S., De Jongh, K. S., Westenbroek, R. E., Reber, B. F. X., Scheuer, T., & Catterall, W. A.** (1995). Structure and function of the β 2 subunit of brain sodium channels, a transmembrane glycoprotein with a CAM motif. *Cell*, **83**(3), 433-442.
- Johansson, L., Gafvelin, G., & Arnér, E. S.** (2005). Selenocysteine in proteins—properties and biotechnological use. *Biochimica et Biophysica Acta (BBA)-General Subjects*, **1726**(1), 1-13.

- Jones, D. P., Go, Y. M., Anderson, C. L., Ziegler, T. R., KINKADE, J. M., & Kirilin, W. G. (2004). Cysteine/cystine couple is a newly recognized node in the circuitry for biologic redox signaling and control. *The FASEB journal*, **18(11)**, 1246-1248.
- Karlsson, M., Kurz, T., Brunk, U. T., Nilsson, S. E., & Frennesson, C. I. (2010). What does the commonly used DCF test for oxidative stress really show?. *Biochemical Journal*, **428(2)**, 183-190.
- Kassmann, M., Hansel, A., Leipold, E., Birkenbeil, J., Lu, S. Q., Hoshi, T., & Heinemann, S. H. (2008). Oxidation of multiple methionine residues impairs rapid sodium channel inactivation. *Pflügers Archiv-European Journal of Physiology*, **456(6)**, 1085-1095.
- Kazen-Gillespie, K. A., Ragsdale, D. S., D'Andrea, M. R., Mattei, L. N., Rogers, K. E., & Isom, L. L. (2000). Cloning, localization, and functional expression of sodium channel β 1A subunits. *Journal of Biological Chemistry*, **275(2)**, 1079-1088.
- Kennett, E., & Kuchel, P. (2003). Redox reactions and electron transfer across the red cell membrane. *IUBMB life*, **55(7)**, 375-385.
- Kenwood, B. M., Weaver, J. L., Bajwa, A., Poon, I. K., Byrne, F. L., Murrow, B. A., Calderone, J.A., Hunag, L., Divakaruni, A.S., Tomsig, J.L., Okabe, K., Ryan, H.L., Coleman, G.C., Colombus, L., Yan Z., Saucerman, J.J., Smith, S.S., Holmes, J.W., Lynch, K.R., Ravichandran, K.S., Uchiyama S., Santos, W.L., Rogers, G.W., Okusa, M.D., Bayliss, D.A., & Hoehn, K.L. (2014). Identification of a novel mitochondrial uncoupler that does not depolarize the plasma membrane. *Molecular metabolism*, **3(2)**, 114-123.
- Killig, F., & Stark, G. (2002). Photodynamic activation of ion transport through lipid membranes and its correlation with a constant constant of the membrane. *Biochimica et Biophysica Acta (BBA) - Biomembranes*, **1564 (1)**, 207-213.
- Kim, G., Weiss, S. J., & Levine, R. L. (2014). Methionine oxidation and reduction in proteins. *Biochimica et Biophysica Acta (BBA)-General Subjects*, **1840(2)**, 901-905.
- Kohen, R., & Nyska, A. (2002). Invited review: Oxidation of biological systems: oxidative stress phenomena, antioxidants, redox reactions, and methods for their quantification. *Toxicologic pathology*, **30(6)**, 620-650.
- Kolbe, K., Schönherr, R., Gessner, G., Sahoo, N., Hoshi, T., & Heinemann, S. H. (2010). Cysteine 723 in the C-linker segment confers oxidative inhibition of hERG1 potassium channels. *The Journal of Physiology*, **588(16)**, 2999-3009.
- Kozai, D., Ogawa, N., & Mori, Y. (2014). Redox regulation of transient receptor potential channels. *Antioxidants & redox signaling*, **21(6)**, 971-986.
- Kranc, K. R., Pyne, G. J., Tao, L., Claridge, T. D., Harris, D. A., Cadoux-Hudson, T. A., Turnbull, J.J., Schofield, C.J., & Clark, J. F. (2000). Oxidative degradation of bilirubin produces vasoactive compounds. *The FEBS Journal*, **267(24)**, 7094-7101.
- Kurata, Y., Hisatome, I., Tsuboi, M., Uenishi, H., Zhang, G., Oyaizu, M., Sato, R., & Imanishi, S. (1998). Effect of sulfhydryl oxidoreduction on permeability of cardiac tetrodotoxin-insensitive sodium channel. *Life sciences*, **63(12)**, 1023-1035.
- Lambeth, J. D. (2004). NOX enzymes and the biology of reactive oxygen. *Nature reviews. Immunology*, **4 (3)**, 181.
- Lang, F., Föllner, M., Lang, K. S., Lang, P. A., Ritter, M., Gulbins, E., Verninov, A., Huber, S. M. (2005). The results of the study are summarized as follows: Ion channels in cell proliferation and apoptotic cell death. *The Journal of Membrane Biology*, **205(3)**, 147-157.
- Lavi, R., Shainberg, A., Friedmann, H., Shneyvays, V., Rickover, O., Eichler, M., Kaplan, D., & Lubart, R. (2003). Low energy visible light induces reactive oxygen species generation and stimulates an increase of intracellular calcium concentration in cardiac cells. *Journal of Biological Chemistry*, **278(42)**, 40917-40922.

- Lavine, T. F.** (1947). The formation, resolution, and optical properties of the diastereoisomeric sulfoxides derived from L-methionine. *Journal of Biological Chemistry*, **169**(3), 477-492.
- Leach, J. K., Van Tuyle, G., Lin, P. S., Schmidt-Ullrich, R., & Mikkelsen, R. B.** (2001). Ionizing radiation-induced, mitochondria-dependent generation of reactive oxygen / nitrogen. *Cancer research*, **61**(10), 3894-3901.
- Li, X., Fang, P., Mai, J., Choi, E. T., Wang, H., & Yang, X. F.** (2013). Targeting mitochondrial reactive oxygen species as novel therapy for inflammatory diseases and cancers. *Journal of hematology & oncology*, **6**(1), 19.
- Li, Z., Chapleau, M. W., Bates, J. N., Bielefeldt, K., Lee, H. C., & Abboud, F. M.** (1998). Nitric oxide as an autocrine regulator of sodium currents in baroreceptor neurons. *Neuron*, **20**(5), 1039-1049.
- Liao, J. C., Roider, J., & Jay, D. G.** (1994). Chromophore-assisted laser inactivation of proteins is mediated by the photogeneration of free radicals. *Proceedings of the National Academy of Sciences*, **91**(7), 2659-2663.
- Lim, J. C., Gruschus, J. M., Kim, G., Berlett, B. S., Tjandra, N., & Levine, R. L.** (2012). A low pKa cysteine at the active site of mouse methionine sulfoxides reductase A. *Journal of Biological Chemistry*, **287** (30), 25596-25601.
- Love, N.R., Chen, Y., Ishibashi, S., Kritsiligkou, P., Lea, R., Koh, Y., & Amaya, E.** (2013). Amputation-induced reactive oxygen species (ROS) are required for successful *Xenopus* tadpole tail regeneration. *Nature cell biology*, **15**(2), 222.
- Lu, J., & Holmgren, A.** (2009). Selenoproteins. *Journal of Biological Chemistry*, **284**(2), 723-727.
- Makino, N., Sasaki, K., Hashida, K., & Sakakura, Y.** (2004). A metabolic model describing the H₂O₂ elimination by mammalian cells including H₂O₂ permeation through cytoplasmic and peroxisomal membranes: comparison with experimental data. *Biochimica et Biophysica Acta (BBA)-General Subjects*, **1673**(3), 149-159.
- Mao, W., You, T., Ye, B., Li, X., Dong, H. H., Hill, J. A., Li, F., & Xu, H.** (2012). Reactive oxygen species suppress cardiac Nav1.5 expression through Foxo1. *PloS one*, **7**(2), e32738.
- Matough, F. A., Budin, S. B., Hamid, Z. A., Alwahaibi, N., & Mohamed, J.** (2012). The role of oxidative stress and antioxidants in diabetic complications. *Sultan Qaboos University Medical Journal*, **12**(1), 5.
- McPhee, J. C., Ragsdale, D. S., Scheuer, T., & Catterall, W. A.** (1998). A critical role for the S4-S5 intracellular loop in domain IV of the sodium channel α -subunit in fast inactivation. *Journal of Biological Chemistry*, **273**(2), 1121-1129.
- Meyer, A. J., & Dick, T. P.** (2010). Fluorescent protein-based redox probes. *Antioxidants & redox signaling*, **13**(5), 621-650.
- Møller, P., & Wallin, H.** (1998). Adduct formation, mutagenesis and nucleotide excision repair of DNA damage produced by reactive oxygen species and lipid peroxidation product. *Mutation Research/Reviews in Mutation Research*, **410**(3), 271-290.
- Morgan, K., Stevens, E. B., Shah, B., Cox, P. J., Dixon, A. K., Lee, K., & Jackson, A. P.** (2000). β 3: a further auxiliary subunit of the voltage-sensitive sodium channel that modulates channel gating with distinct kinetics. *Proceedings of the National Academy of Sciences*, **97**(5), 2308-2313.
- Motterlini, R., Clark, J. E., Foresti, R., Sarathchandra, P., Mann, B. E., & Green, C. J.** (2002). Carbon monoxide-releasing molecules. *Circulation research*, **90**(2), e17-e24.
- Nadal, A., Roperio, A. B., Fuentes, E., Soria, B., & Ripoll, C.** (2004). Estrogen and xenoestrogen actions on endocrine pancreas: from ion channel modulation to activation of nuclear function. *Steroids*, **69**(8), 531-536.

- Nagababu, E., & Rifkind, J. M.** (2004). Heme degradation by reactive oxygen species. *Antioxidants & redox signaling*, **6**(6), 967-978.
- Nathan, C., & Ding, A.** (2010). SnapShot: reactive oxygen intermediates (ROI). *Cell*, **140**(6), 951-951.
- Niwa, H., Inouye, S., Hirano, T., Matsuno, T., Kojima, S., Kubota, M., Ohashi, M., & Tsuji, F. I.** (1996). Chemical nature of the light emitter of the Aequorea green fluorescent protein. *Proceedings of the National Academy of Sciences*, **93**(24), 13617-13622.
- Noda, M., & Hiyama, T. Y.** (2015). The Na^x channel: what it is and what it does. *The Neuroscientist*, **21**(4), 399-412.
- Noda, M., Shimizu, S., Tanabe, T., Takai, T., Kayano, T., Ikeda, T., & Kangawa, K.** (1984). Primary structure of Electrophorus electricus sodium channel deduced from cDNA sequence. *Nature*, **312**(5990), 121-127.
- Noori, S.** (2012). An overview of oxidative stress and antioxidant defensive system. *Open access scientific reports*, **1**(8), 1-9.
- Oien, D. B., Canello, T., Gabizon, R., Gasset, M., Lundquist, B. L., Burns, J. M., & Moskovitz, J.** (2009). Detection of oxidized methionine in selected proteins, cellular extracts and blood serums by novel anti-methionine sulfoxide antibodies. *Archives of biochemistry and biophysics*, **485**(1), 35-40.
- Ojha, N. K., Leipold, E., Schönherr, R., Hoshi, T., & Heinemann, S. H.** (2017). Non-photonic sensing of membrane-delimited reactive species with a Na⁺ channel protein containing selenocysteine. *Scientific Reports*, **7**:46003.
- Ojha, N. K., Nematian-Ardestani, E., Neugebauer, S., Borowski, B., El-Hussein, A., Hoshi, T., Leipold, E., & Heinemann, S. H.** (2014). Sodium channels as gateable non-photonic sensors for membrane-delimited reactive species. *Biochimica et Biophysica Acta (BBA)-Biomembranes*, **1838**(5), 1412-1419.
- Olschewski, A., & Weir, E. K.** (2015). Redox regulation of ion channels in the pulmonary circulation. *Antioxidants & redox signaling*, **22** (6), 465-485.
- O'Malley, H. A., & Isom, L. L.** (2015). Sodium channel β subunits: emerging targets in channelopathies. *Annual review of physiology*, **77**, 481-504.
- Owusu-Ansah, E., Yavari, A., & Banerjee, U.** (2008). A protocol for in vivo detection of reactive oxygen species. *Protocol Exchange*. Epub 27 February 2008.
- Pacher, P., Beckman, J. S., & Liaudet, L.** (2007). Nitric oxide and peroxynitrite in health and disease. *Physiological reviews*, **87**(1), 315-424.
- Poole, L. B., Karplus, P. A., & Claiborne, A.** (2004). Protein sulfenic acids in redox signaling. *Annual Review of Pharmacology & Toxicology*, **44**, 325-347.
- Pryor, W. A., & Godber, S. S.** (1991). Noninvasive measures of oxidative stress status in humans. *Free Radical Biology and Medicine*, **10**(3-4), 177-184.
- Pyne-Geithman, G. J., Morgan, C. J., Wagner, K., Dulaney, E. M., Carrozzella, J., Kanter, D. S., Zuccarello, M., & Clark, J. F.** (2005). Bilirubin production and oxidation in CSF of patients with cerebral vasospasm after subarachnoid hemorrhage. *Journal of Cerebral Blood Flow & Metabolism*, **25**(8), 1070-1077.
- Rack, M., Rubly, N., & Waschow, C.** (1986). Effects of some chemical reagents on sodium current inactivation in myelinated nerve fibers of the frog. *Biophysical journal*, **50**(4), 557-564.
- Rhee, S. G., Bae, Y. S., Lee, S. R., & Kwon, J.** (2000). Hydrogen peroxides: a key messenger that modulates protein phosphorylation through cysteine oxidation. *Science Signaling*, **2000**(53), pe1-pe1.

- Roos, G., Foloppe, N., & Messens, J.** (2013). Understanding the pK_a of redox cysteines: the key role of hydrogen bonding. *Antioxidants & redox signaling*, **18**(1), 94-127.
- Ruggles, E. L., Snider, G. W., & Hondal, R. J.** (2011). Chemical basis for the use of selenocysteine. In selenium (pp. 73-83). Springer New York.
- Ruppersberg, J. P., Stocker, M., Pongs, O., Heinemann, S. H., Frank, R., & Koenen, M.** (1991). Regulation of fast inactivation of cloned mammalian Ik (A) channels by cysteine oxidation. *Nature*, **352**, 711-714.
- Sahoo, N., Hoshi, T., & Heinemann, S. H.** (2014). Oxidative modulation of voltage-gated potassium channels. *Antioxidants & redox signaling*, **21**(6), 933-952.
- Salvemini, D., & Cuzzocrea, S.** (2002). Oxidative stress in septic shock and disseminated intravascular coagulation. *Free Radical Biology and Medicine*, **33**(9), 1173-1185.
- Schmidt, R. L., & Simonović, M.** (2012). Synthesis and decoding of selenocysteine and human health. *Croatian medical journal*, **53**(6), 535-550.
- Seidel, R. A., Claudel, T., Schleser, F. A., Ojha, N. K., Westerhausen, M., Nietzsche, S., Sponholz, C., Cuperus, F., Coldewey, S.M., Heinemann, S.H., Pohnert, G., Trauner, M., & Bauer, M.** (2017). Impact of higher-order heme degradation products on hepatic function and hemodynamics. *Journal of Hepatology*, **67**(2), 272-281.
- Sen, K. I., Hepler, R., & Nanda, H.** (2017). Detection and Measurement of Methionine Oxidation in Proteins. *Current Protocols in Protein Science*, **87**:14.16.1-14.16.11.
- Sharma, P., Jha, A. B., Dubey, R. S., & Pessarakli, M.** (2012). Reactive oxygen species, oxidative damage, and antioxidant defense mechanism in plants under stressful conditions. *Journal of botany*, **2012**, 1-26.
- Shen, H., Zhou, Q., Pan, X., Li, Z., Wu, J., & Yan, N.** (2017). Structure of a eukaryotic voltage-gated sodium channel at near-atomic resolution. *Science*, **355**(6328), eaal4326.
- Shulaev, V., & Oliver, D. J.** (2006). Metabolic and proteomic markers for oxidative stress. New tools for reactive oxygen species research. *Plant Physiology*, **141**(2), 367-372.
- Soh, H., Jung, W., Uhm, D. Y., & Chung, S.** (2001). Modulation of large conductance calcium-activated potassium channels from rat hippocampal neurons by glutathione. *Neuroscience letters*, **298**(2), 115-118.
- Sroussi, H. Y., Berline, J., & Palefsky, J. M.** (2007). Oxidation of methionine 63 and 83 regulates the effect of S100A9 on the migration of neutrophils in vitro. *Journal of leukocyte biology*, **81**(3), 818-824.
- Stadtman, E. R.** (1993). Oxidation of free amino acids and amino acid residues in proteins by radiolysis and by metal-catalyzed reactions. *Annual review of biochemistry*, **62**(1), 797-821.
- Stadtman, E. R.** (2006). Protein oxidation and aging. *Free radical research*, **40**(12), 1250-1258.
- Stadtman, E. R., & Levine, R. L.** (2003). Free radical-mediated oxidation of amino acids and amino acid residues in proteins. *Amino acids*, **25**(3-4), 207-218.
- Stark, G.** (2005). Functional consequences of oxidative membrane damage. *The Journal of Membrane Biology*, **205**(1), 1-16.
- Stone, J. R., & Yang, S.** (2006). Hydrogen peroxide: a signaling messenger. *Antioxidants & redox signaling*, **8**(3-4), 243-270.
- Su, Z., Limberis, J., Martin, R.L., Xu, R., Kolbe, K., Heinemann, S. H., & Gintant, G. A.** (2007). Functional effects of methionine oxidation of hERG potassium channels. *Biochemical pharmacology*, **74**(5), 702-711.

- Sun, Y. M., Favre, I., Schild, L., & Moczydlowski, E.** (1997). On the structural basis for size-selective permeation of organic cations through the voltage-gated sodium channel. *The Journal of General Physiology*, **110**(6), 693-715.
- Tarr, M., Arriaga, E., & Valenzano, D.** (1995). Progression of cardiac potassium exposure after exposure to reactive oxygen. *Journal of Molecular and Cellular Cardiology*, **27**(5), 1099-1109.
- Trimmer, J. S., Cooperman, S. S., Tomiko, S. A., Zhou, J., Crean, S. M., Boyle, M. B., Kalen, R. G., Sheng, Z., Barchi, R. L., Sigworth, F. J., Goodman, R. H., Agnew, W. S., Mandel, G.** (1989). Primary structure and functional expression of a mammalian skeletal muscle sodium channel. *Neuron*, **3**(1), 33-49.
- Tsien, R. Y.** (1998). The green fluorescent protein. *Annual review of biochemistry*, **67**, 509-544.
- Ulbricht, W.** (2005). Sodium channel inactivation: molecular determinants and modulation. *Physiological reviews*, **85**(4), 1271-1301.
- Vogt, W.** (1995). Oxidation of methionyl residues in proteins: tools, targets, and reversal. *Free Radical Biology and Medicine*, **18**(1), 93-105.
- Volinsky, R., & Kinnunen, P. K.** (2013). Oxidized phosphatidylcholines in membrane-level cellular signaling: from biophysics to physiology and molecular pathology. *The FEBS journal*, **280**(12), 2806-2816.
- Wall, S. B., Oh, J. Y., Diers, A. R., & Landar, A.** (2012). Oxidative modification of proteins: an emerging mechanism of cell signaling. *Frontiers in physiology*, **3**: 369.
- Wallace, R. H., Wang, D. W., Singh, R., Scheffer, I. E., George, A. L., Phillips, H. A., Saar, K., Reis, A., Johnson, E.W., Sutherland, G.R., & Berkovic, S. F., Mulley, J.C.** (1998). Febrile seizures and generalized epilepsy associated with a mutation in the Na⁺-channel β 1 subunit gene SCN1B. *Nature genetics*, **19**(4), 366.
- Wang, G. K.** (1984). Modification of sodium channel inactivation in single myelinated nerve fibers by methionine-reactive chemicals. *Biophysical journal*, **46**(1), 121-124.
- Wang, G. K., & Wang, S. Y.** (2002). Modifications of human cardiac sodium channel gating by UVA light. *Journal of Membrane Biology*, **189**(2), 153-165.
- Wardman, P.** (2007). Fluorescent and luminescent probes for measurement of oxidative and nitrosative species in cells and tissues: progress, pitfalls, and prospects. *Free radical biology and medicine*, **43**(7), 995-1022.
- Wessjohann, L. A., Schneider, A., Abbas, M., & Brandt, W.** (2007). Selenium in chemistry and biochemistry in comparison to sulfur. *Biological chemistry*, **388**(10), 997-1006.
- West, J. W., Patton, D. E., Scheuer, T., Wang, Y., Goldin, A. L., & Catterall, W. A.** (1992). A cluster of hydrophobic amino acid residues required for fast Na⁺-channel inactivation. *Proceedings of the National Academy of Sciences*, **89**(22), 10910-10914.
- Winrow, V. R., Winyard, P. G., Morris, C. J., & Blake, D. R.** (1993). Free radicals in inflammation: second messengers and mediators of tissue destruction. *British Medical Bulletin*, **49**(3), 506-522.
- Wojtovich, A. P., & Foster, T. H.** (2014). Optogenetic control of ROS production. *Redox biology*, **2**, 368-376.
- Woo, H. A., Chae, H. Z., Hwang, S. C., Yang, K. S., Kang, S. W., Kim, K., & Rhee, S. G.** (2003). Reversing the inactivation of peroxiredoxins caused by cysteine sulfinic acid formation. *Science*, **300**(5619), 653-656.
- Wood, Z. A., Poole, L. B., & Karplus, P. A.** (2003). Peroxiredoxin evolution and regulation of hydrogen peroxide signaling. *Science*, **300**(5619), 650-653.

- Wu, L., & Wang, R.** (2005). Carbon monoxide: endogenous production, physiological functions, and pharmacological applications. *Pharmacological reviews*, **57(4)**, 585-630.
- Wu, W. S.** (2006). The signaling mechanism of ROS in tumor progression. *Cancer and Metastasis Reviews*, **25(4)**, 695-705.
- Yan, Z., Zhou, Q., Wang, L., Wu, J., Zhao, Y., Huang, G., & Yan, N.** (2017). Structure of the Nav 1.4- β 1 Complex from Electric Eel. *Cell*, **170**, 470–482.
- Yang, F.** (1997). The molecular structure of green fluorescent protein. *PhD thesis*, Rice University, Houston, USA.
- Yang, F., Moss, L. G., & Phillips Jr, G. N.** (1996). The molecular structure of green fluorescent protein. *Nature Biotechnology*, **14(124671251)**, 1392-1395
- Yang, N., & Horn, R.** (1995). Evidence for voltage-dependent S4 movement in sodium channels. *Neuron*, **15(1)**, 213-218.
- Yu, F. H., Westenbroek, R. E., Silos-Santiago, I., McCormick, K. A., Lawson, D., Ge, P., Ferriera, H., Lilly, J., DiStefano, P. S., Catterall, W. A., Scheuer, T., Curtis, R.** (2003). The results are summarized in the following table. Sodium channel beta4, a new disulfide-linked auxiliary subunit with similarity to beta2. *The Journal of Neuroscience*, **23(20)**, 7577-7585.
- Zhang, P. H.** (2005). Effect of hydrogen peroxide on persistent sodium current in guinea pig ventricular myocytes. *Acta pharmacologica Sinica*, **26(7)**, 828-834.

Declaration

I hereby declare that:

1. I am aware of the current course of examination for doctoral studies of the Faculty of Medicine at Friedrich Schiller University of Jena, Germany.
2. I have researched and written the presented thesis myself, no passages of text have been taken from third parties or own exam papers without having been identified. All tools, personal notifications, and sources used by me have been indicated in the thesis.
3. my doctoral supervisor, Prof. Dr. Stefan H. Heinemann has supported me in selecting and analyzing the material and in preparing the manuscript for publications. Most of the part of the presented thesis has already published in three peer-reviewed scientific journals, namely *Biochimica et Biophysica Acta (BBA)-Biomembranes*, *Scientific Reports*, and *Journal of Hepatology*.
4. the assistance of any doctoral consultant has not been utilized and no third parties have either directly or indirectly received monetary benefits from the presented work or from related contents of the submitted thesis.
5. I have not submitted the thesis as an examination paper for state or other academic examinations.
6. I have not submitted the same, largely similar or any different treatises to another university as dissertation.

Jena, 04.09.2017

Navin Kumar Ojha

[German translation]

Ehrenwörtliche Erklärung

Ich erkläre hiermit, dass:

1. mir die geltende Promotionsordnung der Medizinischen Fakultät der Friedrich-Schiller-Universität Jena, Deutschland bekannt ist.
2. ich die vorliegende Arbeit selbst angefertigt habe, keine Textabschnitte von Dritten oder eigene Prüfungsarbeiten übernommen habe ohne diese zu kennzeichnen. Alle von mir verwendeten Hilfsmittel, persönlichen Mitteilungen und Quellen wurden in der Arbeit angegeben.
3. mein Betreuer Herr Prof. Dr. Stefan H. Heinemann mich bei der Auswahl und Analyse des Materials sowie bei der Erstellung des Manuskripts unterstützt hat. Der Großteil der Ergebnisse der vorliegenden Arbeit wurde bereits in drei wissenschaftlichen peer-reviewed Zeitschriften veröffentlicht: *Biochimica et Biophysica Acta (BBA)-Biomembranes*, *Scientific Reports* und *Journal of Hepatology*.
4. die Hilfe eines Promotionsberaters nicht in Anspruch genommen wurde und dass Dritte weder unmittelbar noch mittelbar geldwerte Leistungen von mir für Arbeiten erhalten haben, die im Zusammenhang mit dem Inhalt der vorgelegten Dissertation stehen.
5. ich die Dissertation noch nicht als Prüfungsarbeit für eine staatliche oder andere akademische Prüfung eingereicht habe.
6. ich die gleiche, eine in wesentlichen Teilen ähnliche oder eine andere Abhandlung bei einer anderen Hochschule als Dissertation nicht vorgelegt habe.

Jena, 04.09.2017

Navin Kumar Ojha

Acknowledgements

Independence is important for true progress; however, a difficult journey will be easier and pleasant when you travel together. Although I am only responsible for this thesis, I appreciate contributions of all those persons whose time, ideas, comments, criticism, support, and encouragement led the success of my doctoral project.

The vocabulary fails to express my heartfelt gratitude and unfathomable indebtedness to my esteemed supervisor Prof. Dr. Stefan. H. Heinemann, whose guidance, encouragements, stimulating suggestions, critical analysis, and immense support helped me to accomplish my doctoral research and thesis writing. I am proud and privileged to have a doctoral supervisor like him.

I am thankful to Prof. Dr. Toshi Hoshi (University of Pennsylvania), Dr. Roland Schönherr, and Dr. Enrico Leipold for their interest in my research works, valuable suggestions, and help in preparing manuscripts for publications.

I am also grateful to Dr. Guido Geßner, Dr. Nirakar Sahoo, Dr. Sandip Swain, Dr. Martin Schink, and Bilal Malik for their valuable suggestions, motivation, and discussion both scientific and non-scientific. Special thanks to Dr. Guido Geßner and Johanna Maria Langner for translating some pages of the thesis into the German language.

My sincere gratitude to Mrs. Dorith Schmidt, Mrs. Gudrun Albrecht, Mrs. Elke Müller, and Dr. Franziska Jahn for their unconditional help in accomplishing administrative and official work. I would like to say special thanks to Dr. Franziska Jahn for her ever helping and 'never saying no' attitude. Many thanks to Mr. Holger Sack, Mrs. Angela Roßner, Mrs. Anja Keßler, and Mrs. Eva-Maria Franke for the technical and lab assistance.

Last but not least, I would like to thank my parents, brothers, sisters, and friends. I wish to express my warmest gratitude to the most important person in my life, my wife, who has shown great patience and understanding during the odd time of my life.

-Navin Kumar Ojha

Curriculum Vitae and Publication List

Personal Details

Name, Nationality: Navin Kumar Ojha, Indian

Family status: Married

Date of birth, Place: 07.03.1986, Katni, India

Email: navin.k.ojha@gmail.com

Education and Research experience

From 12/2012: Ph.D. thesis in the Department of Biophysics at the Friedrich Schiller University of Jena, Germany under the supervision of Prof. Dr. Stefan H. Heinemann.

10/2011 – 08/2011: Research Assistant, School of Life sciences, Jawaharlal Nehru University, New Delhi, India

07/2009 – 08/2011: M.Sc. Neuroscience, School of Studies in Neuroscience, Jiwaji University, Gwalior, India

07/2006 – 06/2009: B.Sc., Jain Group of Colleges, Jiwaji University, Gwalior, India

Achievements and Awards

-
1. Travel award from the German Physiological Society for attending the Young Physiologist Symposium (Leipzig, 2015 and Jülich, 2016)
 2. Capacity build-up scholarship from the University Grant Commission (UGC) of India (2011-2012)
 3. Department of Biotechnology (DBT)-Studentship from the Government of India for master studies (2009 - 2011)
 4. John-Miller travel award for attending the Annual Meeting of the Indian Academy of Neurosciences (Jaipur, 2010 and Lucknow, 2011)

Publications

Ojha, N. K., Leipold, E., Schönherr, R., Hoshi, T., & Heinemann, S. H. (2017). Non-photonic sensing of membrane-delimited reactive species with a Na⁺ channel protein containing selenocysteine. *Scientific Reports*, 7: 46003.

Seidel, R. A., Claudel, T., Schleser, F. A., **Ojha, N. K.**, Westerhausen, M., Nietzsche, S., Karailieva, D., Sponholz, C., Cuperus, F., Coldewey, S. M., Heinemann, S. H., Pohnert, G., Trauner, M., and Bauer, M. (2017). Impact of higher-order heme degradation products on hepatic function and hemodynamics. *Journal of Hepatology*, 67 (2), 272 – 281.

Ojha, N.K., Nematian-Ardestani, E., Neugebauer, S., Borowski, B., El-Hussein, A., Hoshi, T., Leipold, E., Heinemann, S. H. (2014). Sodium channels as gateable non-photon sensors for membrane-delimited reactive species. *Biochimica et Biophysica Acta (BBA)-Biomembranes*, 1838(5), 1412-1419.

Posters

Ojha, N.K., Leipold, E., Schönherr, R., Hoshi, T., Heinemann, S. H. (2017). Non-photon sensing of membrane-delimited reactive species with a Na⁺ channel protein containing selenocysteine. *The OCC World Congress and Annual SFRR-E Conference June 21 – 23, 2017, Berlin, Germany*. Free Radical Biology and Medicine, Vol. 108, Suppl. 1, S58. DOI: <https://doi.org/10.1016/j.freeradbiomed.2017.04.203>

Jin, J., **Ojha, N. K.**, Schink, M., Rühl, P., Heinemann, S. H. Membrane potential manipulation with visible flash-light illumination of targeted superparamagnetic beads. *5th Symposium of Young Physiologists, September 22 – 23, 2016*, Forschungszentrum Jülich, Germany.

Ojha, N. K., Leipold, E., Schönherr, R., Heinemann, S. H. Real-time ROS monitoring delimited to the cell membrane by voltage-gated sodium channels containing selenocysteine. *4th Symposium of Young Physiologists, September 24 – 25, 2015*, Faculty of Veterinary Medicine, Leipzig, Germany.

Ojha, N. K., Arifin, J. C., Schink, M., Leipold, E., Heinemann, S. H. Photonic modulation of membrane potential by flash-light illumination of metallic beads. *11th Annual Meeting of the German Neuroscience Society, March 18 – 21, 2015*, Göttingen, Germany.

Sharma, D., **Ojha, N. K.**, Mishra, M., Singh, R. Anti-epileptic effect of sodium valproate, ascorbic acid, and tocopherol in iron-induced epilepsy in wistar rats. *30th Annual meeting of the Indian Academy of Neurosciences, October 27 – 30, 2012*, Amritsar, India.

Scientific talk

Ojha, N.K., Leipold, E., Schönherr, R., and Heinemann, S. H. Artifacts of light in life science research. *6th Symposium of Young Physiologists, September 28 – 29, 2017*, Institute of Physiology II, University Hospital of Jena, Germany (*yet to be done*).

Ojha, N.K., Leipold, E., Schönherr, R., Hoshi, T., Heinemann, S. H. Non-photonic sensing of membrane-delimited reactive species with a Na⁺ channel protein containing selenocysteine. *Blitz presentation, FEBS/EMBO Lecture Course on Ion Channels and Transporters, May 14 – 20, 2017*, Erice, Italy.

Ojha, N.K., Leipold, E., Schönherr, R., and Heinemann, S. H. Monitoring of cellular reactive species with voltage-gated Na⁺ channels containing selenocysteine. *5th Symposium of Young Physiologists, September 22 – 23, 2016*, Forschungszentrum Jülich, Germany.

Jena, 04.09.2017

Navin Kumar Ojha